NOVEL MULTIFUNCTIONAL FILTERING POWER DIVIDERS MADE ON CIRCULAR PATCH RESONATORS

KHOR Y CHUN

MASTER OF ENGINEERING SCIENCE

Faculty of Engineering and Science

Universiti Tunku Abdul Rahman

FEBUARY 2013

ABSTRACT

Microwave power dividers and filters are among the key passive components in any microwave circuits and subsystems. The former has been broadly employed for dividing or combining microwave signals; whereas, the later is to be used for selecting the wanted and unwanted signals. Both components are found necessary in circuitries such as power amplifiers, phase shifters, antenna arrays and so on. In practice, a power divider is usually cascaded with a bandpass filter in order to eliminate noise contributed by the surrounding subsystems or components. However, it results in a bulkier circuit size and higher loss, suffering by microwave signals along the signal paths.

The latest trend of miniaturizing a wireless communication system is to merge various components into a single RF module and, also sometimes, with the use of reconfigurable designs. In this thesis, for the first time, several types of multifunctional microstrip bandpassing power dividers are presented. This project is composed by two parts. Part 1 will be describing the double-layered dual-mode microstrip bandpassing power dividers; while a reconfigurable one will be presented in Part 2. Both of them will be elaborated in the subsequent paragraphs.

ACKNOWLEDGEMENT

I would like to thank Dr. Lim Eng Hock and Prof. Chung Boon Kuan for their directions, ideas and guidance. Throughout the completion of this research project, invaluable recommendations and suggestions have been shared. In addition, they were always available whenever I faced doubt.

I also wish to thank Mr. Ho, who guided me on fabrication process. With his experience, I am able to fabricate my design precisely. Besides that, I also like to extend my gratitude to all the seniors and friends during problem solving.

Special thanks should be given to UTAR for supporting all the equipments, facilities, and materials. Furthermore, the online database such as IEEE Xplore and ProQuest are very handy where most of the related information is available.

APPROVAL SHEET

This thesis entitled **'NOVEL MULTIFUNCTIONAL FILTERING POWER DIVIDERS MADE ON CIRCULAR PATCH RESONATORS'** was prepared by KHOR Y CHUN and submitted as partial fulfillment of the requirement for the degree of Master of Engineering Science at Universiti Tunku Abdul Rahman.

Approved by,

_____

(Dr. Lim Eng Hock) Date: _____

Supervisor

Department of Electrical and Electronic Engineering

Faculty of Engineering Science

Universiti Tunku Abdul Rahman

_____

(Prof. Dr. Chung Boon Kuan) Date: _____

Professor/Co-supervisor

Department of Electrical and Electronic Engineering

Faculty of Engineering Science

Universiti Tunku Abdul Rahman

FACULTY OF ENGINEERING SCIENCE

UNIVERSITI TUNKU ABDUL RAHMAN

Date: 22th Feb 2013

SUBMISSION OF FINAL YEAR PROJECT /DISSERTATION/THESIS

It is hereby certified that **KHOR Y CHUN** (ID No: **10 UEM 07362**) has completed this dissertation entitled "**NOVEL MULTIFUNCTIONAL FILTERING POWER DIVIDERS MADE ON CIRCULAR PATCH RESONATORS**" under the supervision of Dr. Lim Eng Hock (Supervisor) from the Department of Electrical and Electronic Engineering, Faculty of Engineering and Science (FES), and Prof. Ir. Dr. Chung Boon Kuan (Co-Supervisor) from the Department of Electrical and Electronic Engineering, Faculty of Engineering and Science (FES).

I understand that University will upload softcopy of my final dissertation in pdf format into UTAR Institutional Repository, which may be made accessible to UTAR community and public.

Yours truly,

(KHOR Y CHUN)

DECLARATION

I hereby declare that the thesis is based on my original work except for citations and quotations which have been duly acknowledged. I also declare that it has not been previously and concurrently submitted for any other degree or award at UTAR or other institutions.

Name : KHOR Y CHUN

Date : 22th Feb 2013

NOVEL MULTIFUNCTIONAL FILTERING POWER DIVIDERS MADE ON CIRCULAR PATCH RESONATORS

In Part 1, two bandpassing power dividers, for both the two and three outputs**,** are investigated. To demonstrate the design ideas, two prototypes are designed to work at 6 GHz with the use of a circular patch resonator. The filter synthesis method is employed to generate coupling matrix for each of the bandpassing power dividers. Here, it will be showcased that the design freedom can be made higher by having more outputs while keeping the design ideology. Another distinct advantage of the proposed bandpassing power divider is that a pair of transmission zeroes can be clearly identified at finite frequencies. This is due to tight coupling between the resonator and the output patches of the double-layered structure.

Now, another new idea for multifunctional power dividers is proposed. As for Part 2, the idea of integrating an PIN diode as a switching element is presented. The proposed reconfigurable bandpassing power divider consists of a 2.4 GHz circular patch resonator and an embedded PIN diode at each output port. The design principle of this part is to individually optimize both the **in-phase** and **out-of-phase** performances. Later, both of them are combined into one resonator. It was found that the prototype has very good performances. Also, the idea of reconfiguration can be

easily achieved by incorporating the PIN diodes, either by turning anyone of them ON or OFF.

Finally, a comprehensive parametric analysis is carried out for each project in order to completely understand each of the parameters and their limitations. All the simulations were done by using Ansoft HFSS software and prototypes were fabricated. Measurements were then carried out to verify the simulated results.

TABLE OF CONTENTS

LIST OF TABLES

LIST OF FIGURES

CHAPTER 1

Introduction

1.1 Background

Radiofrequency and microwave refer to the frequency spectrums ranging from 300 MHz to 30 GHz, which correspond to wavelengths from 100cm to 1cm. In any microwave circuits and subsystems such as power amplifiers, phase shifters, and antenna arrays, microwave power dividers/combiners and bandpass filters are among the key passive components. The former are usually deployed to divide or combine signals in specific frequency bands and the latter are generally used to remove the unwanted signals in certain spectrums.

In the past, many power dividers with different number of output ports, ranging from 1-to-2 (Jia, Z. et al., 2006; Cohn, S. B., 1986; Tang, X., and Mouthaan, K., 2009; Rosloniec, S., 1996), 1-to-3 (Tahara, Y. et al., 2005; Chiu, J. C. et al., 2006; Goldfarb, M. E., 1991; Eccleston, K. W., 2005; Abbosh, M., 2008; David, M. et al., 1996; Mgombelo, H. R. and Gardiner, J. G., 1990), 1-to-4 (Lin, Z. and Chu, Q. X., 2008) up till 1-to-N (Kishihara, M. et al., 2004; Yau, W. et al., 1986; Nakatsugawa, M. and Nishikawa, K., 2001; Wilkinson, E. J., 1960; Shor, 1988; Hung, Y. Y. et al., 1970; Saleh, 1980) , have been reported. As mentioned in (Chiu, J. C. et al., 2006),

however, some designs are facing difficulties in configuring odd number of output ports (Rosloniec, S., 1996; Yau, W. et al., 1986; Shor, 1988).

Among the aforementioned, the Wilkinson Power Divider is the most widely used. It was proposed by E. J. Wilkinson in 1960, and the schematic is shown here in *Figure 1.1*. The microwave signal at the input port (Port P1) is split into two identical output signals (at Ports P2 and P3) through a pair of quarter-wavelength impedance transformers. On the other hand, it can also work as a power combiner when two identical signals are fed at P2 and P3.

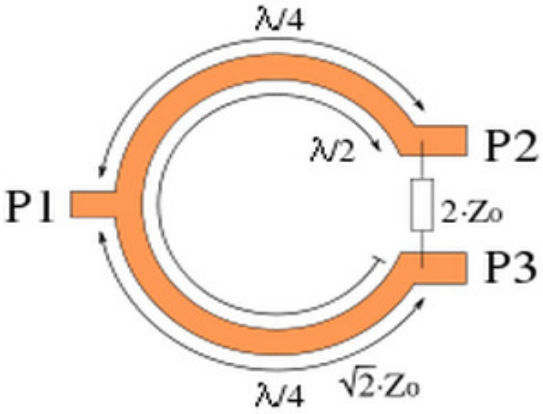

Figure 1.1: Wilkinson Power Divider.

There are two major drawbacks of the Wilkinson power divider. Firstly, in order to split a signal into more outputs (beyond two outputs), the divider needs to combine several sections of microstrip lines and add more isolation resistors as well as quarter-wavelength impedance transformers, which significantly complicates the design procedures and sacrifices the space efficiency. Secondly, as mentioned in (Kishihara, M. et al., 2004), as the number of output ports increases, the characteristic impedance of the transformers needs a higher value. In other words, it requires the use of thinner transmission lines. But this is limited by the fabrication

technologies in most of the time. On top of that, the performance of the divider may degrade significantly caused by the parasitic effect at the multi-section branching junctions.

In most cases, a standalone microwave power divider does not have bandpassing effect. To improve the frequency selectivity, such component is usually cascaded with a bandpass filter (BPF) to eliminate the noise contributed by the surrounding subsystems or components. However, at lower microwave frequencies, circuits that are designed by the classical method occupy excessive space. In order to address this issue, some researchers integrated power divider with a bandpass filter (Cheong, P. et al., 2010; Song, K. and Xue, Q., 2010; Wong, S. W. and Zhu, L., 2008; Wong, S. W. and Zhu, L., 2009; Shao, J. Y. et al., 2011). In (Wong, S. W. and Zhu, L., 2009), a quarter-wavelength short-circuited stub and a parallel-coupled line is incorporated into the two output ports of a traditional single-stage Wilkinson power divider. According to the analysis in (Wong, S. W. and Zhu, L., 2008), in order to achieve sharp roll-off skirt, a divider is constructed by introducing a pair of stepped-impedance open-circuited stubs and parallel-coupled lines in the two output ports. Alternatively, the quarter-wavelength transformers of the conventional Wilkinson power divider were simply replaced either by two quasi-elliptic filters in (Shao, J. Y. et al., 2011) or by the stepped impedance interdigital coupling structure in (Cheong, P. et al., 2010). For (Song, K. and Xue, Q., 2010), the authors successfully implemented an ultra-wideband (UWB) bandpassing power divider using the multilayer slotline structure. However, this idea requires an isolation resistor to be embedded into the substrates. It complicates the fabrication process.

As one of the possible solutions to the mentioned limitations, it will be shown in this thesis (**Chapter 3**) that a double-layered bandpass power divider can be made without the use of any isolation resistor or quarter-wavelength impedance transformer. With this, the proposed configuration can be easily extended to have multiple output ports. And also, it serves as an alternative solution to introduce band-passing effect to a power divider, while keeping compact size.

In some wireless applications such as WLAN and Bluetooth systems, balun (Lew, D. W. et al., 2001; Cho, C. and Gupta, K. C., 1998; Zhang, Z. Y. et al., 2005; Tang, C. W. and Chang, C. Y., 2002; Ng, C. Y. et al., 2002; Bialkowski, M. E. and Abbosh, A. M., 2007), and (Basraoui, M. and Prasad, S. N., 1998) is an essential element. It transforms a single-ended signal into a pair of differential ones, which are 180° out-of-phase, or vice versa. For instance, *Figure 1.2* shows the typical schematic of a Bluetooth system where a balun is used to combine two differential signals coming from a chip into a single-ended one that is transmissible by the antenna. In order to further improve the compactness and cost efficiency, some researchers have come up with microwave baluns that have bandpassing effect, as reported in Jung, (E. Y. and Hwang, H. Y., 2005; Yeung, L. K. and Wu, K. L., 2006; Yeung, L. K. and Wu, K. L., 2007; Yeung, L. K. and Wu, K. L., 2007; Wu C. H. et al., 2008; Huang, G. S. and Chen, C. H., 2011; Huang, G. S. et al., 2007; Sun, S. and Menzel, W., 2011; Kang, S. J. and Hwang, H. Y., 2010).

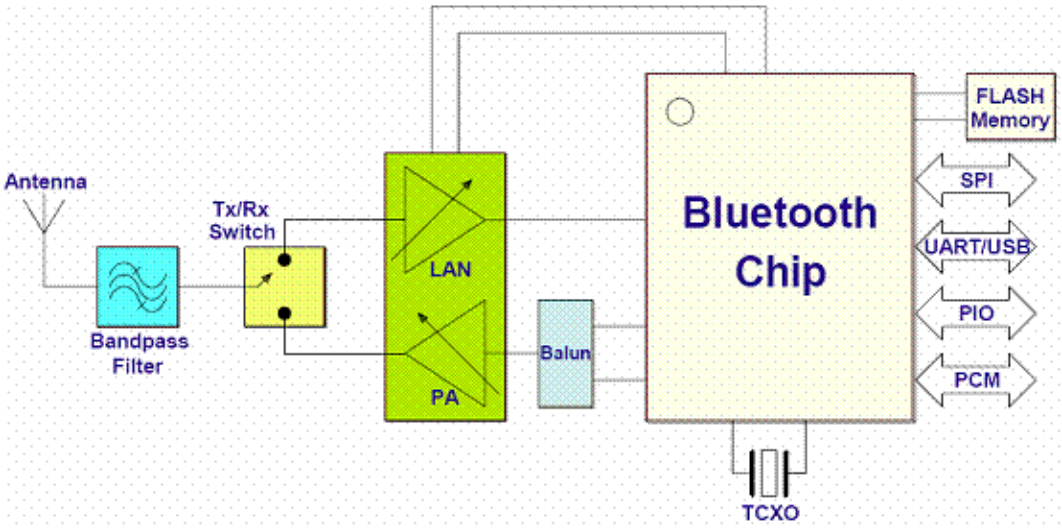

Figure 1.2: Schematic of a Bluetooth module.

In a microwave system, circuit size and production cost are the two most important criteria. Therefore, devices that can perform multifunctional operations are in high demand by various modern communication systems and applications. Recently, engineers have come up with a few reconfigurable designs (Chiou, Y. C. and Rebeiz, G. M., 2011; Chen, J. Y. et al., 2011; Mung, W. Y. and Chan, W. S., 2011; Wong, P. W. and Hunter, I. C., 2009; Zheng, S. Y. et al., 2011; Li, Y. C. and Xue, Q., 2011; Hsieh, L. H. and Chang, K., 2003; Lehmann, T. et al., 2009; Kim, S. and Leong, J., 2009; Tae, H. S. et al., 2012; Marim, M. F. et al., 2006; Park, J. H. et al., 2005; Deng, P. H. and Jheng, J. H., 2011) where different switching technologies, such as silicon and GaAs varactor diodes, RF PIN diodes, ferroelectric diodes, and RF microelectromechanical systems (RF-MEMS), were used. Generally, the abovementioned reconfigurable designs can be categorized into two major subcategories, namely tunable (Chiou, Y. C. and Rebeiz, G. M., 2011; Chen, J. Y. et al., 2011; Mung, W. Y. and Chan, W. S., 2011; Wong, P. W. and Hunter, I. C., 2009; Zheng, S. Y. et al., 2011; Li, Y. C. and Xue, Q., 2011; Hsieh, L. H. and Chang, K.,

2003), and switchable (Lehmann, T. et al., 2009; Kim, S. and Leong, J., 2009; Tae, H. S. et al., 2012; Marim, M. F. et al., 2006; Park, J. H. et al., 2005; Deng, P. H. and Jheng, J. H., 2011). However, they do not provide both the power dividing and bandpassing effects at the same time.

In order to further improve the miniaturization level and cost efficiency, it will be shown in this thesis (**Chapter 4**) that a single-layered multifunctional and reconfigurable power divider with bandpassing effect can be achieved by integrating an RF PIN diode at each of the output ports. By incorporating switches, the proposed bandpass power divider can be configured either to be in-phase or out-of-phase.

1.2 Research Objectives and Motivations

The main objective of this thesis is to explore the multifunction of the microstrip patch resonator as either a passive or an active device. In the first part, a double-layered structure is deployed for designing the in-phase power dividers with multiple outputs. Later, a single-layered circular patch is made a dual-functional coupler that provides in-phase and out-of-phase operations in one. The details are covered in ***Chapter 3*** and ***4***.

Chapter 3 is to explore multifunction in a circular patch resonator and to develop a double-layered dual-mode power divider with bandpassing effect. For the first time, a 1-to-2 bandpassing power divider is designed, following by another with 1-to-3 power division. Both of them do not involve the usage of any isolation resistor and impedance transformer. Another distinctive advantage is that the overall circuit size remains even if the number of output ports is increased. Both of the proposed prototypes have been designed at 6 GHz. Experiments were conducted to verify the simulated models. In addition, a thorough study on performances, including filter synthesis and coupling modeling, for both designs will be carried out.

In ***Chapter 4*** of this project, a compact, multifunctional, and reconfigurable bandpassing power divider has been designed by utilizing several RF PIN-diodes as switching elements. By sharing a single resonator, it can work either as an in-phase or out-of-phase reconfigurable bandpassing power divider. The design procedure of the proposed configuration is very simple and straightforward. To start with, the in-

and out-of-phase couplers are designed separately. Then, it will be shown that both of them can be easily combined into one that has both functions without modifying the original design parameters. In this case, biasing circuitries are needed to power up the RF PIN diodes.

1.3 Thesis Organization

Chapter 1 briefly introduces the background of the microwave power dividers and bandpass filters. In this chapter, some recent developments and current issues that are relevant to the works presented in this thesis are discussed. The objectives of this research work are briefly outlined.

Chapter 2 discusses the fundamental theory of microstrip technologies. Here, microstrip lines and resonators are investigated. At the same time, several types of losses that are common in microstrip lines have been reviewed. It follows by the discussion of transfer function where the insertion loss, return loss, and group delay of filters are studied. In the final part, filter synthesis is illustrated.

Chapter 3 analyses the proposed double-layered 1-to-2 and 1-to-3 bandpassing power dividers. The design procedures for both the proposed designs are outlined. The return losses as well as insertion losses will be discussed in the following sections. Subsequently, the amplitude difference between the output ports and group delays are presented. Lastly, the effects of all design parameters are reviewed.

In ***Chapter 4*** the proposed single-layered reconfigurable band-passing power divider is investigated in detail. It starts with the discussion of the performance of the proposed in-phase reconfigurable band-passing power divider, following by the out-of-phase one. Its design procedures and the operation principles of the switching element are reviewed in the following section. Next, the return losses, insertion losses, amplitude and phase differences are presented. It is followed by the discussion of the effect of each parameter.

Chapter 5 summarizes the research works presented in this thesis. Finally, some personal opinions are also given for the future works.

CHAPTER 2

Literature Review

2.1 Microstrip Lines

Microstrip lines are one of the most commonly used microwave transmission lines in the wireless systems. The general configuration of a microstrip is depicted in *Figure 2.1*. This type of transmission line has been popular because of it is relatively easy to fabricate. Also, integration with other surface-mount components is convenient. It consists of a conducting line suspending above a ground plane, separated by a substrate. The conducting line (microstrip line), with width of W and thickness of t, is made on a substrate that comes with a relative dielectric constant of ε_r and a thickness of h.

As well known, wave propagating in a microstrip is not purely in the transverse electromagnetic (TEM) mode because of its inhomogeneous structure, to be precise the dielectric substrate and air, shown in *Figure 2.2*. A pure TEM wave has only transverse electric fields and it propagates at the speed of light c. In general, the properties of a microstrip depend not only on the materials, but its propagation characteristics can also be varied by the physical dimension of the transmission line.

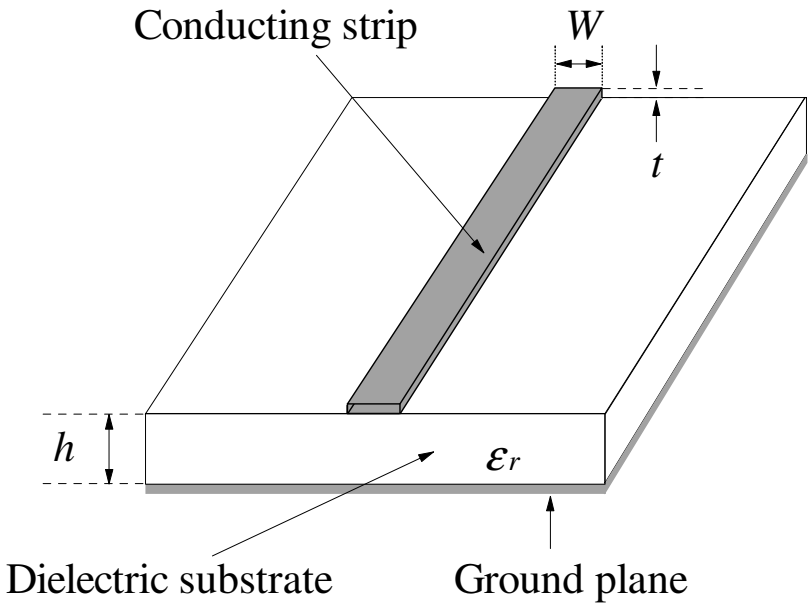

Figure 2.1: Configuration of a general microstrip.

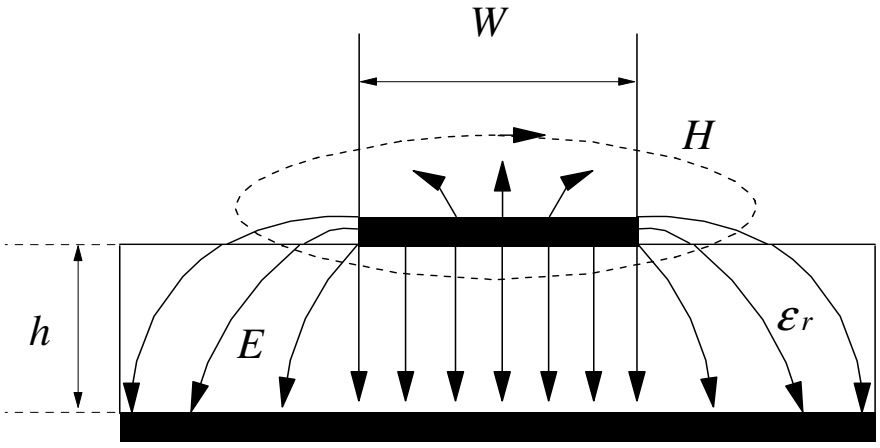

Figure 2.2: Internal and external field distribution of a microstrip.

2.1.1 Effective Dielectric Constant and Characteristic Impedance

The field distribution in a microstrip is assumed to be quasi-TEM. This is because the longitudinal components of the fields for the dominant mode is minute compared to the transverse ones, and they can be neglected. Being quasi-TEM, the microwave signal propagates like a plane wave in a microstrip. This approximation is valid over most of the operating frequency ranges (Hong, J. S. and Lancaster, M. J., 2001). To ease calculation, the homogeneous dielectric material with an effective permittivity replaces the inhomogeneous dielectric-air media of microstrip. As a result, the transmission characteristics of a microstrip can be described by only two parameters, namely, the effective dielectric constant ε_{reff} and characteristic impedance Z_0, which can be determined as follows

$$\varepsilon_{reff} = \frac{C_d}{C_a} \tag{2.1}$$

$$Z_0 = \frac{1}{c\sqrt{C_d C_a}} \tag{2.2}$$

C_d = capacitance per unit length with presence of dielectric substrate.
C_a = capacitance per unit length with the dielectric substrate replaced by air.
C = velocity of electromagnetic wave in free space or speed of light ($c \approx 3.0\times10^8$ m/s).

Over the past years, much effort has been dedicated to improve the accuracy of calculation for both the effective permittivity and characteristic impedance, which can be estimated by the empirical *eqn. (2.3) – (2.6)*. It is better than one percent.

For $W/h \leq 1$:

$$\varepsilon_{reff} = \frac{\varepsilon_r + 1}{2} + \frac{\varepsilon_r - 1}{2}\left\{\left(1 + 12\,\frac{h}{W}\right)^{-0.5} + 0.04\left(1 - \frac{W}{h}\right)^2\right\} \tag{2.3}$$

$$Z_0 = \frac{\eta}{2\pi\sqrt{\varepsilon_{reff}}}\ln\left(\frac{8h}{W} + 0.25\frac{W}{h}\right) \tag{2.4}$$

For $W/h \geq 1$:

$$\varepsilon_{reff} = \frac{\varepsilon_r + 1}{2} + \frac{\varepsilon_r - 1}{2}\left\{\left(1 + 12\,\frac{h}{W}\right)^{-0.5}\right\} \tag{2.5}$$

$$Z_0 = \frac{\eta_0}{\sqrt{\varepsilon_{reff}}}\left\{\frac{W}{h} + 1.393 + 0.677\ln\left(\frac{W}{h} + 1.44\right)\right\}^{-1} \tag{2.6}$$

η_0 = the wave impedance in free space (120π ohm).
W = width of microstrip
h = substrate height

A microstrip can normally have characteristic impedance ranging from 20 to 120 Ω. Thinner line leads to higher characteristic impedance, and vice versa. However, the upper limit is restricted by the technological constraints on the minimum line width that can be realized as well as the production tolerances. But broad line usually introduces higher-order modes.

2.1.2 Wavelength λ_g and physical length l

The velocity c of any propagating electromagnetic waves is given by the product of frequency and wavelength. In free space, the velocity is defined as $c = f\lambda_0$. However, when the wave is travelling in different media, it experiences a mixed dielectric environment. As a result, the wave velocity in microstrip is $v_p = f\lambda_g$, and the guided wavelength is defined as

$$\lambda_g = \frac{\lambda_0}{\sqrt{\varepsilon_{eff}}} \tag{2.7}$$

and the effective permittivity is approximated by

$$\varepsilon_{eff} \approx \frac{1}{2}(\varepsilon_r + 1) \tag{2.8}$$

2.1.3 Microstrip losses

Microstrip suffers from losses (Chang, K. et al., 2002), which can be categorized into three types, namely conductive, dielectric, and radiation losses. Conductive loss, more frequently referred as ohmic loss, is caused by the current flow in the conductor and ground, dominating at microwave frequencies. Dielectric loss describes the dissipation inside the dielectric substrate of a microstrip. The former can be calculated by *eqn. (2.9)* and the latter by *eqn. (2.10).*

$$a_c = 0.072\frac{\sqrt{f}}{WZ_0}\lambda_g \ dB/guided\ wavelength \tag{2.9}$$

$$\alpha_d = 27.3\ \frac{\varepsilon_r(\varepsilon_{reff}-1)\tan\delta}{\varepsilon_{reff}(\varepsilon_r-1)}\ dB/guided\ wavelength \tag{2.10}$$

Here, f is defined to be the operating frequency in GHz, λ_g is the guided wavelength, and $tan\ \delta$ is the loss tangent of the substrate. Radiation loss occurs when the energy is radiated to the surrounding environment. It is usually introduced by the discontinuities in the transmission lines.

2.2 Circular Patch Resonator

Resonator is a microwave structure that contains one or more standing waves in it. It can be constructed by lumped elements, quasi-lumped elements, or distributed components. Microstrip resonator is a distributed resonator that becomes very popular recently because of a number of advantages such as planar, low cost, and easy integration with other surface-mount components. The Q factor is also reasonably high for a microstrip resonating structure which is available in different configurations such as line, ring, and patch. A brief introduction on various resonators will be given next.

Lumped-element and quasi-lumped-element resonators are formed by the lumped or quasi-lumped capacitors and inductors shown in *Figure 2.3(a) and (b)*. At

high frequency, the coupling mechanism between two open-ended lines is used for implementing different capacitances (*C*). Also, an inductor (*L*) is usually a high-impedance line. As seen in *Figure 2.3 (b)*, an open stub and a high-impedance line are cascaded to form an *LC* resonator that resonates at $\omega_0 = 1/\sqrt{LC}$. Sometimes, they are not considered as lumped elements because the size and length of the high-frequency lines are in multiple of a wavelength, leading to a large footprint.

As for the distributed line resonator, it is usually $\lambda_{g0}/4$ in length, where λ_{g0} is the guided wavelength at the fundamental resonant frequency f_0. Examples on quarter-wavelength resonators are given in *Figure 2.3(c)* and *(d)*. Another typical distributed line resonator is the half-wavelength resonator, as depicted in *Figure 2.3(e)*.

The ring resonator described in *Figure 2.3(f)* is also one of the distributed line resonators, where *r* is the median radius of the ring. The fundamental resonance frequency f_0 occurs when the median circumference $2\pi r \approx \lambda_{g0}$. Ring resonator has a distinctive feature due to its symmetrical geometry, where a resonance can occur in either one of the two orthogonal coordinates. Therefore, it can support a pair of degenerate modes that have the same resonance frequency but with energy distribution in orthogonal.

Patch is a simple and compact resonator which has been extensively explored for various component designs in microwave. It can be made into different shapes such as rectangular, circular, triangular, and elliptical. *Figure 2.3(g)* and *(h)* show the typical circular and triangular patch resonators, respectively.

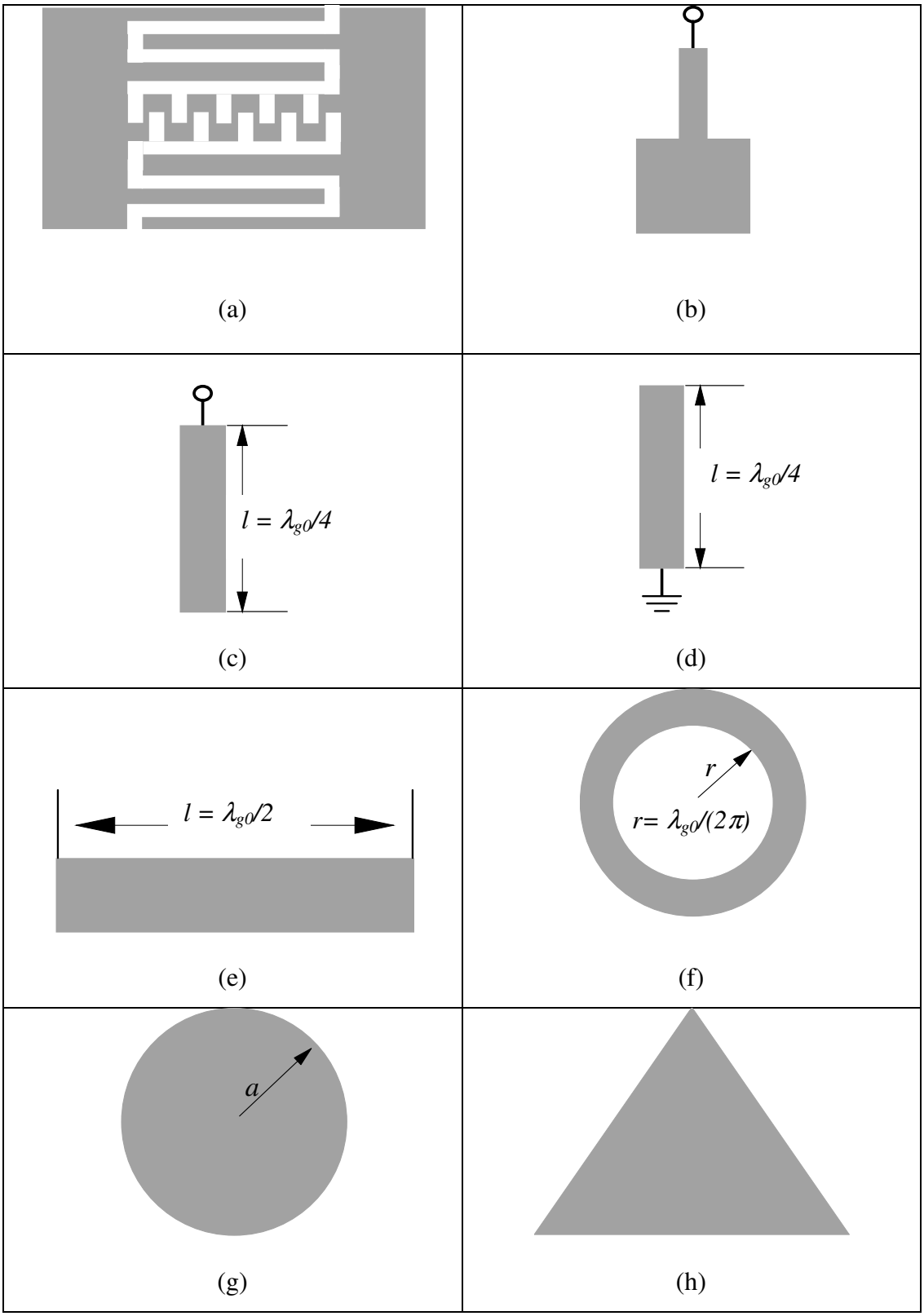

Figure 2.3: Different microstrip resonators: (a) lumped-element *L* and *C*; (b) quasi-lumped-element *LC* resonator; (c) $\lambda_{g0}/4$ line (shunt series resonance); (d) $\lambda_{g0}/4$ line (shunt parallel resonance); (e) $\lambda_{g0}/2$ line resonator; (f) ring resonator; (g) circular patch resonator; (h) triangular patch resonator.

As circular patch has been used throughout this thesis for designing different types of power dividers, it is imperial to study its characteristics here. The microstrip patch resonator can be considered as a waveguide cavity with magnetic wall on the side surface, but electric walls on the top and bottom, as shown in *Figure 2.4* (Hong, J. S. and Lancaster, M. J., 2001). With the use of the cavity model, the electric and magnetic fields inside the cavity can be described by *eqn. (2.11)* at the TM^{z}_{mn0} mode, where z is defined perpendicular to the ground plane in the cylindrical coordinate system *(r, θ, z)*. It does not have current along the dielectric edge when operating at this mode. Here, A_{nm} is the reference amplitude, J_{n} is the Bessel function of the first kind of order n, J'_{n} is the derivative of J_{n}, and K_{nm} is the m^{th} order zero of J'_{n}. For m = 1, the zeros are

$$K_{n1} = \begin{cases} 3.83171 & n = 0 \\ 1.84118 & n = 1 \\ 3.05424 & n = 2 \\ 4.20119 & n = 3 \end{cases}$$

$$E_z = A_{nm} J_n (K_{nm} r/a) \cos(n\theta) \tag{2.11a}$$

$$H_r = \frac{j}{\omega\mu}\left(\frac{1}{r}\frac{\partial E_z}{\partial \theta}\right) = -\frac{j}{\omega\mu}\frac{n}{r} A_{nm} J_n (K_{nm} r/a) \sin(n\theta) \tag{2.11b}$$

$$H_\theta = \frac{-j}{\omega\mu}\left(\frac{\partial E_z}{\partial r}\right) = -\frac{j}{\omega\mu}\frac{K_{nm}}{a} A_{nm} J_n^{'} (K_{nm} r/a) \cos(n\theta) \tag{2.11c}$$

$$E_\theta = E_r = E_z = 0 \tag{2.11d}$$

The resonance frequency of the TM^z_{mn0} mode can be calculated by

$$f_{nm0} = \frac{K_{nm}c}{2\pi a_e\sqrt{\varepsilon_r}} \tag{2.12}$$

and the effective radius a_e is given by

$$a_e = a\sqrt{1 + \frac{2h}{\pi a}\left[\ln\left(\frac{\pi a}{2h}\right) + 1.7726\right]} \tag{2.13}$$

The effective radius takes the fringing fields into account. For a simple circular microstrip patch resonator, the fundamental mode is the TM^z_{110} mode. Some of the field patterns of different *TM* modes are shown in *Figure 2.5* (Watkins, J., 1969).

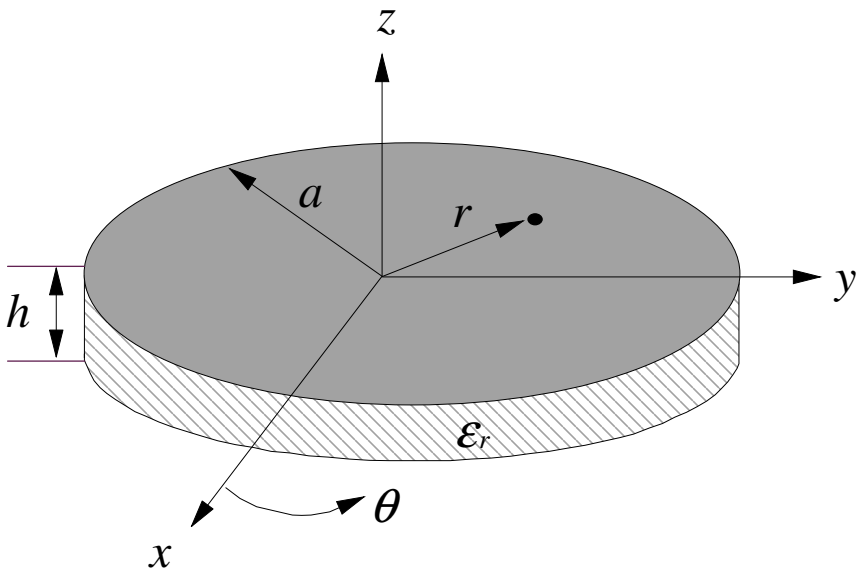

Figure 2.4: Cavity model of the circular microstrip patch resonator.

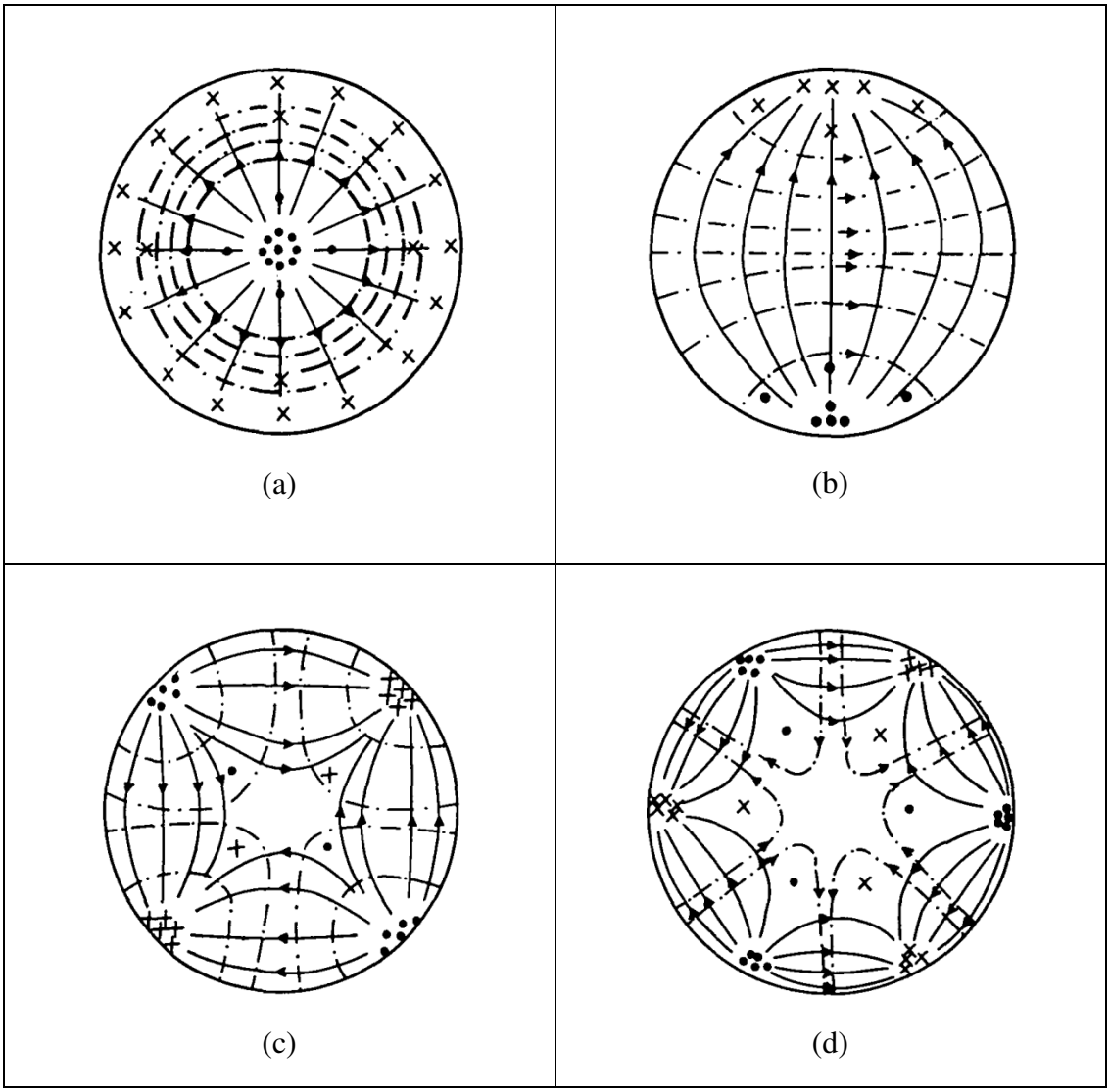

Figure 2.5: Field patterns at different transverse modes: (a) TM_{010}^{z} , (b) TM_{110}^{z} , (c) TM_{210}^{z} , (d) TM_{310}^{z} .

2.3 Transfer Function for Filters

The transfer function of a two-port filter network is a mathematical description of its system response, which relates a network output to its input source. In microwave engineering, the transmission coefficient S_{21}, depicting the power flow of a microwave signal from input to the output, is commonly used as the transfer function. For a lossless filter network, the amplitude-squared transfer function is defined as,

$$|S_{21}(j\Omega)|^2 = \frac{1}{1 + \varepsilon^2 F_n^2(\Omega)} \tag{2.14}$$

where ε describes the ripple constant, $F_n(\Omega)$ represents the filtering function, and Ω denotes the frequency variable. For the given transfer function mentioned above, its insertion loss can be computed by

$$L_A(\Omega) = 10 \log \frac{1}{|S_{21}(j\Omega)|^2} \; dB \tag{2.15}$$

For lossless condition, $|S_{11}|^2 + |S_{21}|^2 = 1$, the return loss of the filter can be defined using

$$L_R(\Omega) = 10 \log[1 - |S_{21}(j\Omega)|^2] \; dB \tag{2.16}$$

And the group delay of the network can be calculated by

$$\tau_d(\Omega) = \frac{d\Phi_{21}(\Omega)}{-d\Omega} \; seconds \tag{2.17}$$

where $\phi_{21}(\Omega)$ represents the phase response in radians, and Ω is the angular frequency in radians per second. Three types of commonly seen filter responses will be briefly discussed here. The transfer function for the Butterworth response is given by

$$|S_{21}(j\Omega)|^2 = \frac{1}{1 + \Omega^{2n}} \tag{2.18}$$

where *n* is the order of the filter. It is a lowpass filter with flat response and no ripple in the passband.

The transfer function that describes the Chebyshev response is

$$|S_{21}(j\Omega)|^2 = \frac{1}{1 + \varepsilon^2 T_n^2(\Omega)} \tag{2.19}$$

where ε represents the ripple constant, which can be computed from the ripple amplitude L_{Ar} in dB using *eqn. (2.1)*. $T_n(\Omega)$ is a Chebyshev function of the first kind of order n-th, and it is defined in *eqn. (2.22)*.

$$\varepsilon = \frac{1}{\sqrt{10^{-\frac{L_{Ar}}{10}} - 1}} \tag{2.20}$$

$$T_n(\Omega) \begin{cases} \cos(n\, cos^{-1}\, \Omega) & |\Omega| \leq 1 \\ \cosh(n\, cos^{-1}\, \Omega) & |\Omega| \leq 1 \end{cases} \tag{2.21}$$

The demand for high-performing microwave filters is ever increasing today to meet the stringent requirements of the wireless systems. One of the most sought-after performances is to have a pair of transmission zeros near to the cutoff frequencies for a better selectivity. However, the conventional Butterworth a Chebyshev filters do not provide any zeros.

With the introduction of transmission zeros, the Chebyshev response can be tailored into a better-performing one that has fast rolloff. The new transfer function has Elliptic response and defined as

$$|S_{21}(j\Omega)|^2 = \frac{1}{1 + \varepsilon^2 F_n^2(\Omega)} \tag{2.22}$$

$$\varepsilon = \frac{1}{\sqrt{10^{-\frac{L_{Ar}}{10}} - 1}} \tag{2.23}$$

$$F_n(\Omega) = cosh\left\{(n-2)cosh^{-1}(\Omega) + cosh^{-1}\left(\frac{\Omega_a\Omega - 1}{\Omega_a - \Omega}\right) + cosh^{-1}\left(\frac{\Omega_a\Omega + 1}{\Omega_a + \Omega}\right)\right\} \tag{2.24}$$

where ε is a ripple constant that can be calculated from a given return loss $L_R = 20 \log|S_{11}|$ in dB. n is the order of the filter. Ω is the frequency variable normalized to the cutoff frequency. The locations of the pair of transmission zeros are defined as $\Omega = \pm\Omega_a$ ($\Omega_a > 1$). For an elliptic bandpass filter, the angular frequency can be determined using the frequency mapping method as shown in *eqn. (2.25)*,

$$\Omega = \frac{1}{\text{FBW}} \cdot \left(\frac{\omega}{\omega_0} - \frac{\omega_0}{\omega}\right) \tag{2.25}$$

ω is the frequency variable of the bandpass filter, ω_0 is the midband frequency and FBW is the fractional bandwidth. Now, the locations of two finite-frequency attenuation poles of the bandpass filter can be found by

$$\omega_{a1} = \omega_0 \frac{-\Omega_a\text{FBW} + \sqrt{(\Omega_a\text{FBW})^2 + 4}}{2} \tag{2.26a}$$

$$\omega_{a2} = \omega_0 \frac{\Omega_a\text{FBW} + \sqrt{(\Omega_a\text{FBW})^2 + 4}}{2} \tag{2.26b}$$

$$\omega_0 = \sqrt{\omega_L \omega_H} \tag{2.26c}$$

$$FBW = \frac{Bandwidth}{Centre\ frequency} \tag{2.27}$$

Both the conventional Chebyshev and Elliptic filters have the same ripple level inside the passband. The only difference is that the former does not have any transmission zeros. *Figure 2.6* shows the typical frequency responses of the 6th-order Chebyshev and Elliptic filters. The selectivity of the Elliptic filter is much better than that for the Chebyshev because of the existence of the transmission zeros.

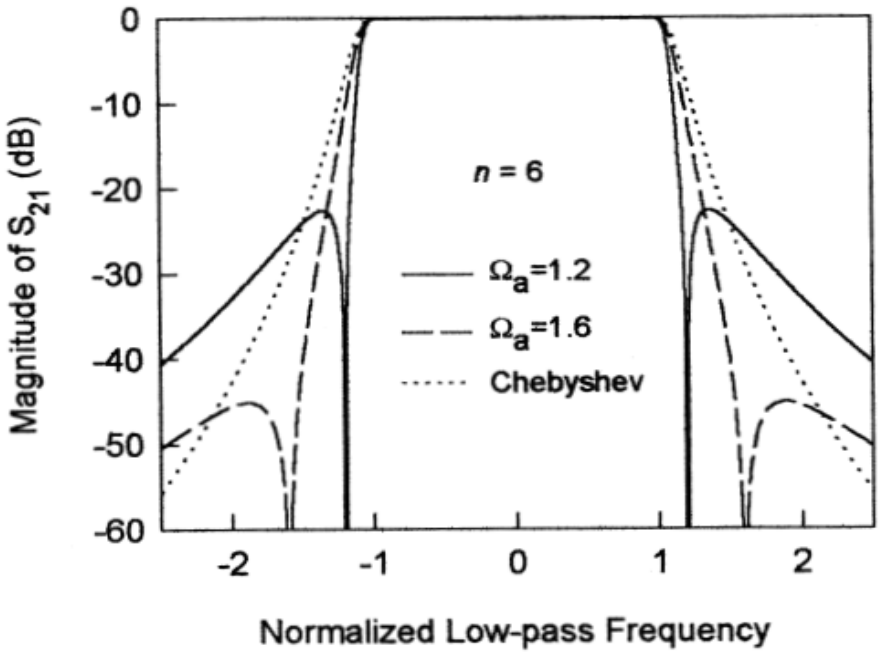

Figure 2.6: Comparison of the frequency responses of the Chebyshev and Elliptic filters. The later has pair of attenuation poles (n = 6).

2.4 Filter Synthesis

By only cross-coupling a pair of the nonadjacent resonators in a standard Chebyshev filter, the transmission zeros of the Elliptic filter can be easily realized. In (Levy, R., 1976), a synthesis method has been developed for the elliptic filters based on the lowpass prototype ones. *Figure 2.7* illustrates the lowpass prototype filter that is used for filter synthesis. Here, the rectangular boxes represent the ideal admittance inverters, each with characteristic admittance *J*.

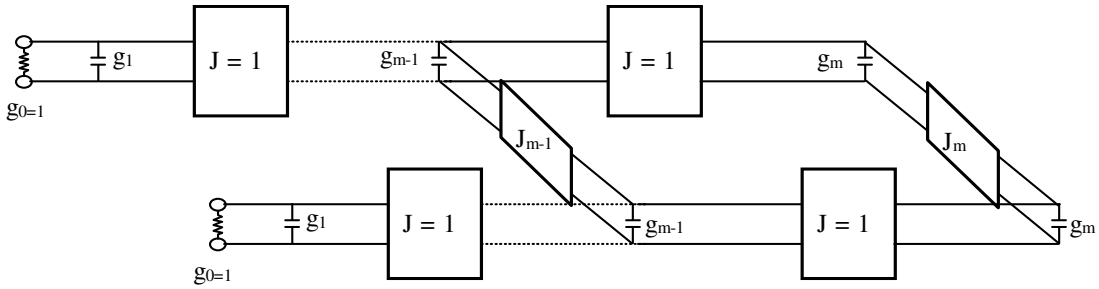

Figure 2.7: Lowpass prototype filter for the filter synthesis.

Hence, the approximate synthesis starts with the element values of the Chebyshev filters:

$$g_1 = \frac{2 \sin \frac{\pi}{2n}}{\gamma} \tag{2.28a}$$

$$g_i g_{i-1} = \frac{4 \sin \frac{(2i-1)\pi}{2n} \sin \frac{(2i-3)}{2n}}{\gamma^2 + \ sin^2 \frac{(i-1)\pi}{n}} \tag{2.28b}$$

(i = 1, 2, …..m), $m = n/2$, n = order of filter

$$\gamma = sinh\left(\frac{1}{n}\, sinh^{-1}\frac{1}{\varepsilon}\right) \tag{2.28c}$$

$$S = \left(\sqrt{1 + \varepsilon^2} + \varepsilon\right)^2 \tag{2.28d}$$

$$J_m = \frac{1}{\sqrt{S}} \qquad , \qquad J_{m-1} = 0 \tag{2.28e}$$

In order to introduce transmission zeros at $\Omega = \pm\Omega_a$, the required value of J_{m-1} is

$$J_{m-1} = \frac{-J'_m}{(\Omega_a g_m)^2 - J'^2_m} \tag{2.29}$$

$$J'_m = \frac{J_m}{1 + J_m J_{m-1}} \tag{2.30}$$

where J'_m is interpreted as the updated J_m. Both the *eqn. (2.29)* and *(2.30)* are solved iteratively with the initial values of J_m and J_{m-1} given in *eqn. (2.28)*. *Figure 2.8* illustrates the general coupling structure of the bandpass filter with a single pair of transmission zeros at two finite frequencies. It consists of the coupling coefficient and the external quality factors, which can be determined by the following formulas:

$$Q_{ei} = Q_{eo} = \frac{g_1}{FBW} \tag{2.31}$$

$$M_{i,i+1} = M_{n-i,n-i+1} = \frac{FBW}{\sqrt{g_i g_{i+1}}} \qquad , \qquad for\ i = 1\ to\ m-1 \tag{2.32}$$

$$M_{m,m+1} = \frac{FBW\ .J_m}{g_m} \tag{2.33}$$

$$M_{m-1,m+2} = \frac{FBW\ .J_{m-1}}{g_{m-1}} \tag{2.34}$$

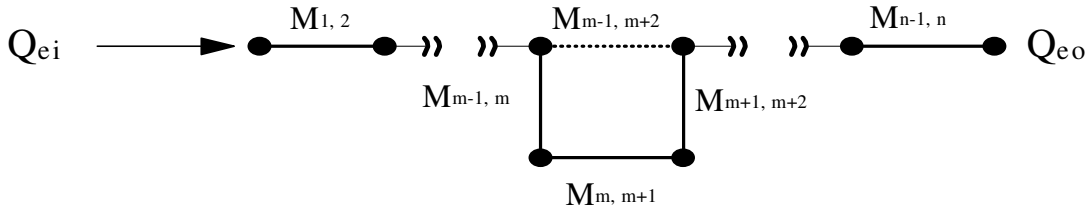

Figure 2.8: General coupling structure of the bandpass filter with a pair of finite-frequency zeros.

The general coupling matrix and scaled external quality factors can be obtained by the following formulas:

$$M_{ij} = m_{ij} FBW \tag{2.35}$$

$$Q_{e1} = \frac{q_{e1}}{FBW} \tag{2.36}$$

$$Q_{en} = \frac{q_{en}}{FBW} \tag{2.37}$$

where q_{e1} and q_{en} are the external quality factors and m_{ij} denotes the normalized coupling coefficient. Since in most cases, bandpass filters are symmetrical, thus they will have symmetrical set of couplings ($M_{12} = M_{n-1,n}$, $M_{23} = M_{n-2,n-1}$) and external quality factors ($Q_{e1} = Q_{en}$). The structure of the general coupling matrix of the second-order bandpass filter can be written as

$$[m] = \begin{bmatrix} 0 & m_{12} \\ m_{12} & 0 \end{bmatrix} \qquad n = 2 \tag{2.38}$$

and the scaled external quality factors are $q_{e1} = q_{en}$.

The calculated values of design parameters, general coupling matrix, and scaled external quality factors of the proposed bandpassing power dividers will be comprehensively discussed in **Section 3.2.1** and **3.3.1**.

CHAPTER 3

Double-layered Bandpassing Power Dividers

3.1 Introduction

In this chapter, two double-layered bandpassing power dividers are proposed and investigated. Both of them are designed on a circular microstrip resonator to provide 3 dB (named as 'BPD-A') and 4.8 dB (named as 'BPD-B') power division. The circular patch, with etched-away slots and sectors, is utilized as the resonator for both of the proposed designs. It will be shown that the etched slots are able to perturb the energy distribution on the resonator so that additional modes can be introduced. Both the BPD-A and BPD-B power dividers have double resonances, which are very desirable for wideband performance.

Next, sectorial notches are cut around the circular edge of the patch for the purpose of improving impedance matching. The inclusion of the notches causes the Q-factor of the resonator to reduce; as a result, the bandwidth of the power divider is increased. In order to cut off unwanted signals in a wireless system, transmission zeros are usually introduced into the microwave components to improve the selectivity. In my work, a double–layered structure has been employed to provide tight coupling where two zeros are obtainable.

In this project, high frequency simulation software, Ansoft HFSS (Ansoft Corporation, HFSS), was used throughout the design process for simulation, optimization, and troubleshooting. Measurements were done by utilizing the R&S®ZVB8 Vector Network Analyzer (VNA). Both the proposed designs are fabricated on the Duroid RO4003C substrate with a dielectric constant of ε_r = 3.38, tan δ = 0.0027, and a thickness of h = 1.524 mm. In this chapter, the configurations, results, discussions, and parametric analysis of the proposed power dividers BPD-A and BPD-B will be discussed in **Section 3.2** and **Section 3.3**, respectively.

3.2 3 dB Double-layered Bandpass Power Divider (BPD-A)

3.2.1 Configuration

Figure 3.1 shows the schematic of the proposed BPD-A. With reference to the figure, it consists of a circular patch resonator (bottom patch) that is sandwiched in between *Substrate 1* and *Substrate 2*. The resonator is excited by an input coaxial feed (*Port 1*) connected to the center of the patch. As can be seen in the figure, an additional circular patch (top patch) is directly made on *Substrate 2* to couple the electromagnetic signal out to the two output ports (*Port 2* and *Port 3*). Both the patches share the common ground on the bottom-most surface and they must be properly aligned for a maximum coupling. In order to demonstrate the idea, the resonator was designed to operate at 6 GHz; of course it can be designed in any other frequencies.

Figure 3.1(a) shows the bottom patch which is placed on *Substrate 1*. The resonator (with radius of R_a = 15mm) consists of a pair of arc-shape slots and two pairs of sectorial notches. Each of the two arc-shape slots has an arc length of c = 8.2 mm and a width of d = 0.5 mm. Two pairs of notches, which are cut symmetrically along the arc, have the dimensions of a = 5 mm, θ_a = 64.6˚, b = 10.5 mm, and θ_b = 38.6˚, shown in *Figure 3.1(a)*.

The dimension of the patch that is made on *Substrate 2* is shown in *Figure 3.1(b)*. It consists of two identical metallic radial sectors with R_b = 15 mm and θ_t = 90˚. It is interesting to note that the two radial sections with a length of almost half a wavelength are also functioning as an embedded impedance transformer. To further improve the impedance matching, a small circular patch (R_c = 1 mm) is centrally intersected with the top patch. The microwave signal is then guided to the two 50-Ω microstrip lines at the output ports (*Port 2* and *Port 3*). *Figure 3.2* is the photograph of the fabricated prototype.

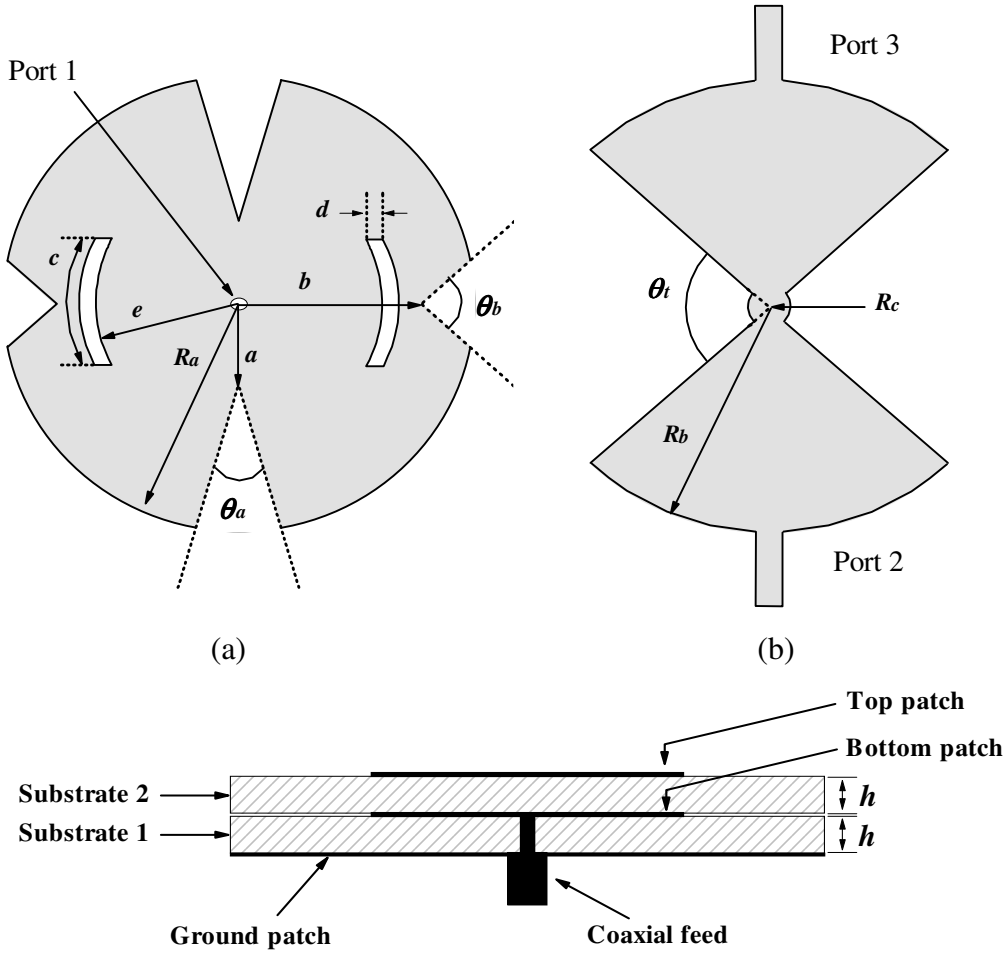

Figure 3.1: Schematic of the proposed BPD-A, (a) Bottom patch, (b) Top patch, (c) Side view.

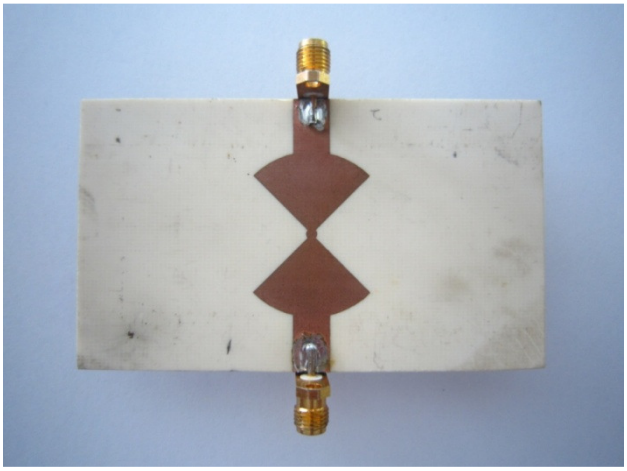

Figure 3.2: Prototype of the proposed BPD-A.

3.2.2 Synthesis Analysis

Synthesis formulas that have been discussed in **Section 2.3** (Elliptic Response) will be applied in this section. MATLAB is used to generate the frequency responses. Target specifications are then set for the calculation of the S parameters. To begin, the synthesis process of the BPD-A is conducted, with the targets defined as follows:

Return Loss (L_R):	-15 dB
Fractional bandwidth (FBW):	15%
Frequency of transmission zero (Ω_a):	2.1
Center frequency (ω_0):	6

As illustrated in *Figure 3.3*, the frequency response of the synthesized transfer function is compared with that of the HFSS simulation. In general, good agreement has been observed in between the synthesized and simulated data. Minor discrepancy is observed as losses are not accounted for the synthesis. However, in the practical filter design process, the required frequency response of a filter is usually synthesized to obtain the transfer function and the equivalent circuit. Suitable resonators are then incorporated for the implementation of the circuit (Hong, J. S. and Lancaster, M. J., 2001). Since it has a second-order filter response, the synthesis order is defined to be $n = 2$. Next, the element values are calculated in *eqn. (3.1)*.

$$g_1 = \frac{2\sin\frac{\pi}{2n}}{\gamma} = \mathbf{0.9301} \qquad (3.1a)$$

$$\gamma = sinh\left(\frac{1}{n}\, sinh^{-1}\frac{1}{\varepsilon}\right) = \mathbf{1.5204} \qquad (3.1b)$$

$$\varepsilon = \frac{1}{\sqrt{10^{-\frac{L_R}{10}} - 1}} = \mathbf{0.1807}, \text{with } L_R = -15 \text{ dB} \qquad (3.1c)$$

$$S = \left(\sqrt{1 + \varepsilon^2} + \varepsilon\right)^2 = \mathbf{1.4326} \qquad (3.1d)$$

$$J_1 = \frac{1}{\sqrt{S}} = \mathbf{0.8355} \qquad (3.1f)$$

$$J_0 = \frac{-J_1}{(\Omega_a g_1)^2 - J_1^2} = -\mathbf{0.4636} \qquad (3.1g)$$

With all the element values defined in *eqn. (3.1)*, the general coupling matrix and scaled external quality factors can be easily obtained.

$$[m] = \begin{bmatrix} 0 & 0.8983 \\ 0.8983 & 0 \end{bmatrix}$$

$$q_{e1} = q_{en} = 0.9301$$

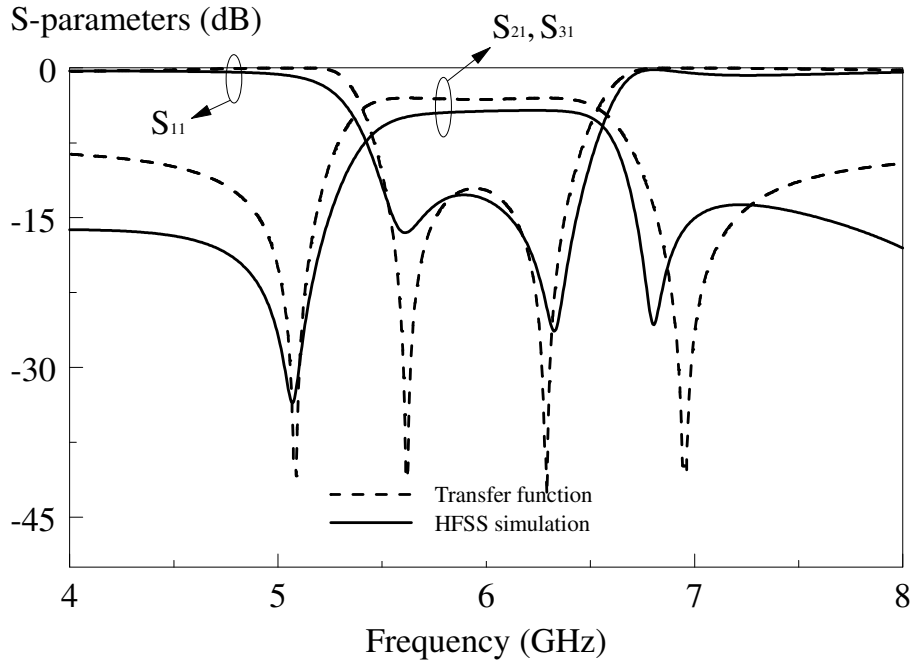

Figure 3.3: Comparison of frequency response of the transfer function for BPD-A. Also given is that generated by HFSS simulation.

3.2.3 Simulation and Experiment Results

The proposed BPD-A was simulated using the Ansoft HFSS software, whereas the fabricated prototype were measured using the R&S®ZVB8 Vector Network Analyzer (VNA). In experiment, all of the unused ports were terminated by the 50-Ω loads.

Figure 3.4(a) depicts the simulated and measured return losses and transmission coefficients. The measured and simulated center frequencies are 5.85 and 6.03 GHz, respectively, with an error of 2.98%. With reference to the same figure, the bandwidths are 12.49% and 15.25%, as can be seen in the simulation and measurement. In general, the measured result agrees well to the simulation. The slight discrepancy can be caused by various tolerances in experiment. As it involves double layers, minor misalignment is inevitable although care has been taken for. In the measurement process, marking is also made on both the substrates for a better alignment.

As can be seen from *Figure 3.4(a)*, the measured insertion loss is slightly lower than for the simulation. This is because simulation does not account for the losses caused by the SMA connectors and cables. As each SMA connector has contributed a loss of around 0.15-0.2 dB, the measured result is in reasonable agreement with the simulated one. Additional loss can be introduced by the conductive and dielectric losses of the metallic patch and substrate layers.

With reference to the same figure, the measured transmission zeros (Z_1 and Z_2), located at 4.90 at the lower and 6.62 GHz at the higher cut-off frequencies, are caused by the tight coupling of the double-layered structure. Two resonance modes (P_1 & P_2) can be clearly seen inside the passband. This makes the proposed BPD-A power divider to have two modes, along with high selectivity. *Figure 3.4(b)* gives the simulated and measured coupling of the two output ports, showing good agreement.

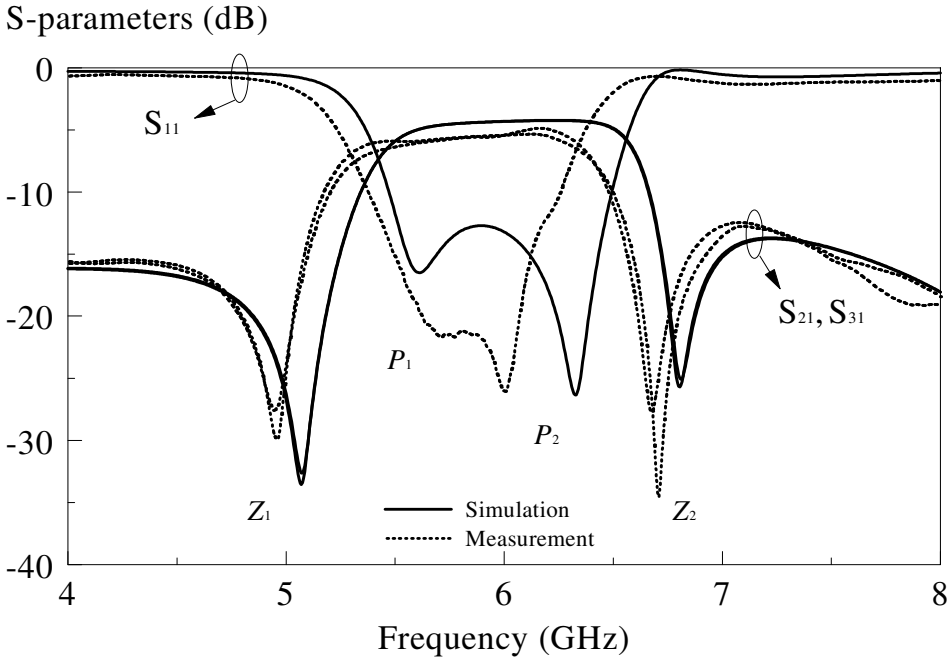

(a)

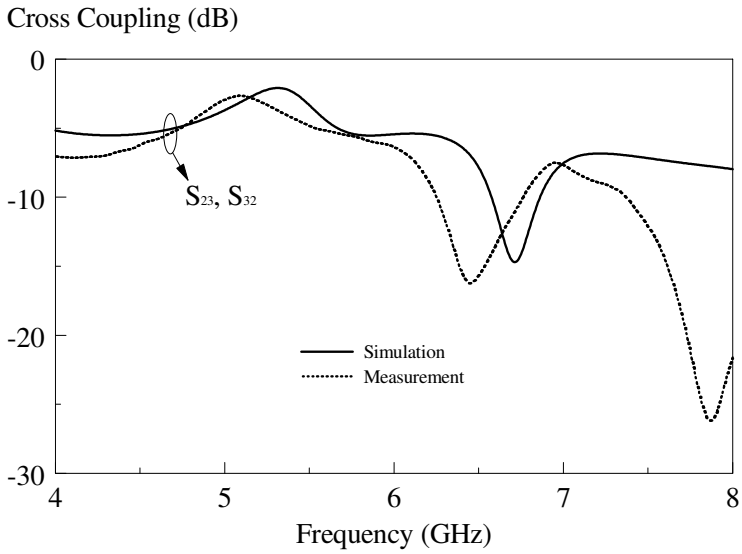

(b)

Figure 3.4: Simulated and measured (a) return and insertion losses and (b) isolation of the output ports of the proposed BPD-A.

Figure 3.5 shows the simulated and measured group delays of the proposed BPD-A. Both of them are almost constant inside the passband. This result is very positive as it shows that the proposed power divider does not cause any distortion to the input signal even if the frequency bandwidth is very broad.

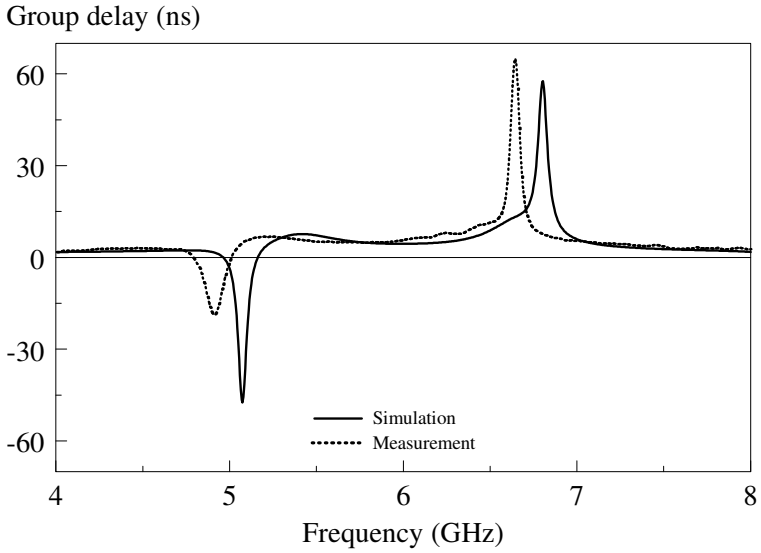

Figure 3.5: Simulated and measured group delays of the proposed BPD-A.

3.2.4 Theoretical and Parametric Studies

It is very important to understand the properties of the circular patch resonator since all the proposed power dividers are made on it. To further study its characteristics, a simple simulation model is constructed. In this case, a circular microstrip resonator, with a radius of 15 mm (with substrate thickness of h = 1.524 mm and dielectric constant of ε_r = 3.38), is centrally fed by a coaxial probe. This radius was also used by all our designs. A ground plane (not shown) is also made on the reverse surface of the substrate. The simulated return loss of this single-port resonator is shown in *Figure 3.6*. As can be seen, a resonance is found at 6.4GHz. The electric and magnetic fields of this mode are further illustrated in *Figure 3.7*. With reference to them, this resonance is indeed the transverse TM^{z}_{010} mode of the circular patch resonator, and the resonant frequency can be calculated using *eqn. (2.12)* in **Chapter 2**.

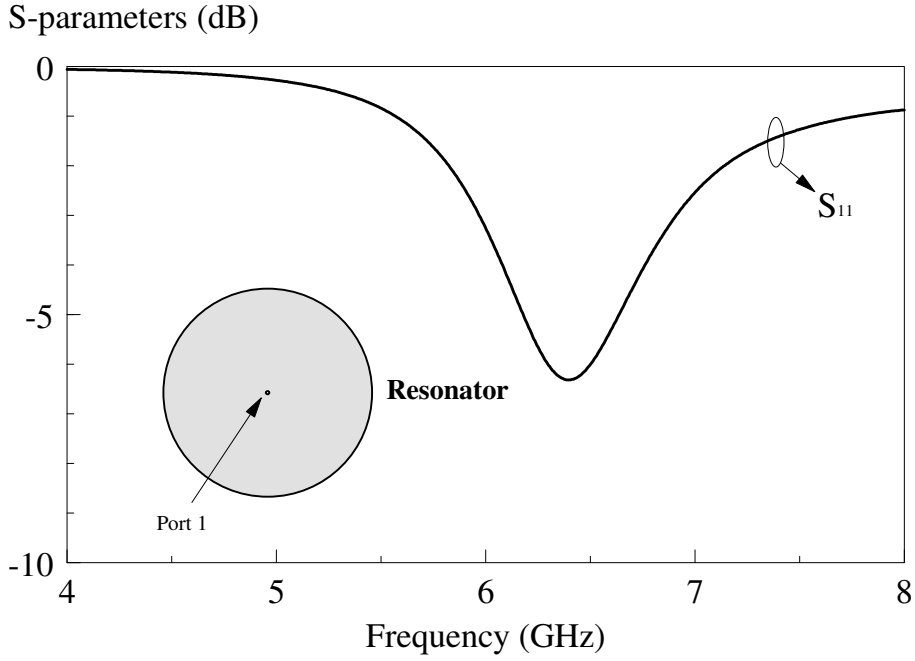

Figure 3.6: Simulated return loss of the simple circular patch resonator.

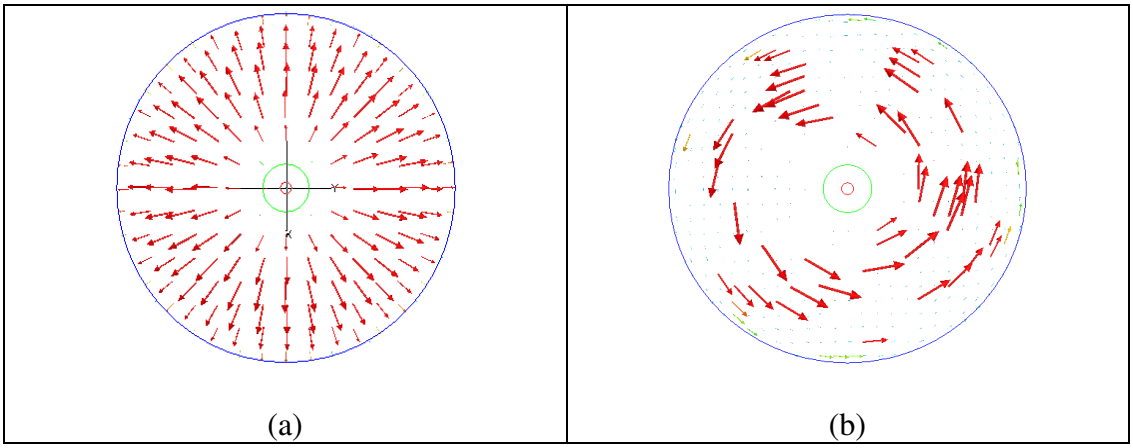

Figure 3.7: (a) Electric and (b) magnetic fields of the simple circular patch resonator.

The proposed power dividers in this thesis are developed based on the aforementioned circular microstrip patch resonator. In order to have a wider bandwidth and higher selectivity, the configuration of the proposed power dividers is made multilayer with some slot cuts for exciting more resonances so that additional poles and zeros can be obtained. To do that, two arc-shape slots, which are positioned at 180˚ against each other, are etched on the patch, as shown in *Figure 3.8*. The purpose of introducing slots is to perturb the current distribution on the circular patch resonator. It is first done on the single-layered simple patch (*Figure 3.7*) for the ease of analysis. The simulated return loss is shown of *Figure 3.8*. Here, it is obvious that the introduction of such slots makes the resonator to have two resonances. This is good for achieving broadband performance. A deeper physical insight can be gained by exploring the electric field distribution of the first (4.985 GHz) and second (6.095 GHz) modes of the single-layered patch resonator, as depicted in *Figure 3.9(a)* and *(b)*, respectively. Based on the field distributions, the former is found to be the transverse TM^{z}_{210} mode and the latter is the original TM^{z}_{010} patch resonance. The resonant frequency and patch radius can be calculated by *eqns. (2.12) and (2.13)*.

Also clear is that the introduction of the slots enables the excitation of the TM^{z}_{210} mode. Similar techniques were also used in (Tan, B. T. *et al.*, 2002; Vargas, S. R. *et al.*, 2007; Li, J. L. *et al.*, 2010; Serrano, A. L. and Correra, F. S., 2009; Serrano, A. L. *et al.*, 2010; Serrano, A. L. *et al.*, 2010; Abunjaileh, A. I. *et al.*, 2007; Singh, Y. K. and Chakrabarty, A., 2008) for perturbing multiple modes. In addition to that, open-circuited stubs were also used by Eriksson *et al*. (Eriksson, A. *et al.*, 2002) for the excitation of the degenerate modes.

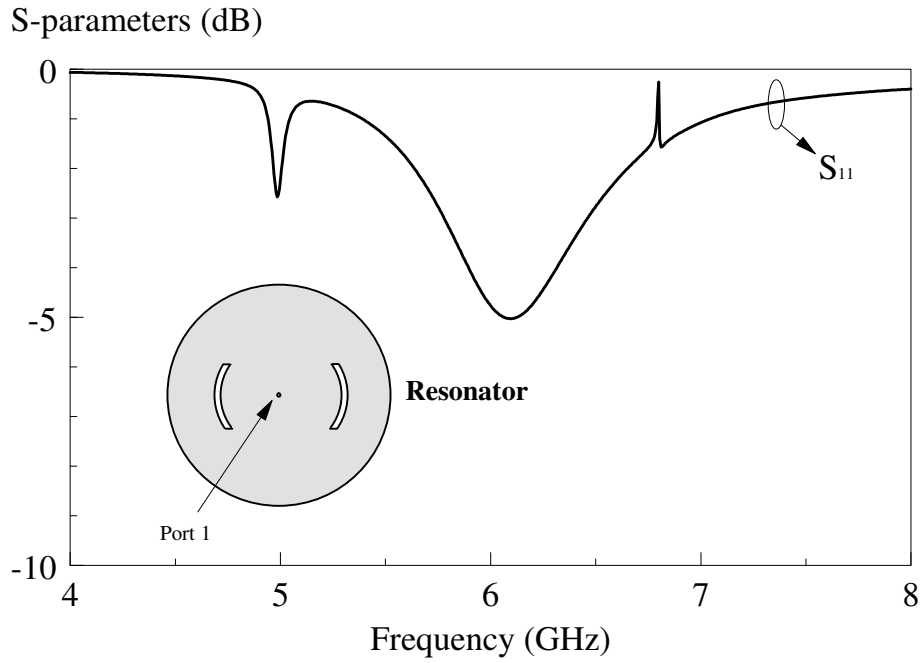

Figure 3.8: Simulated return loss of the circular patch resonator with slot *c*.

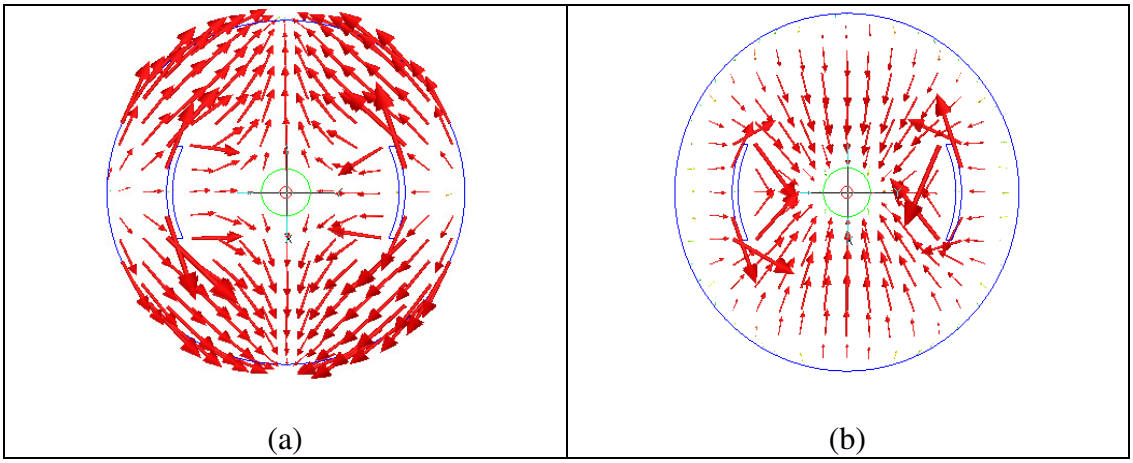

Figure 3.9: Electric fields of the (a) first and (b) second mode of the simple circular patch resonator with slots.

Then a top metallic layer is directly stacked onto the circular patch resonator that is etched with the arc-shaped slots (*Figure 3.9*). The top-down views of the patches are shown in *Figure 3.10* along with the simulated S parameters. Referring to the same figure, poor impedance matching has been observed. To overcome this issue, two sectors are etched on the top metallic layer and a small circular patch is placed in the middle to connect the two sectorial output patches, as shown in *Figure 3.11*. This configuration is very close to that of the proposed multilayered power divider in *Figure 3.1*, except without having any notches. From *Figure 3.11*, two poles at 5.7 and 6.0 GHz as well as two zeros at 4.96 and 6.71 GHz can be clearly identified, which approximate those (*Figure 3.4*) of the final structure (with notches).

As can be seen from *Figure 3.11*, although wideband signature is imminent, it requires further improvement on the impedance matching. To do so, two pairs of notches are then etched on the circular patch resonator so that its input impedance can match with the 50-Ω feedlines (Dey, S. *et al.*, 1993). Also depicted in *Figure*

3.12 are the simulated S parameters. Now, this configuration that comes with slots, sectors, small circular patch and notches forms the proposed multilayered power divider in *Figure 3.1*.

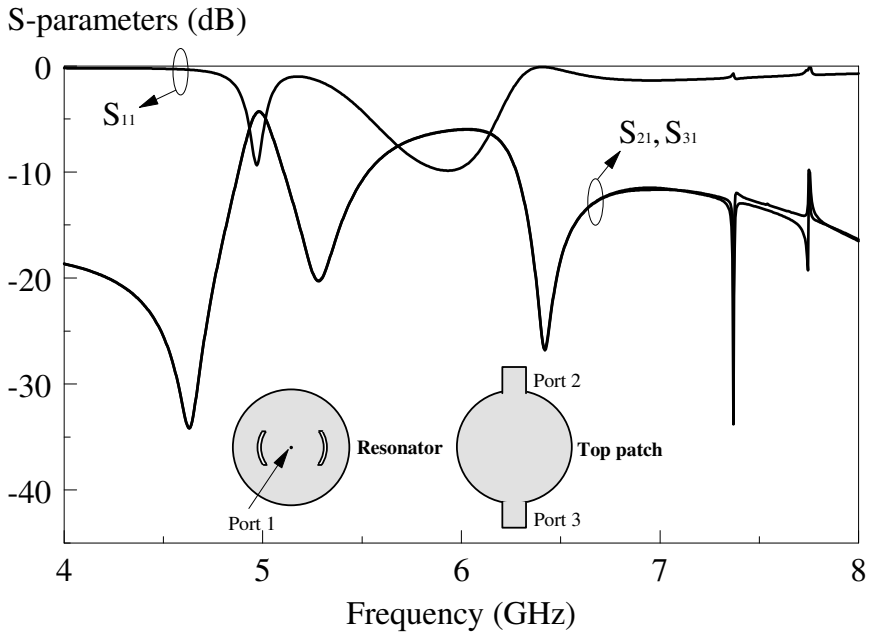

Figure 3.10: The simulated S parameters of the double-layered power divider without any notches.

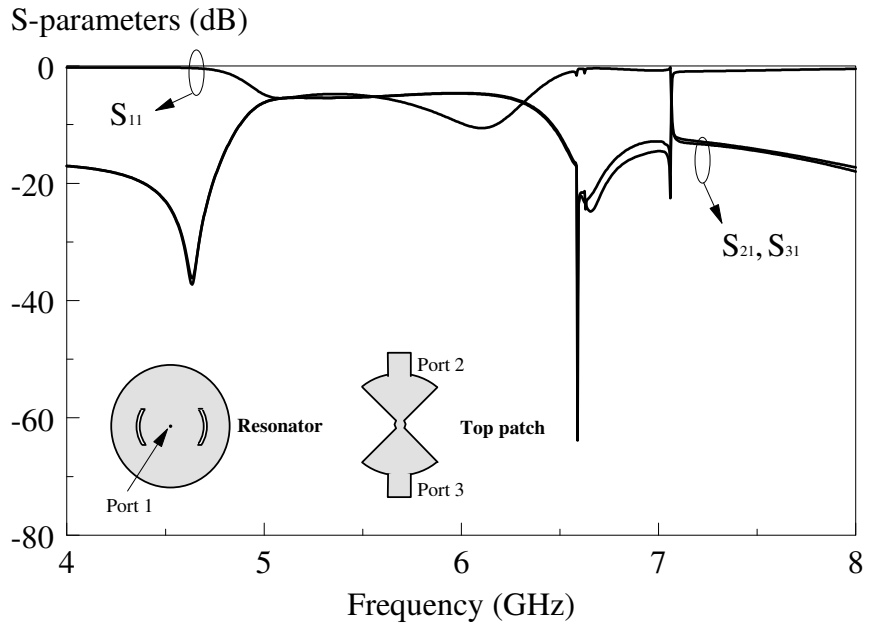

Figure 3.11: The simulated S parameters of the double-layered power divider (with top patch etched but no notch on the bottom resonator).

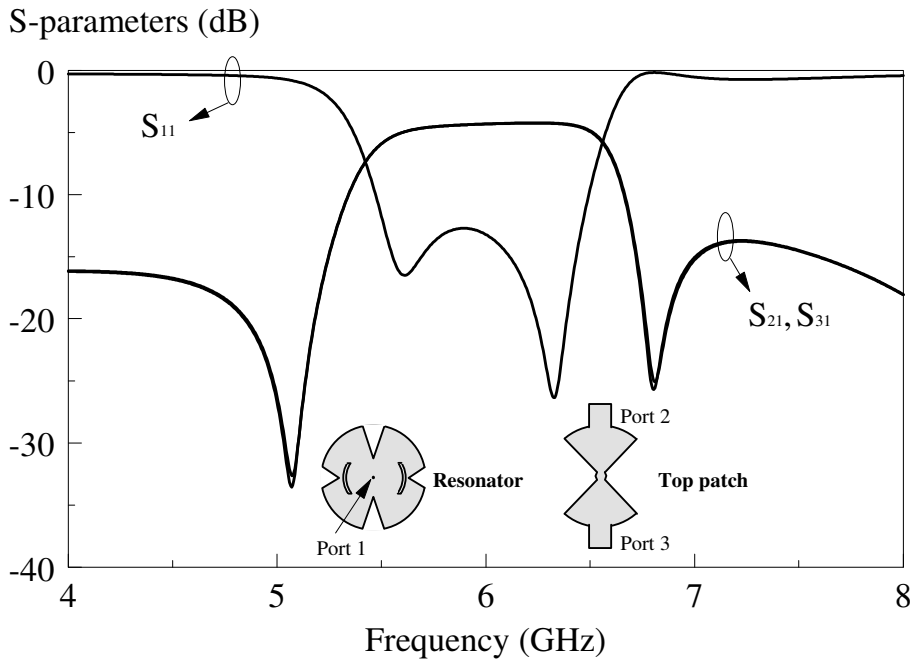

Figure 3.12: The simulated S parameters of the proposed double-layered power divider.

Along with the discussion, some of the crucial design parameters are studied here. Parametric analysis is important for understanding the physical effects. They are very useful for optimization and tuning. As the model was already verified by experiment in the previous sections, the analysis here will be done by simulation. Important design parameters such as R_c, c, θ_b, and θ_a are studied. They can significantly affect the resonances that generate the zeroes (Z_1 and Z_2) and poles (P_1 and P_2) of the proposed power dividers.

3.2.4.1 Slot *c*

To understand the effect of this parameter on the proposed configuration (*Figure 3.1*), the length of slot *c* is varied from 7.2 till 9.2 mm and the effect is studied. From *Figure 3.13*, it can be seen that both the P_1 and Z_1 frequencies become lower as the length of slot *c* is increased. This is because the current path on the resonator travels farther for the longer slots. In this case, the passband can be slightly tuned by adjusting the arc length.

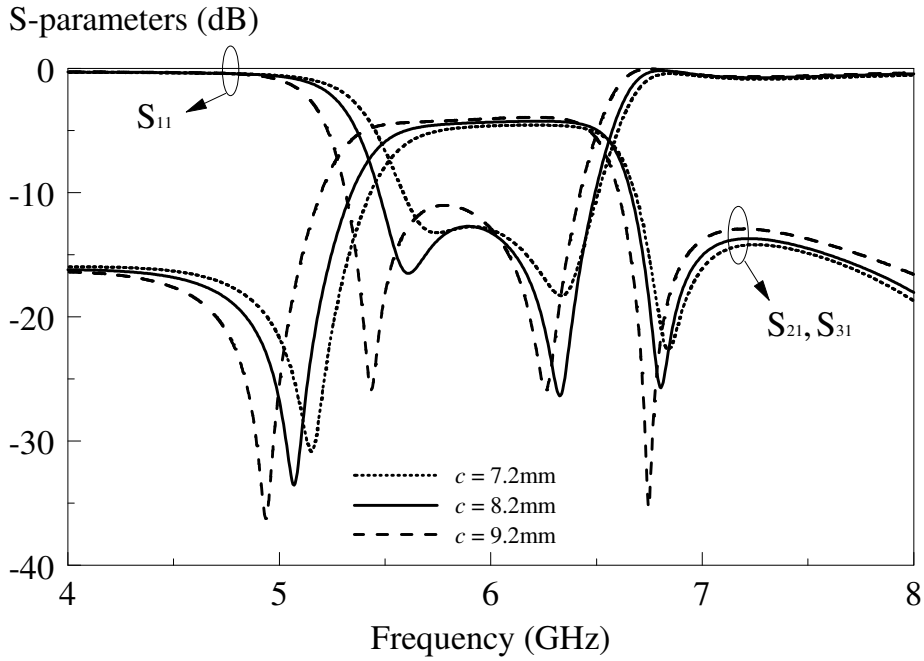

Figure 3.13: Effect of the length of slot c on the S parameters.

3.2.4.2 Notches θ_a and θ_b

The effects of the notch angles θ_a and θ_b are studied next. *Figure 3.14* shows the S parameters of removing either the shallow or the deep notches. The former are removed from the power divider (*Figure 3.1*) so that the effect of θ_a can be visualized. Also shown in the same figure is the result for that with θ_a removed. It is very interesting to note that the positions of the zeros can be easily adjusted by changing the two notch angles. This is crucial for tuning and optimizing the selectivity of the component.

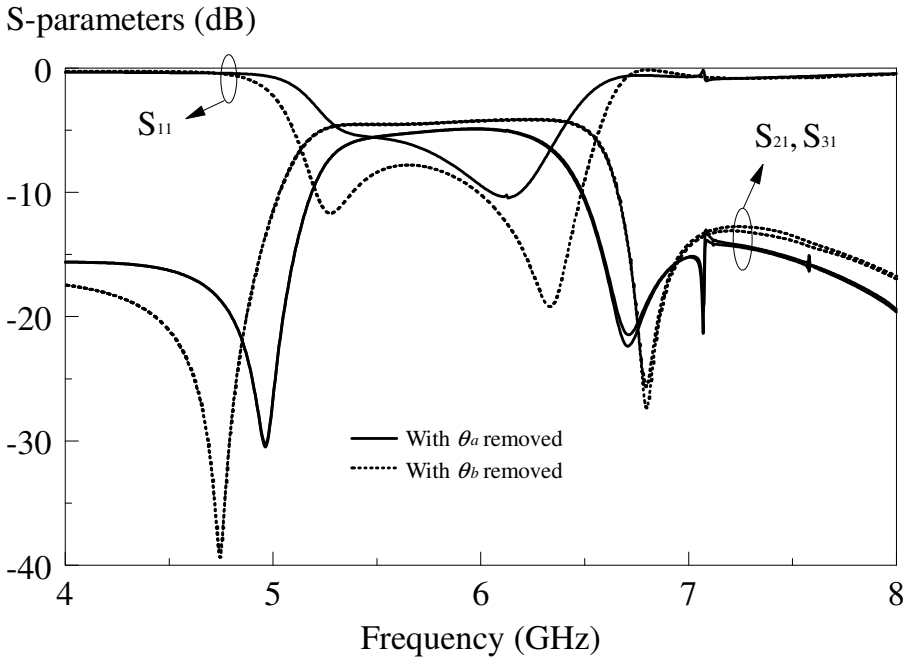

Figure 3.14: The proposed power divider with either θ_a or θ_b removed.

Next, the effect is studied by including both the notches to form the circuit configuration in *Figure 3.1*, which has the frequency response in *Figure 3.2*. For this case, the electric field distributions of the two zeros are depicted in *Figure 3.15*.

It can be seen that two resonances, with orthogonal electric fields, are excited on the bottom patch resonator. Nevertheless, no field energy is able to reach the output ports as the top patch does not get resonated at both.

Here, the effect of θ_b (with $\theta_a = 38.6^\circ$ as in *Figure 3.1*) is explored. By reducing this angle, it can be seen from *Figure 3.16* that the transmission zero Z_1 moves to lower frequencies. This is due to the shorter current path for a smaller θ_b value. The total perimeter of the bottom circular patch resonator is calculated according to θ_b and tabulated in *Table 3.1*. It increases with the decrease of θ_b.

Table 3.1: The perimeter of the circular patch resonator with respect to θ_b. The corresponding zeros frequencies are also appended.

Angle of shallow notches, θ_b (deg)	**Total perimeter (mm)**	**Position of zeros (GHz)**	
		Z_1	**Z_2**
30.0	135.00	4.85	6.80
64.6	130.68	5.08	6.80
90.0	127.74	5.31	6.80

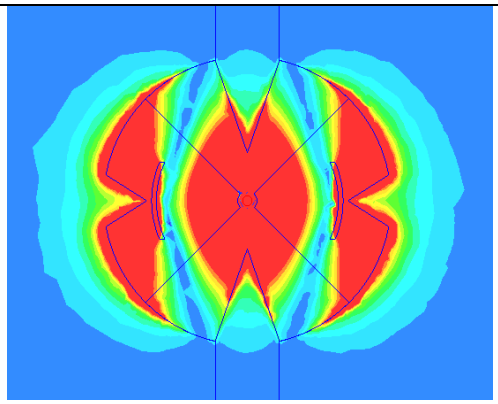

(a)

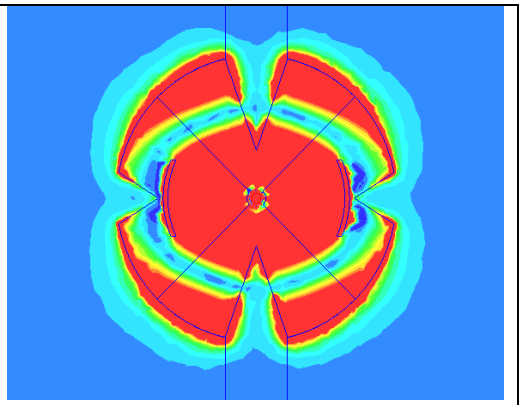

(b)

Figure 3.15: Electric field distributions (a) the first zero Z_1 at 5.08 GHz and (b) the second zero Z_2 at 6.80 GHz.

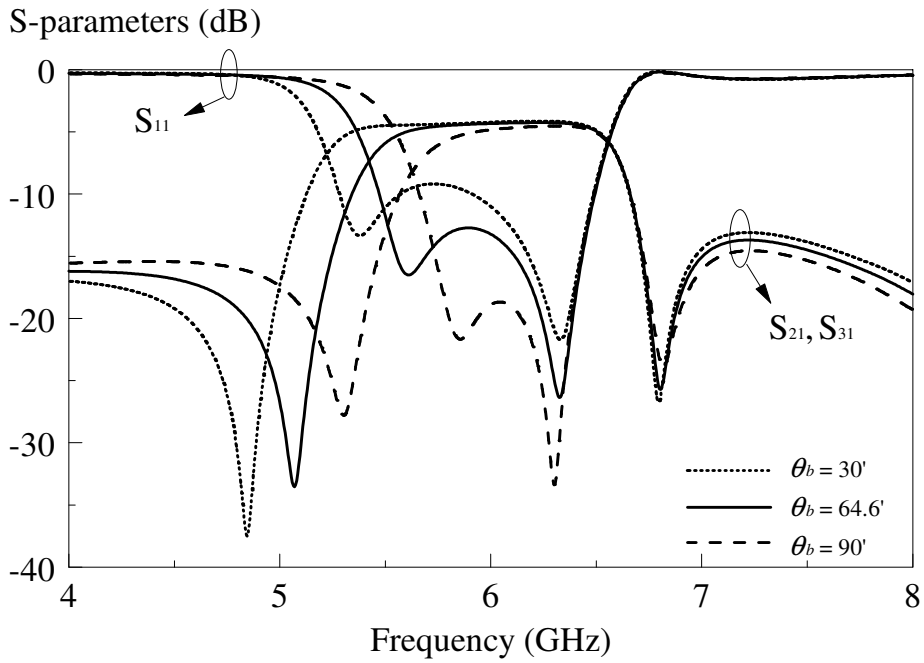

Figure 3.16: Effect of the shallow notch angle θ_b on the S parameters.

Figure 3.17 shows the effect of the deep notch θ_a on the S parameters. It is demonstrated for the lower and upper bounds of 30˚ and 60˚, respectively. Obviously, the second pole P_2 can be shifted up with the increase of θ_a. Again, this is mainly caused by the increment of perimeter. With reference to *Table 3.2*, as θ_a increases, the perimeter of the circular patch resonator reduces.

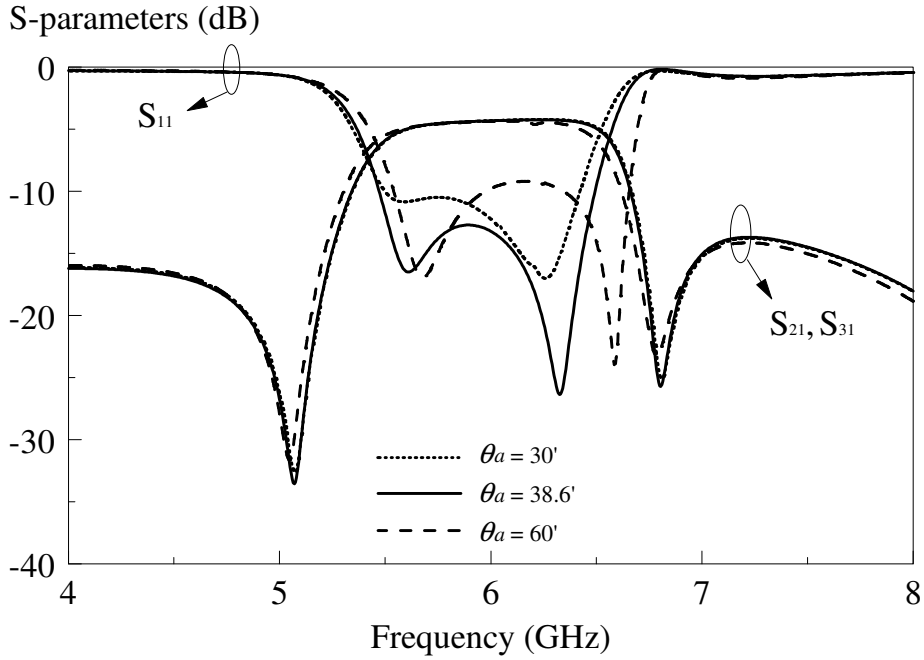

Figure 3.17: Effect of the deep notch θ_a on the S parameters.

Table 3.2: Perimeter of the circular patch resonator with respect to θ_a. The corresponding pole frequencies are also appended.

Angle of deep notches, θ_a (deg)	**Total perimeter (mm)**	**Position of poles (GHz)**	
		P_1	P_2
30.0	133.32	5.57	6.26
38.6	130.68	5.61	6.33
60.0	122.11	5.68	6.60

3.2.4.3 Small Circular Patch R_c

Figure 3.18 shows the effect of the radius of the small circular patch R_c on the frequency response when it is varied from 1 to 3 mm. It can be clearly seen that Z_2 moves lower when R_c increases. But, smaller patch radius is better for the impedance matching of the second pole. The fractional bandwidth ($|S_{11}| < -10$ dB) deteriorates as R_c goes higher. So, it is imperative to keep this radius small, say below 3 mm.

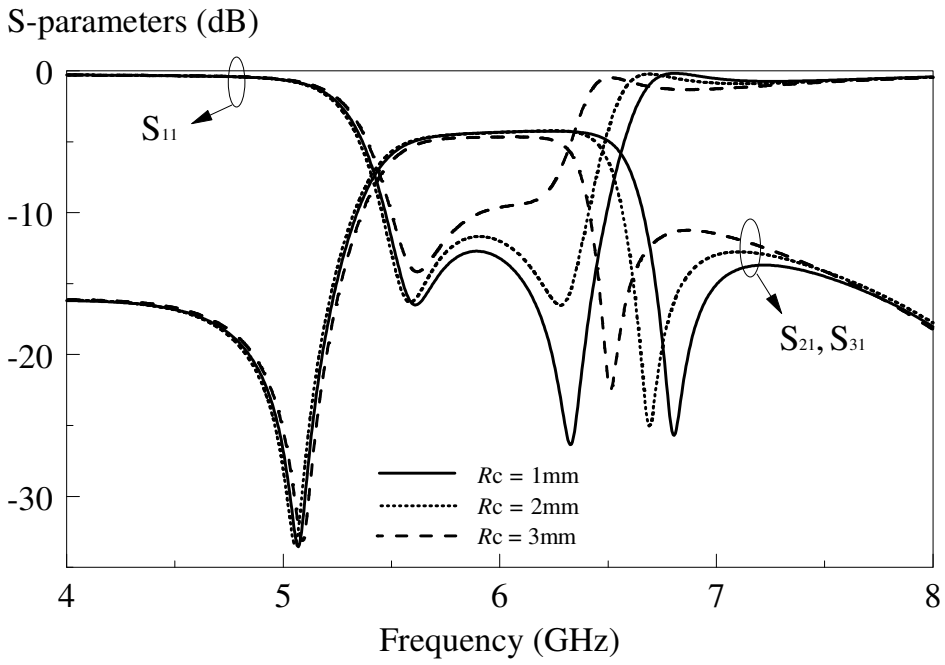

Figure 3.18: Effect of the radius of R_c on the S parameters.

3.3 4.8 dB Double-layered Bandpass Power Divider (BPD-B)

3.3.1 Configuration

The schematic of the proposed BPD-B is illustrated in *Figure 3.19*. It is a 4.8 dB power divider which has similar design to BPD-A. Again, both the resonator and output patch are sharing the same ground plane. In order to demonstrate the idea, the circular patch resonator is design to operate at 6 GHz with a radius of R_a = 15 mm. It is placed on top of *substrate 1* and excited by a coaxial-feed port (*Port 1*). For this configuration, of course, it has three arc slots (with arc width d = 0.5 mm and length c = 6.2 mm), along with two sets of notches (θ_a and θ_b), which are 120° apart from each other among themselves. Each of the slots is formed by a sectorial slit centering at the origin (with e = 9.5 mm) of the resonator. The dimensions of the notches are given by θ_a = 8.2°, θ_b = 14.3°, a = 8 mm and b = 11 mm. With reference to *Figure 3.19(b)*, three sectorial metallic patches (R_b = 15 mm and θ_t = 93.7°), made on *substrate 2*, are used to couple the signals to the output ports. A small circular patch with radius of R_c = 5 mm is placed at center of the output patch for improving the impedance matching as well as optimizing the zero position. *Figure 3.20* is the photograph of the fabricated prototype.

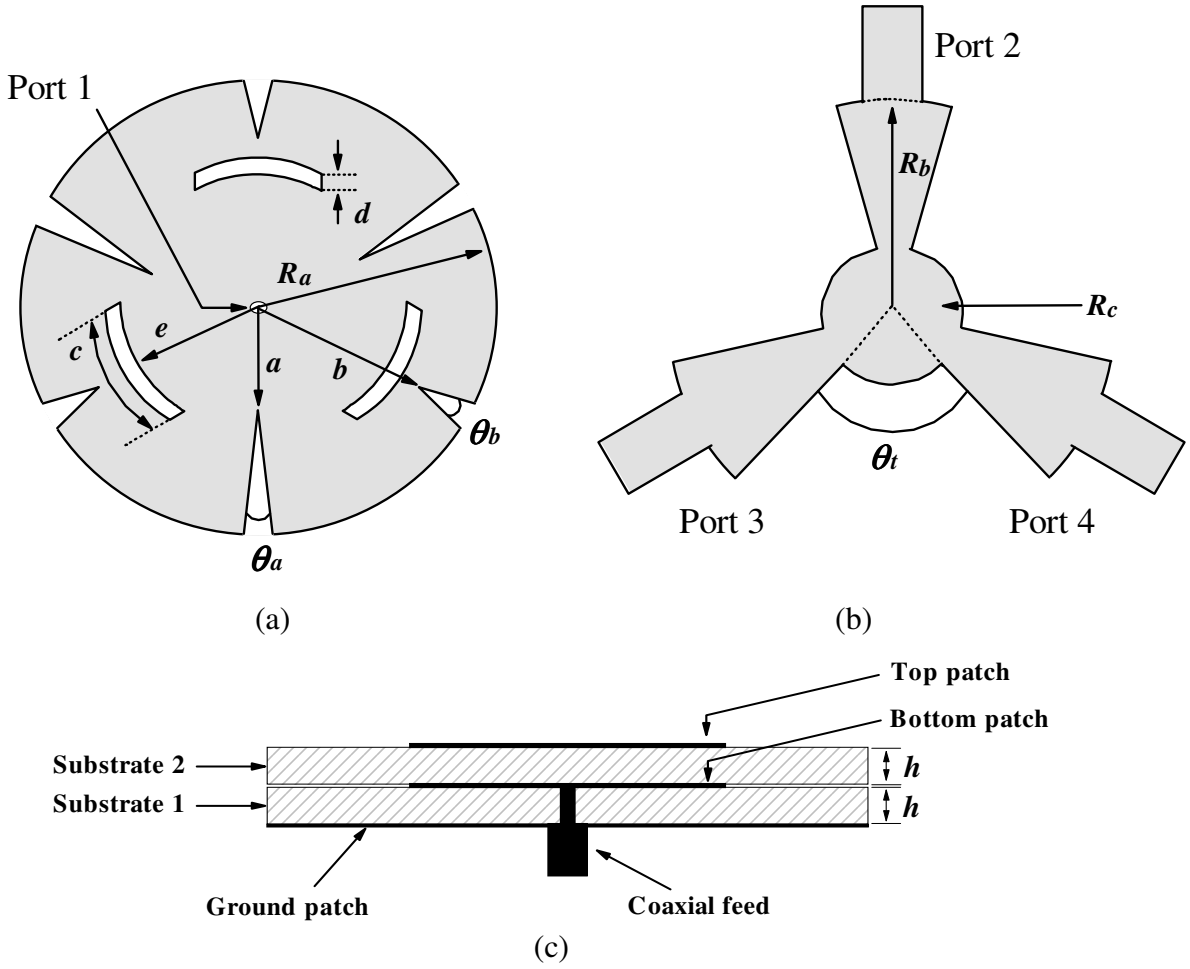

Figure 3.19: Schematic of the proposed BPD-B (a) Circular patch resonator, (b) Output patch, (c) Side view.

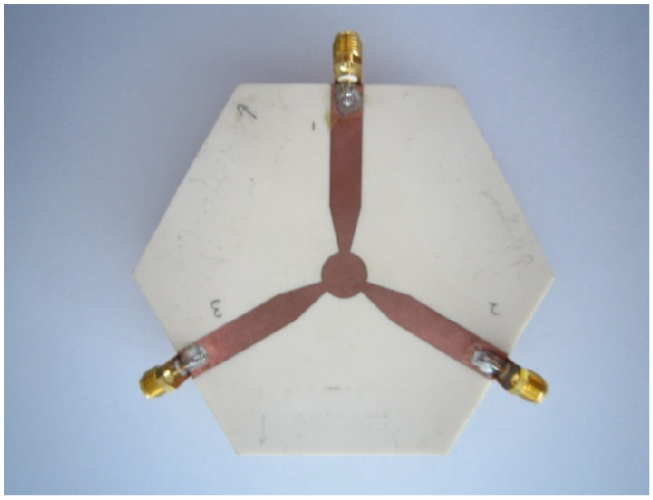

Figure 3.20: Prototype of the proposed BPD-B.

3.3.2 Synthesis Analysis

The same synthesis procedure will be employed to meet the following targets:

Return loss (L_R):	-20 dB
Fractional bandwidth (FBW):	10%
Frequency location of transmission zero (Ω_a):	3.8
Center frequency (ω_0):	6

The frequency responses of the transfer function (Elliptic response), as well as the simulation, are illustrated in *Figure 3.21*. The element values are calculated and shown as below. ($n = 2$, $m = n/2$)

$$g_1 = \mathbf{0.6667}$$
$$\gamma = \mathbf{2.1213}$$
$$\varepsilon = \mathbf{0.1005}, \quad \text{with } L_R = -20 \text{ dB}$$
$$S = \mathbf{1.2222}$$
$$J_1 = \mathbf{0.9045}$$
$$J_0 = \mathbf{-0.7921}$$

With all these element values, the general coupling matrix and scaled external quality factors can be obtained as:

$$[m] = \begin{bmatrix} 0 & 1.3567 \\ 1.3567 & 0 \end{bmatrix} \quad , q_{e1} = q_{en} = 0.6667$$

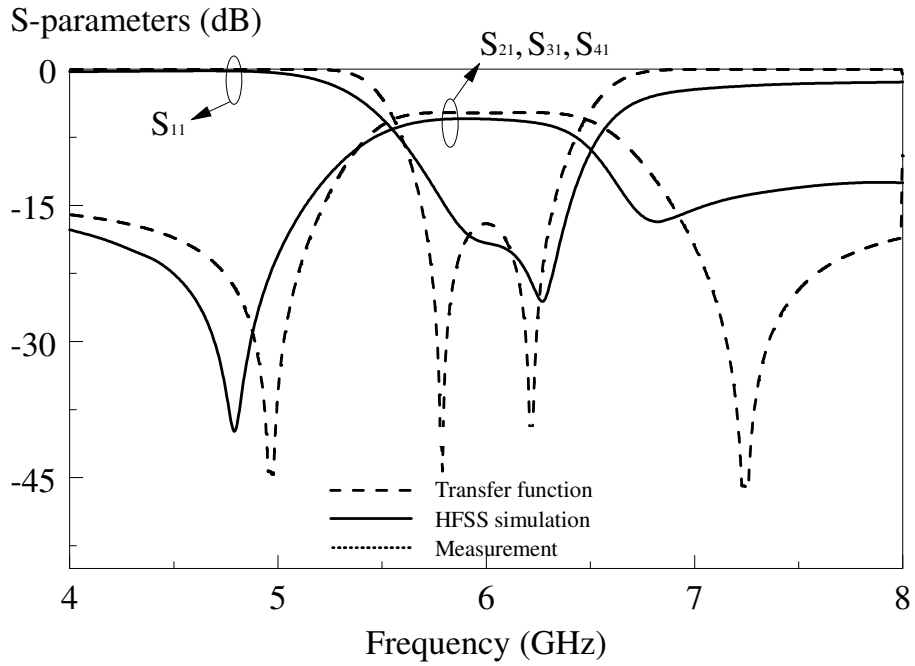

Figure 3.21: Comparison of frequency responses generated by the transfer function (elliptic response) and HFSS simulation.

3.3.3 Simulation and Experiment Results

Figure 3.22(a) shows the simulated and measured S parameters of the proposed BPD-B. Two transmission zeros (Z_1 & Z_2) are clearly seen near to the cut-off frequencies (4.74 and 6.80 GHz). With reference to the same figure, the simulated and measured center frequencies are around 6.0 and 5.9 GH, which has an error of 1.83%. The measured bandwidth is found to be 11.96% (simulation 11.25%). The insertion loss (S_{21}) is measured ~ -6.5 dB at the maximum point. It is slightly higher than that of simulation. This discrepancy can be caused by the SMA

connectors in experiment, which are not accounted for. *Figure 3.22(b)* demonstrates the measured and simulated isolation for each two of the output ports (S_{23}, S_{24}, and S_{34}). Again, reasonable agreement is observed between the simulation and measurement.

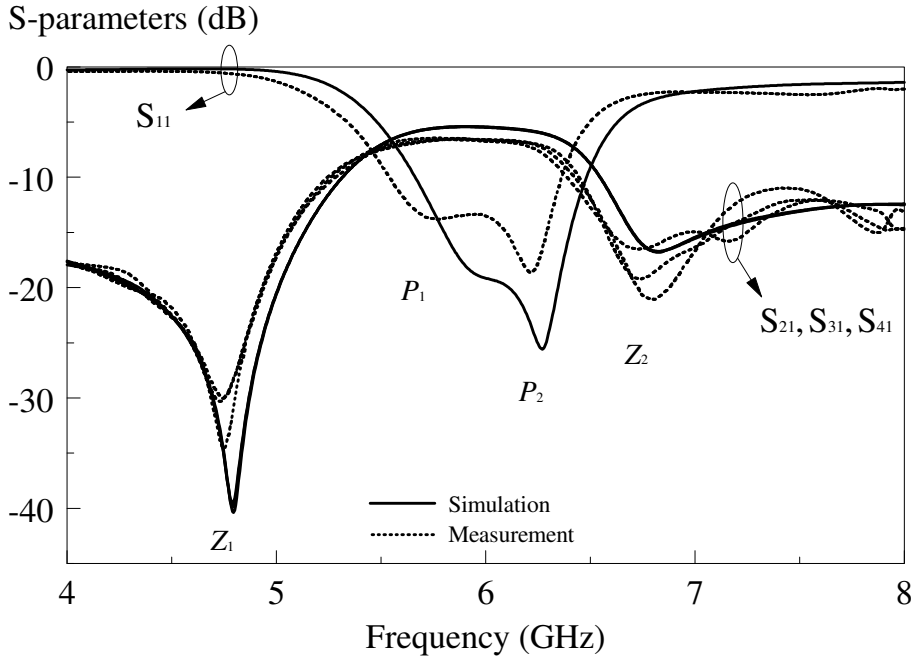

(a)

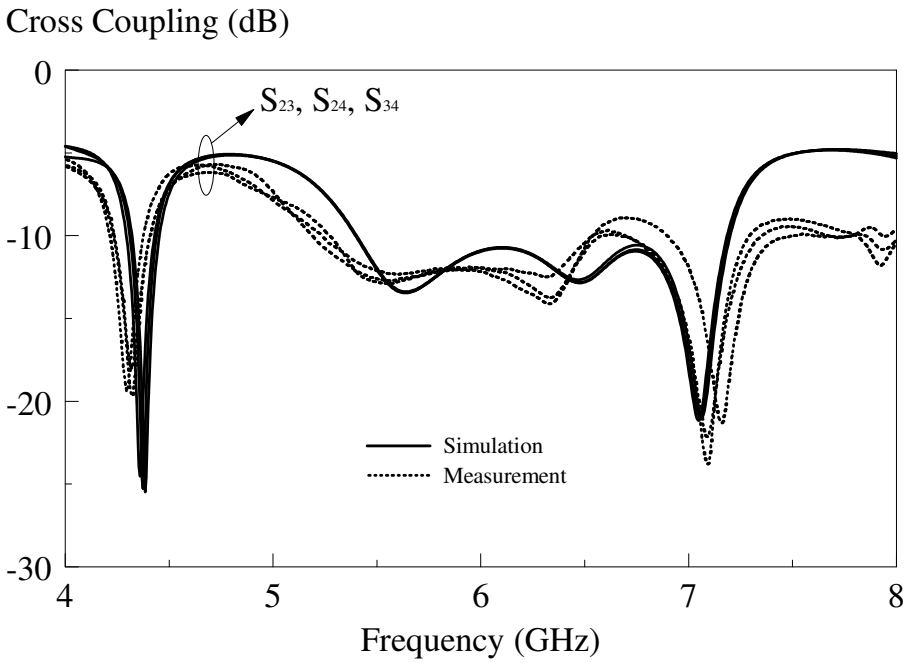

(b)

Figure 3.22: Simulated and measured (a) return and insertion losses and (b) isolation of the output ports of the proposed BPD-B.

The simulated and measured group delays of proposed BPD-B are shown in *Figure 3.23*. As can be seen in the figure, a constant time delay has been observed across the entire passband. This shows that distortion in the input signal should be minimal as all the frequency components are getting through the power divider almost at the same time.

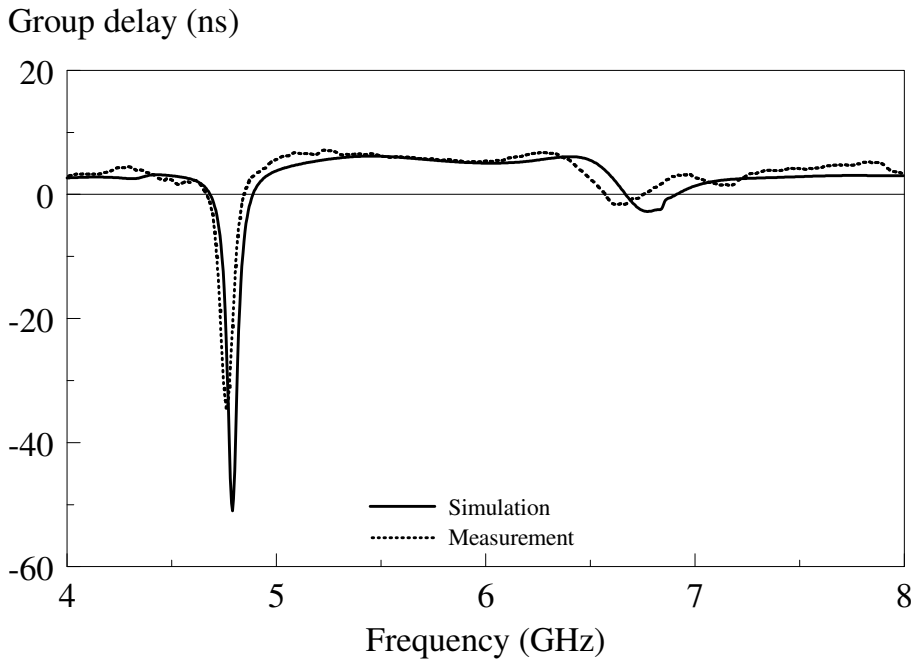

Figure 3.23: Simulated and measured group delay of the proposed BPD-B.

Although two poles and zeros can be obtained in the frequency response of BPD-B, they are not the same resonances as those in BPD-A. This configuration will be further investigated in **Section 3.3.4**.

3.3.4 Parametric Analysis

The parameters that will be discussed are: small circular patch R_c, slot c, shallow notch θ_b, deep notch θ_a, and top etched-away sectors θ_t. Since experimental verification was already given in the previous section, simulation results will be shown for the parametric analysis. Again, poles and zeros are represented by P_1, P_2 and Z_1, Z_2, respectively.

3.3.4.1 Slot *c*

Again, the arc-shaped slots are used to perturb the current distribution on the circular patch resonator. The electric and magnetic fields, including the current distribution of the simple single-layered circular patch resonator were already analyzed in **Section 3.2.4**. *Figure 3.24* shows the simulated return loss of this resonator but now with three arc-shaped slots made on it. These slots are 120˚ separated from each other.

To have a deeper physical insight, the electric fields of the first resonance pole (6.27 GHz) are depicted in *Figure 3.25(a)*, followed by those for the second pole (7.03 GHz) in *Figure 3.25(b).* With reference to the same figure, they are identified to be the transverse mode TM^{z}_{010} for the first pole P_1 while TM^{z}_{310} is for P_2.

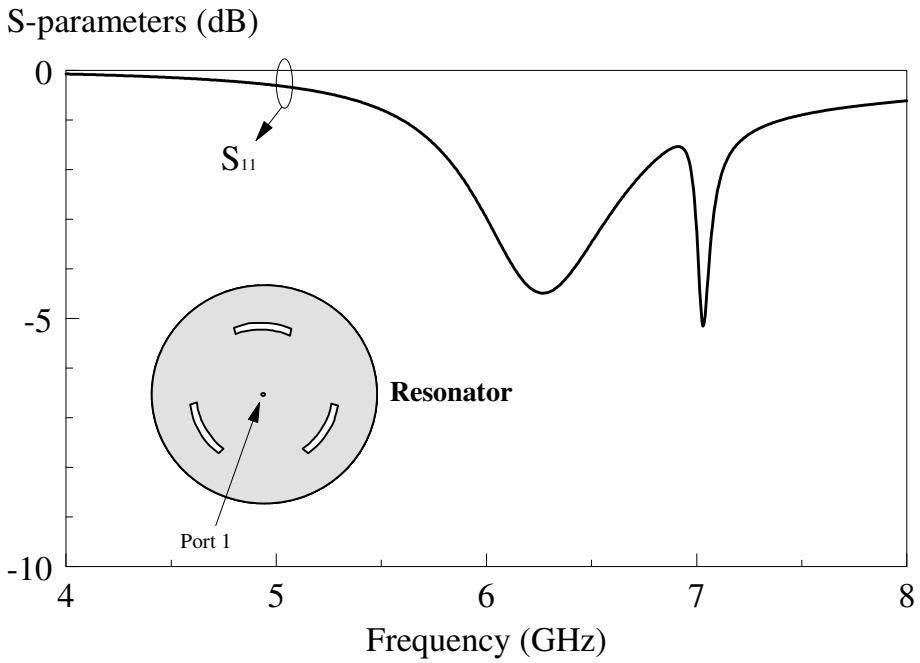

Figure 3.24: Simulated return loss of the circular patch resonator with slot *c*.

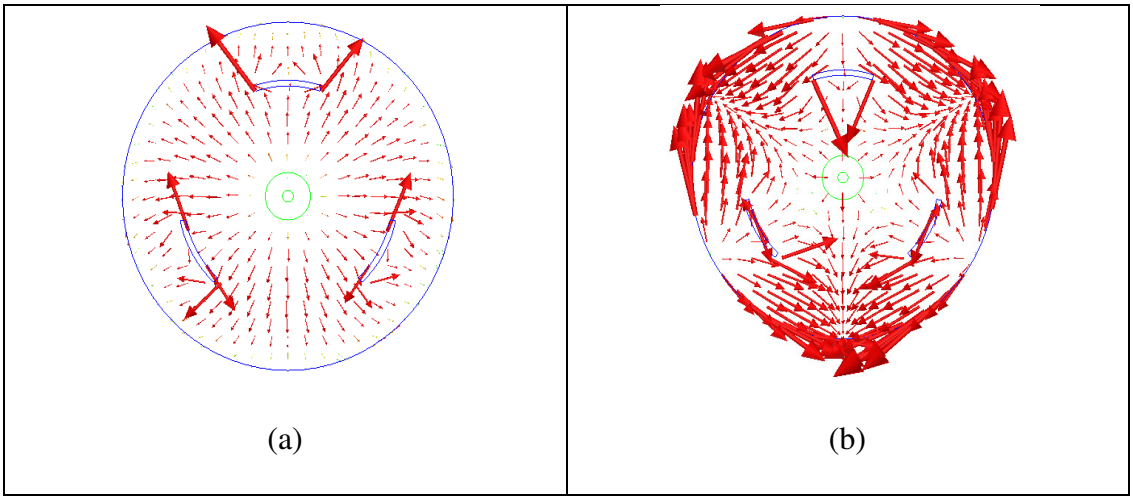

Figure 3.25: Simulated electric fields of (a) the first pole at 6.27 GHz and (b) the second pole at 7.03 GHz.

Next, the effect of the arc-shaped slot *c* is studied, with the results shown in *Figure 3.26.* Both the P_1 and Z_1 move to lower frequency when slot length is increased. On the other hand, this parameter does not affect the second pole (P_2) and zero (Z_2) much. Again, this is due to the increase in electrical length. Longer current travelling path pulls down the operating frequency of the resonator. In this case, a longer arc length can also be used to make the zero position tunable in a broader range. As can be seen in *Figure 3.26*, however, the return loss at the center frequency deteriorates when the two poles move farther apart. Tradeoff is therefore necessary in the tuning range and bandwidth performance. Similar trend was also observed in the 3 dB configuration in **Section 3.2.4**.

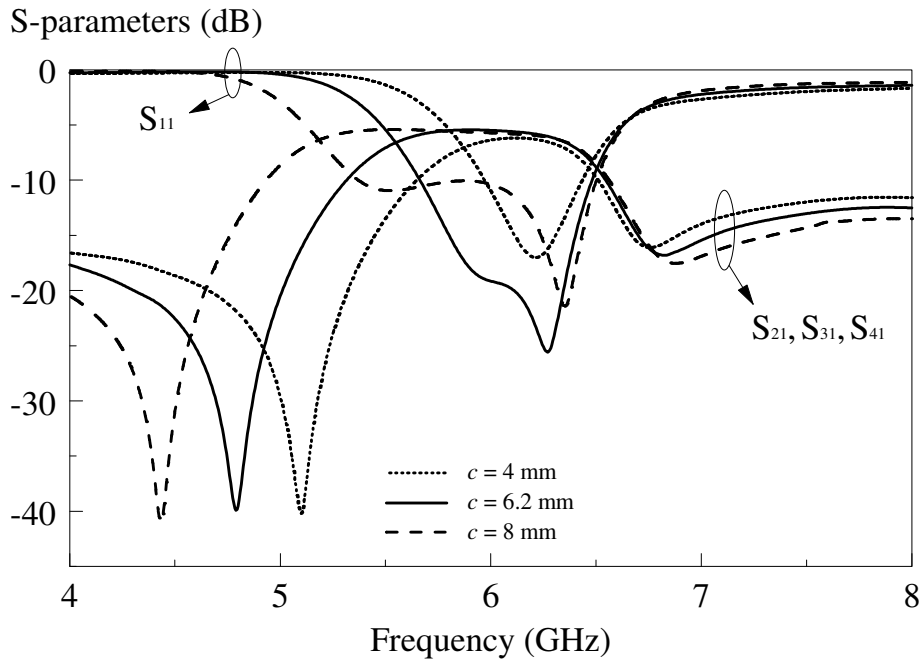

Figure 3.26: Effect of the slot length *c* on the S parameters.

3.3.4.2 Small Circular Patch R_c

Figure 3.27 shows the effect of the radius R_c on the S parameters. It is interestingly to note that this parameter affects the first zero only. It implies that the roll-off rate at the lower cutoff frequency can be tuned independently without bothering others. As R_c reduces, the filtering performance can get improved. This is because of the Z_1 approaches the lower cut-off frequency.

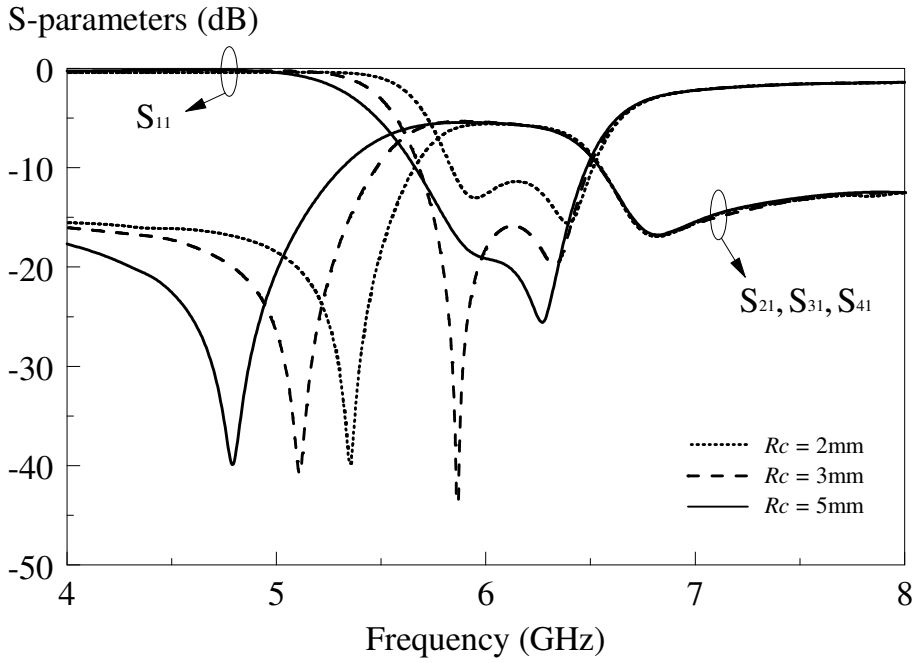

Figure 3.27: Effect of the radius R_c on the S parameters.

3.3.4.3 Shallow Notch θ_b

The influence of the shallow notch angle θ_b on the overall performance is now investigated. Again, as shown in *Figure 3.28*, it is found that the angle of the shallow notches mainly affect the zero Z_1 at the lower bound. As the angle is increased from 5˚ to 90˚, Z_1 increases from 4.7 to 5.1 GHz. To have a deeper physical insight, the parameter corresponding to each angle is compared with its Z_1 position in *Table 3.3*. Here, greater angle leads to a shorter perimeter, hence increasing the Z_1 frequency.

Table 3.3: Total perimeter of circular patch resonator with respect to angle of shallow notches θ_b.

θ_b (deg)	**5**	**14.26**	**60**	**90**
Perimeter, (mm)	156.03	154.24	146.41	141.85
Position of zero Z_1, (GHz)	4.7	4.8	4.9	5.1

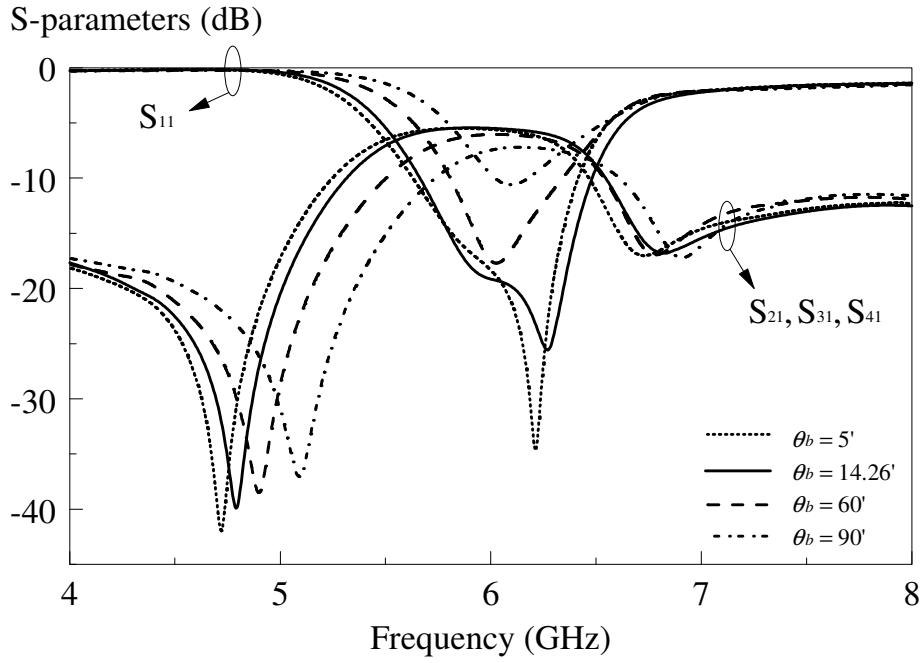

Figure 3.28: Effect of the shallow notch angle θ_b on the S parameters.

3.3.4.4 Sector θ_t on Top Patch

The effect of θ_t, which is an etched-away from the top patch, is studied with the simulated S parameters explored in *Figure 3.29*. It has been noted that only the position of Z_1 is affected but others stay. As the angle decreases from 93.7˚ to 70˚, the position of Z_1 moves nearer the lower bound of the cut-off frequency. In other words, minimizing θ_t can improve the roll-off rate (as shown in *Table 3.4*).

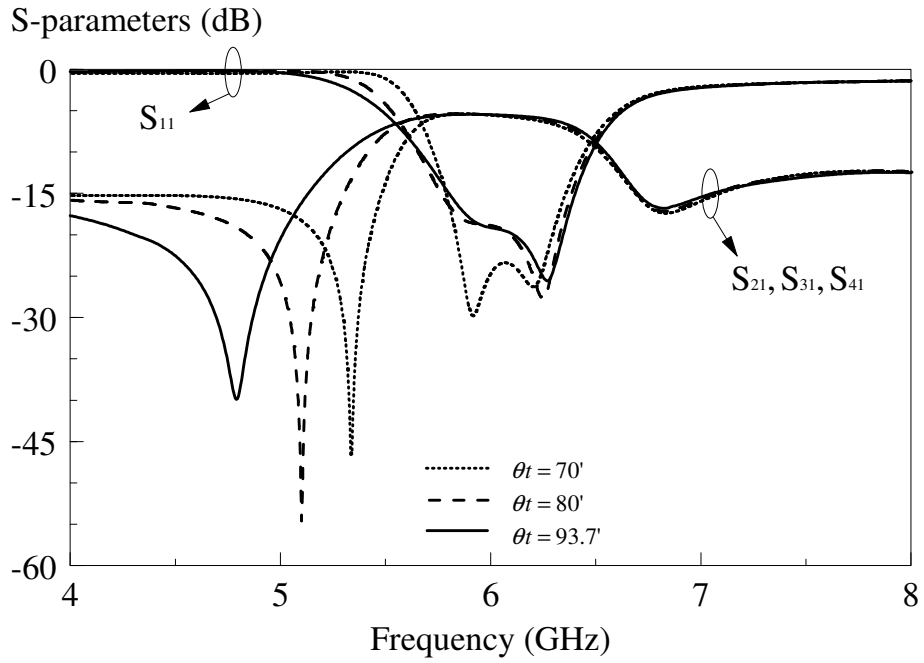

Figure 3.29: Effect of the top sector angle θ_t on the S parameters.

Table 3.4: Calculated roll-off rate and position of Z_1 with respect to the angle of θ_t.

Angle of top sector θ_t	**70**	**80**	**93.7**
Roll-off rate (dB/GHz)	168.86	141.55	56.97
Position of Z_1 (GHz)	5.34	5.10	4.79

3.4 Conclusion

In this chapter, for the first time, two band-passing power dividers have been proposed and the design methodology has been described. The proposed design is different from the conventional Wilkinson power divider. It significantly reduces the design complexity because it does not involve any isolation resistors and quarter-wavelength impedance transformers. Besides that, as more outputs are involved, the proposed design does not require combining several sections of microstrip lines. The slots on the resonator enable double resonances which greatly broaden the bandwidth. Another distinctive advantage is that a pair of transmission zeros (elliptic filter characteristic) can be found near to the cut-off frequencies without cascading to any filter element. This improves both the filter selectivity and compactness. The return loss, insertion loss, and parameters for each of the power dividers have been analyzed. In addition, a comprehensive study on the filter synthesis and coupling matrix has been carried out. Reasonable agreement has been observed between the simulated and experimental data.

CHAPTER 4

Reconfigurable Bandpassing Power Divider

4.1 Introduction

In this chapter, a microwave component that can be configured into either an in-phase or out-of-phase bandpassing power divider is explored. To begin, its passive counterpart which is workable in both the in-phase and out-of-phase settings is discussed in **Section 4.2** and **4.3**. For ease of description, the passive power dividers are named as BPD-1 and BPD-2, respectively, referring to *Table 4.1*. The resonator was then incorporated with the RF PIN diodes for the design of a reconfigurable active power divider, called BPD-3. All the proposed bandpassing power dividers are made on a circular patch resonator, needing only a single-layer, to work at 2.4 GHz. In this case, the output phase can be controlled by switching ON/OFF the diode. Ansoft HFSS (Ansoft Corporation, HFSS) a commercial software, was used for conducting all the simulations. Experiment was conducted utilizing the R&S®ZVB8 Vector Network Analyzer (VNA). In experiment, all the unused ports were terminated by 50-Ω loads. The substrate Duroid RO4003C, with a dielectric constant of ε_r = 3.38, tan δ = 0.0027 and a thickness of h = 1.524 mm, was used throughout the entire project.

Table 4.1: Naming of the proposed bandpassing power dividers.

Name	Circuit configuration
BPD-1	Passive with in-phase outputs (0˚).
BPD-2	Passive with out-of-phase outputs (180˚).
BPD-3	Active reconfigurable power divider (0˚ or 180˚).

4.2 In-phase Bandpassing Power Divider (BPD-1)

4.2.1 Configuration

Figure 4.1 displays the schematic of the proposed BPD-1. The optimized configuration consists of a circular patch resonator with radius of R = 24 mm and a Y-shaped slit, which is formed by combining a 'V' and an 'I' slots. With reference to the figure, microwave signal is fed to *Port 1* and split equally to the two output ports, *Port 2* and *Port 3*, which are designed to have the identical phase. The output feedlines, having the same length, are slightly deviated (d = 8 mm) from the center line of the circular patch for tuning purpose. As the configuration is symmetric, it is good for in-phase power division as the input signals travel through the same distance. Other design parameters are given as: a = 6 mm, b = 0.8 mm, c = 0.4 mm, e = 42 mm and θ = 52˚. The photograph of the proposed prototype BPD-1 is as shown in *Figure 4.2*.

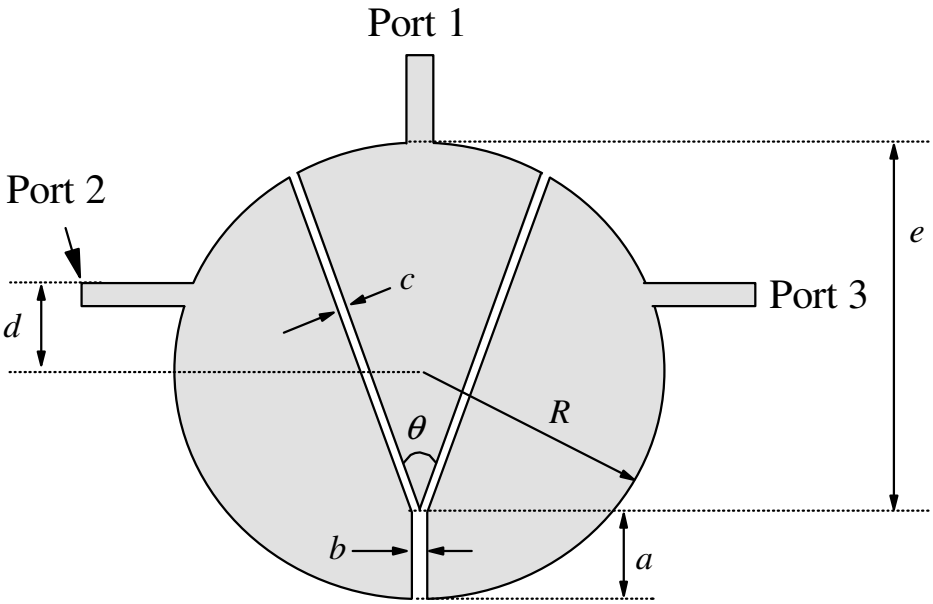

Figure 4.1: Schematic of the proposed BPD-1.

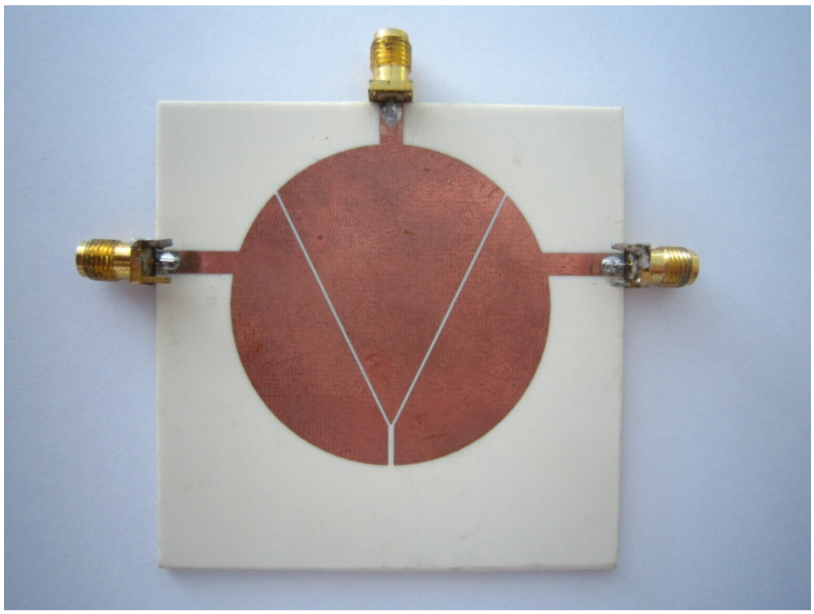

Figure 4.2: Photograph of the prototype of the proposed BPD-1.

4.2.2 Simulation and Experimental Results

The simulated and measured S parameters are depicted in *Figure 4.3(a)*. Two closely coupled resonances centering at 2.35 GHz are observed. It has a measured bandwidth of 5.02%, being slightly smaller than the simulation (7.29%). For both, the amplitude imbalance falls within 0.5 dB across the passband. From the same figure, a pair of transmission zeros are found at Z_1 = 1.32 and Z_2 = 3.26 GHz, which are introduced by the coupling effect in the slits. In *Figure 4.3(b)*, the measured and simulated coupling between the output ports is also depicted, showing reasonable agreement. The phase characteristics are shown in *Figure 4.4*. It is found that the phase imbalance between two output ports is very minute in the range of 0.5 GHz – 4GHz.

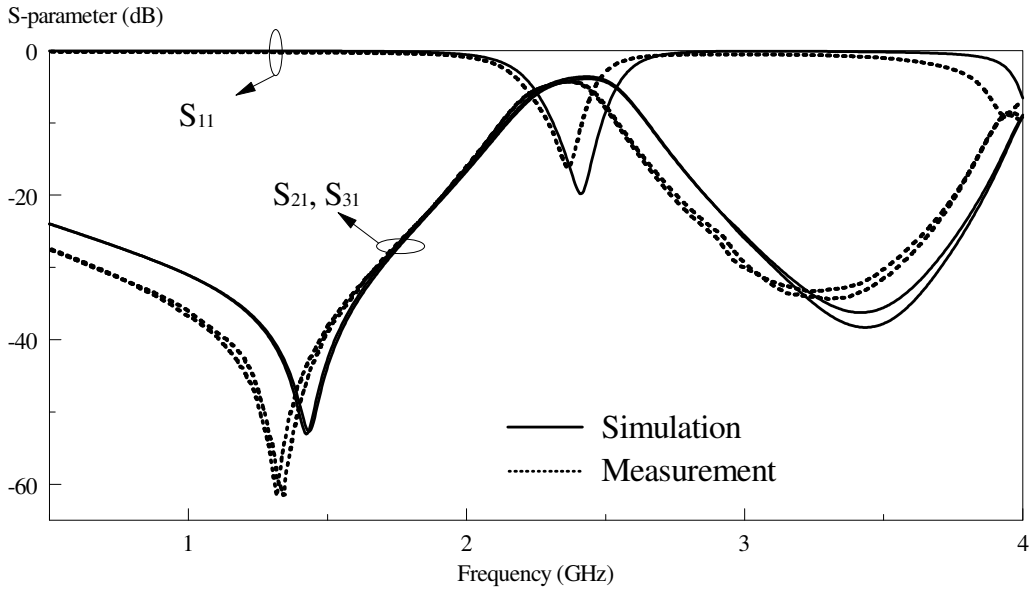

(a)

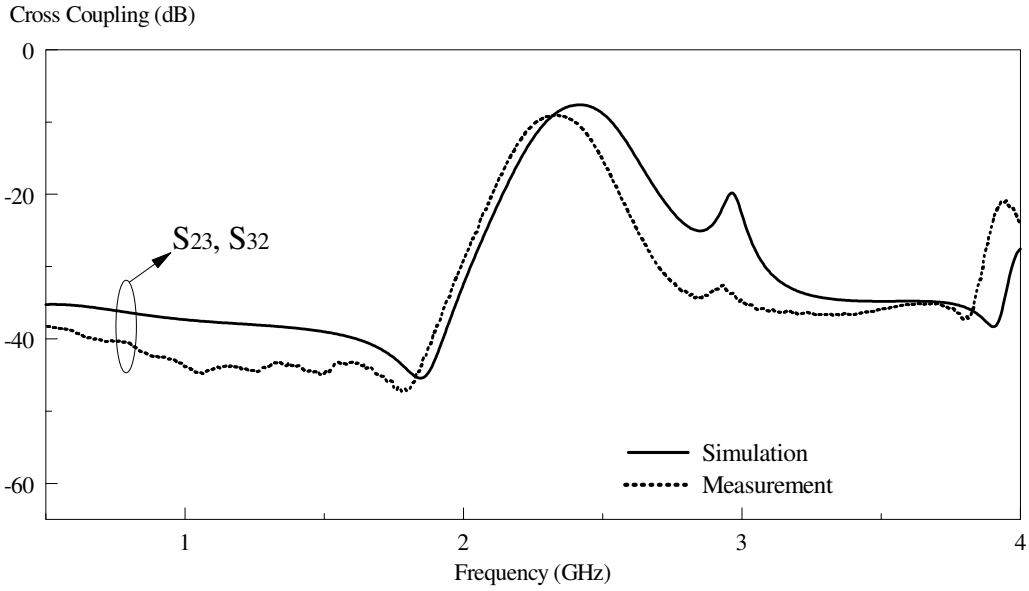

(b)

Figure 4.3: Simulated and measured (a) return and insertion losses, and (b) isolation between the output ports of the proposed BPD-1.

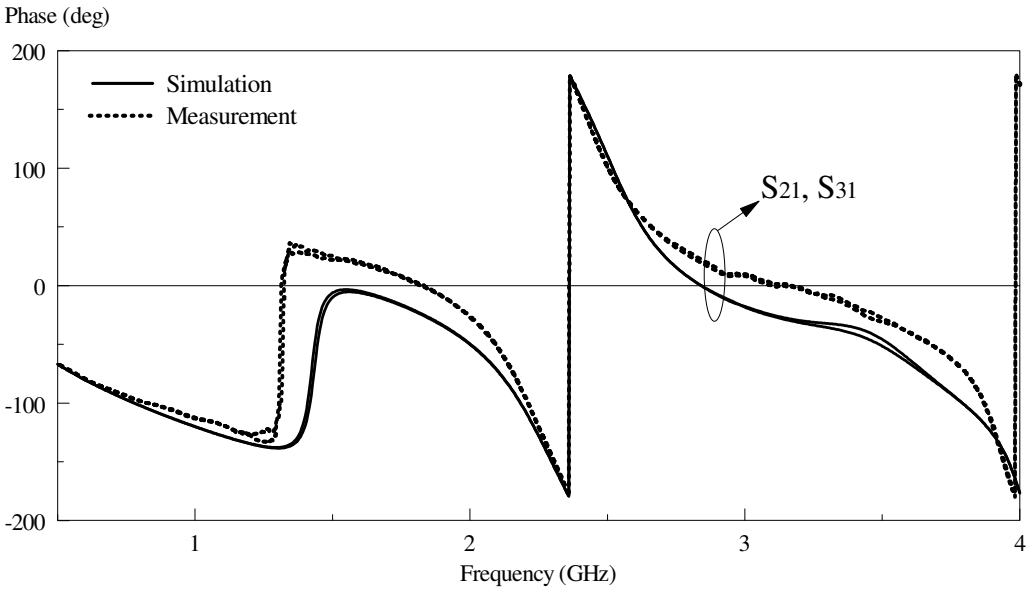

Figure 4.4: Simulated and measured phase responses of the proposed BPD-1.

4.2.3 Theoretical and Parametric Studies

Next, the 'Y' slit of the configuration in *Figure 4.1* is sealed to form a simple circular patch resonator. This analysis is performed to understand the characteristics of this resonator. It will be compared with the proposed power divider. For the simple patch, the lowest zero was observed to be 1.65 GHz while the fundamental pole was found to be ~ 2GHz. *Figure 4.5(a)* depicts the electric field distribution of the zero. Obviously, this resonance allows no field leakage to the output. On the other hand, the boundary condition of the patch is altered by the two output ports such that a new pole can be formed at 2 GHz, as shown in *Figure 4.5(b)*.

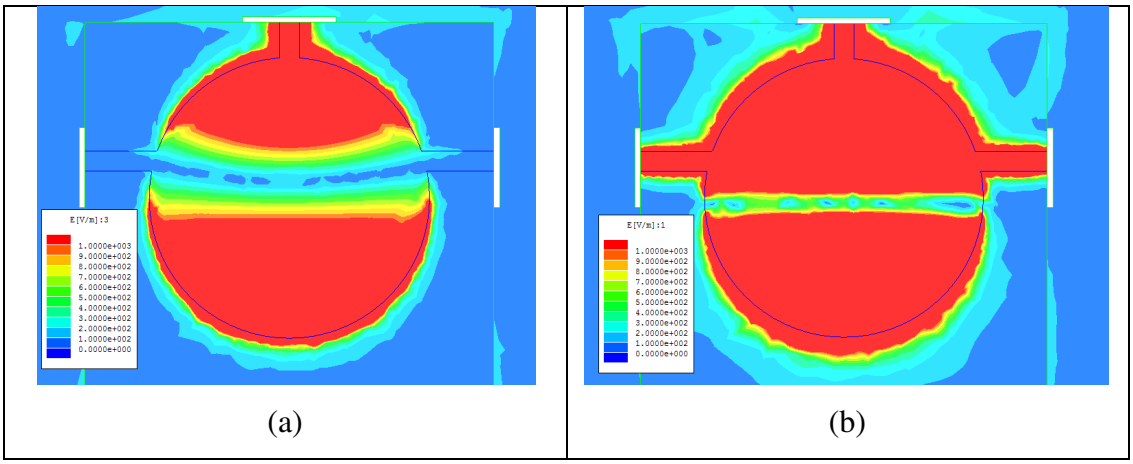

Figure 4.5: The electric field distributions of the simple circular patch at (a) the first transmission zero observed at 1.65 GHz, and (b) the first pole observed at 2 GHz.

The resonances of the proposed configuration are now analyzed. It was already simulated in *Figure 4.3(a)* that two poles could be found close to 2.41 GHz. In order to visualize the two modes clearer, the electric fields at the lower and upper bounds of the passband are chosen to be 2.2 GHz and 2.6GHz, respectively. As can be seen

from *Figure 4.6 (a) and (b)*, two new resonances emerge because of the existence of the Y-shaped slit. On the other hand, the field distributions in *Figure 4.6(c)* and *(d)* show that very little field can travel to the output ports at the zero frequencies. It can be concluded that new resonant modes are made possible by the Y-shaped slit. To understand the configuration better, all the design parameters for BPD-1 are analyzed individually.

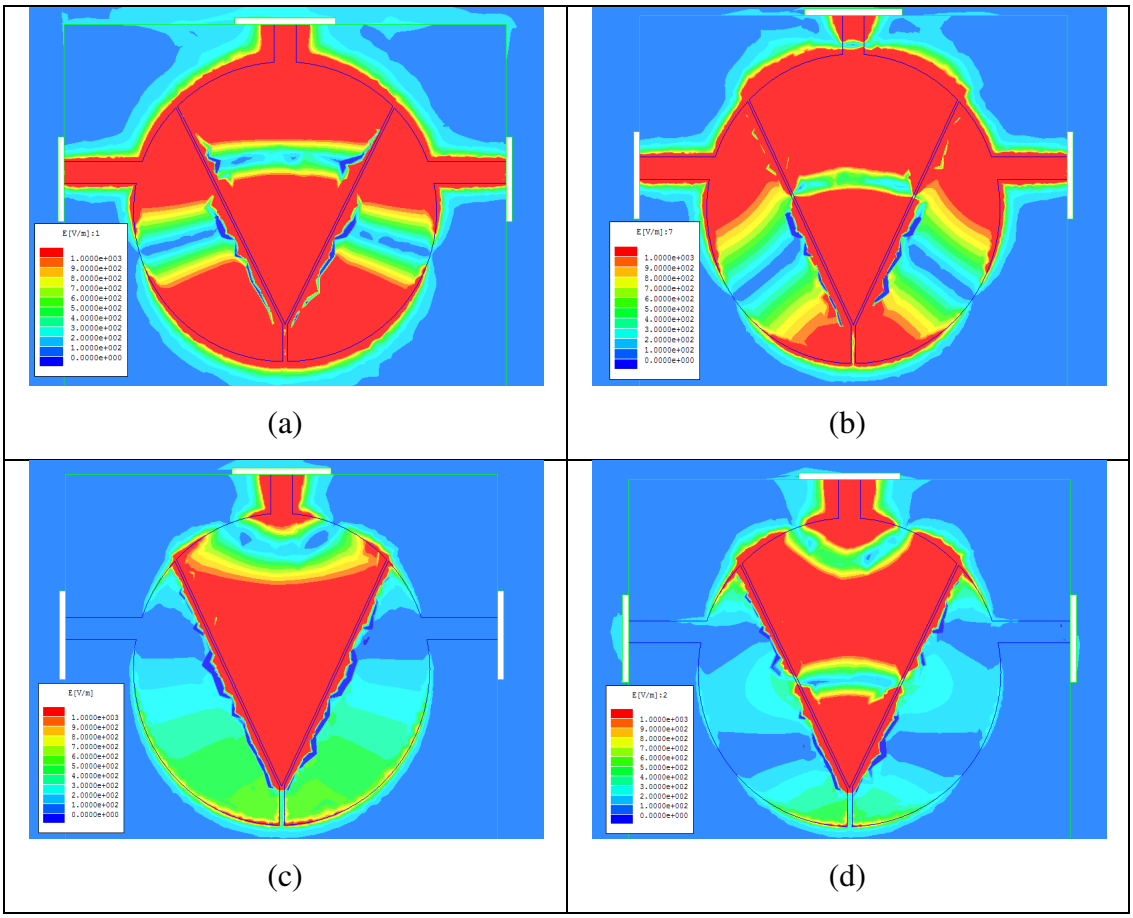

Figure 4.6: The electric field distributions of the proposed in-phase power divider at (a) 2.2 GHz near to P_1, and (b) 2.6 GHz near to P_2, and (c) Z_1 at 1.44 GHz, and (d) Z_2 at 3.44 GHz.

4.2.3.1 Flaring Angle θ of the Y-shaped Slit

Figure 4.7 shows the effect of the flaring angle θ on the S parameters. It is found that the frequency of Z_2 becomes lower as θ is reduced. It implies that this parameter can be deployed for selectivity tuning in the upper bound. Also noted is that the first pole slightly varies with the change of θ. The perimeter of the 'V' portion of the Y-shaped slit is calculated for different flaring angle in *Table 4.2*. It is noted that longer perimeter, corresponding to a larger sector area, results in lower Z_2 frequency.

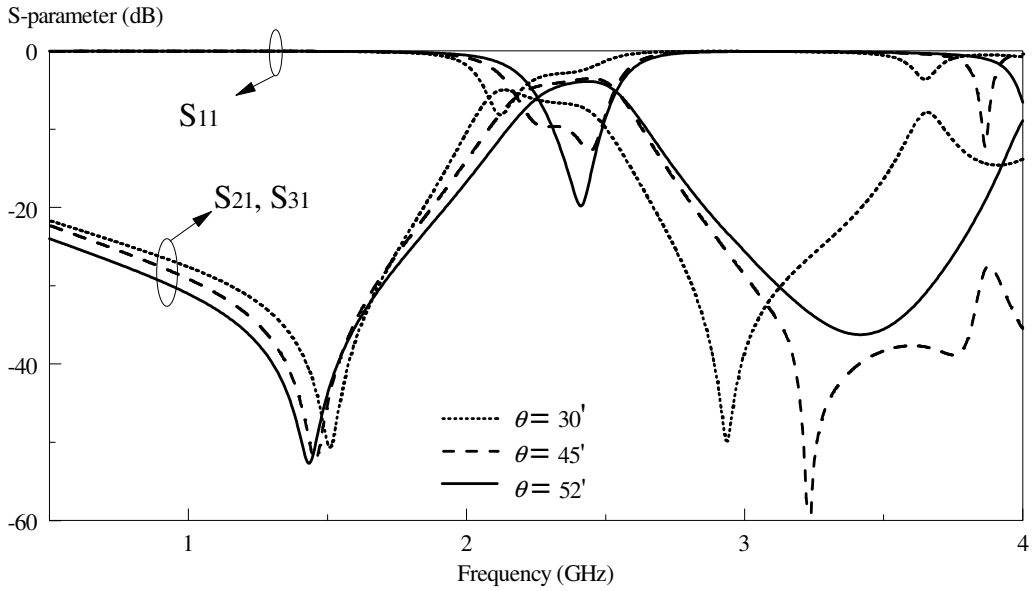

Figure 4.7: Effect of the flaring angle θ on the S parameters.

Table 4.2: Total length of V-branch according to angle θ.

Angle of V-branch, θ (deg)	**30**	**45**	**52**
Total length (mm)	81.8	79.2	77.7
Position of Z_2 for S_{21}(GHz)	2.94	3.23	3.43
Position of Z_2 for S_{31}(GHz)	2.98	3.13	3.43

4.2.3.2 Offset Distance *d* of Output Ports

The offset distance *d* is now studied. *Figure 4.8* illustrates the simulated S parameters with respect to the change of *d*. With reference to the figure, the Z_1 frequency is greatly affected. It moves from 1.26 GHz to 1.58 GHz as the offset distance is decreased from 12 mm to 4 mm. Again, it shows that this design parameter can be applied for optimizing the selectivity of the lower bound of the passband.

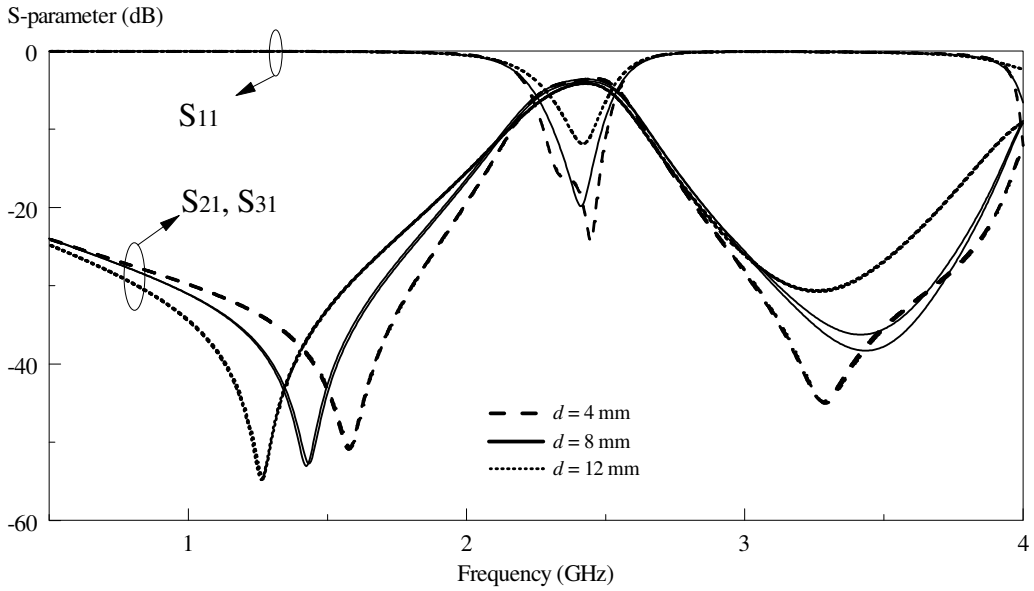

Figure 4.8: Effect of the offset d on the S parameters.

4.3 Out-of-phase Bandpassing Power Divider (BPD-2)

4.3.1 Configuration

By shifting the feedline position of *Port 3*, it was found that the circular patch, loaded with a Y-shaped slit, can also be re-designed into an out-of-phase power divider, which is named as BPD-2 for the ease of discussion later. *Figure 4.9* displays the schematic of the proposed structure, which is quite similar to that in BPD-1. But now, *Port 3* is reallocated in order to tap out the signal at bottom of the resonator. With reference to the same figure, the offset distance is chosen to be g = 9.5 mm from the center line of the resonator Asymmetry in structure causes microwave signal to experience different travelling paths. In this design, the phase difference of the output signals can be easily tuned to become 180±5° in the passband. The photograph of the fabricated prototype is shown in *Figure 4.10*.

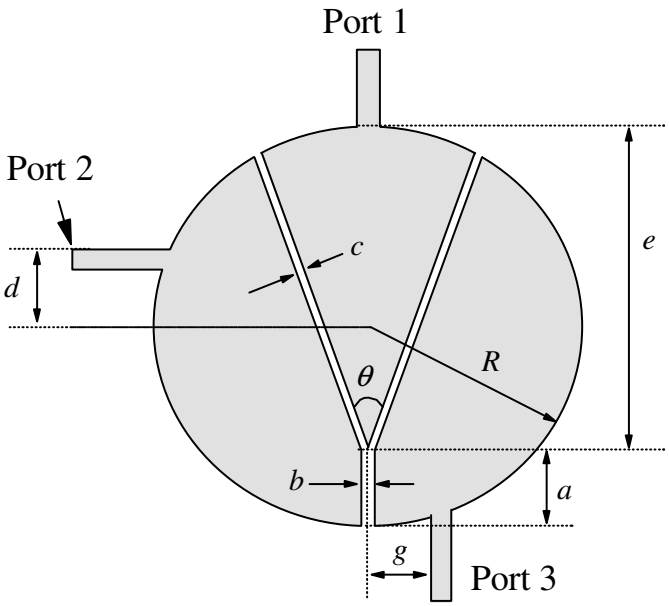

Figure 4.9: Photograph of the prototype of the proposed out-of-phase BPD-2.

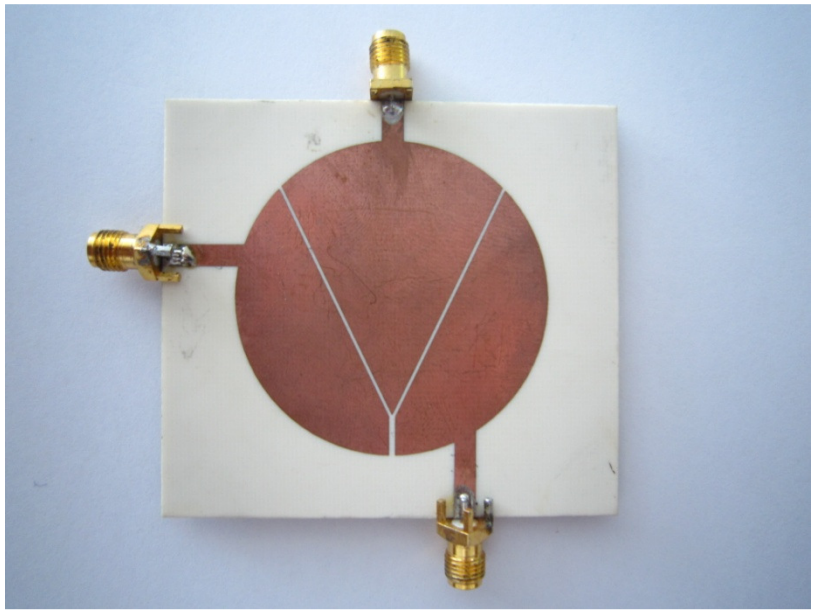

Figure 4.10: Prototype of the proposed BPD-2.

4.3.2 Simulation and Experiment Results

The simulated and measured S parameters of the proposed BPD-2 are illustrated in *Figure 4.11(a)*. The center frequency is found to be 2.36 GHz, being slightly greater than that (2.35GHz) for BPD-1. Different from the previous case, here, only one transmission zero is available in the upper bound of the passband at *Port 3*. Two modes have been observed, giving a measured fractional bandwidth of 4.26% (simulation 5.44%). The measured coupling coefficient, shown in *Figure 4.11(b)*, comes pretty close to the simulation, as expected. *Figure 4.12* gives the amplitude imbalance and phase difference, both in simulation and measurement, of BPD-2. Overall, the phase difference falls within 180±5˚ stretching across the frequency range 2.3 GHz – 2.5 GHz. Nevertheless, the amplitude imbalance limits its usage beyond 2.45 GHz as it exceeds the ±1 dB criteria. It shows that the same type

of resonator can be made either as an in-phase or out-of phase power divider at the same time. This feature will be used to design the reconfigurable active power divider with bandpassing effect in **Section 4.4**.

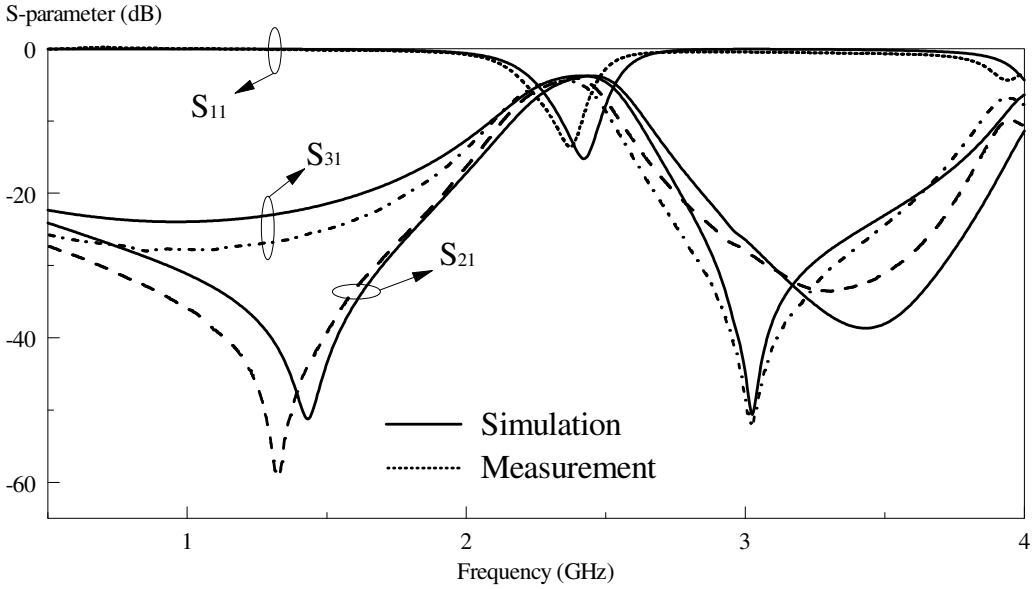

(a)

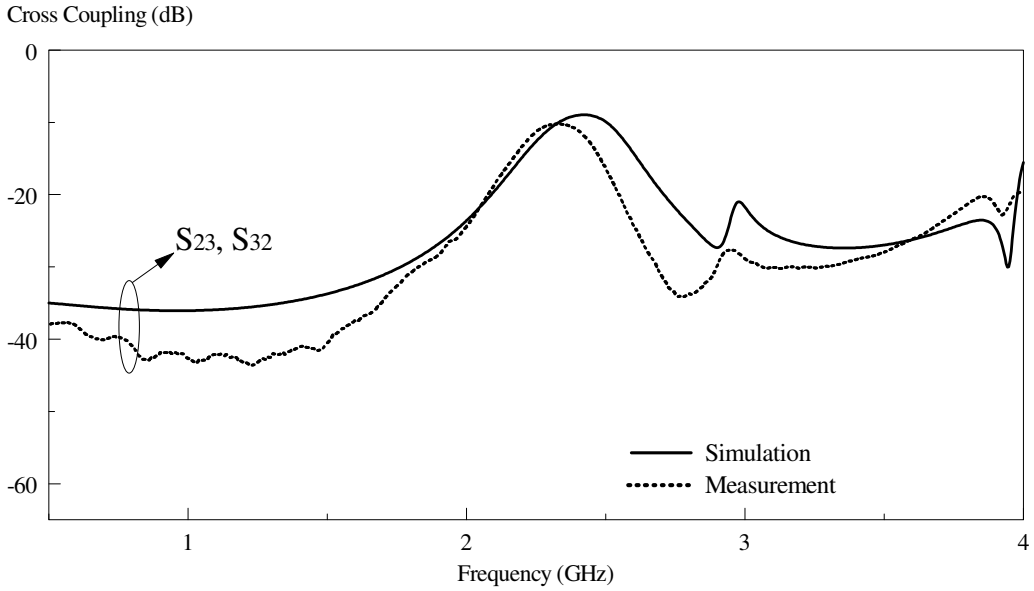

(b)

Figure 4.11: Simulated and measured (a) return and insertion losses and (b) isolation between the output ports of the proposed BPD-2.

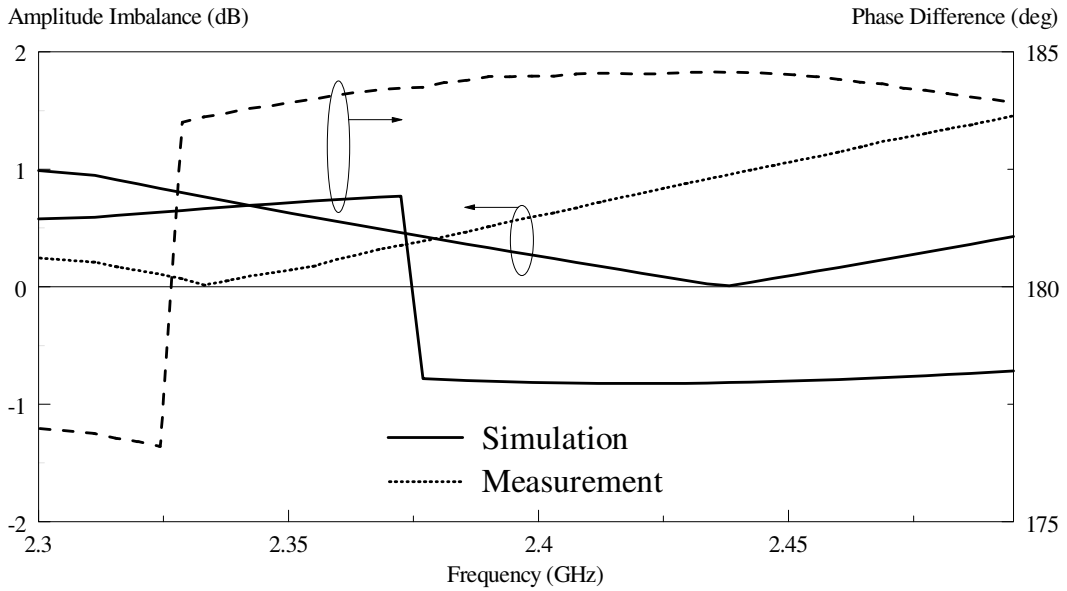

Figure 4.12: Simulated and measured amplitude imbalance and phase difference of the proposed BPD-2.

4.3.3 Theoretical and Parametric Studies

To understand better, the electric field distributions for all the resonances are illustrated in *Figure 4.13*. The fields of the closely coupled poles are shown at 2.2 GHz (*Figure 4.13(a)*, near to P_1) and 2.6 GHz (*Figure 4.13(b)*, near to P_2) so that the individual resonances can be visualized without the disturbance of one another. They are the same modes to those in *Figure 4.6(a)* and *(b)* as the fields appear similar. As can be seen in the frequency response, there are two zeros in both the lower and upper bounds in S_{21}, with their fields shown in *Figure 4.13 (c)* and *(d)*. Despite the change in the feeding position (*Port 3*), the zero resonances are identical to those in *Figure 4.6 (c)* and *(d)*. With reference to *Figure 4.13 (e)*, the field distribution of the upper-bound zero of S_{31} indicates that it has the same resonance mode as that in *(d)*. The effect of the major design parameters will be scrutinized next.

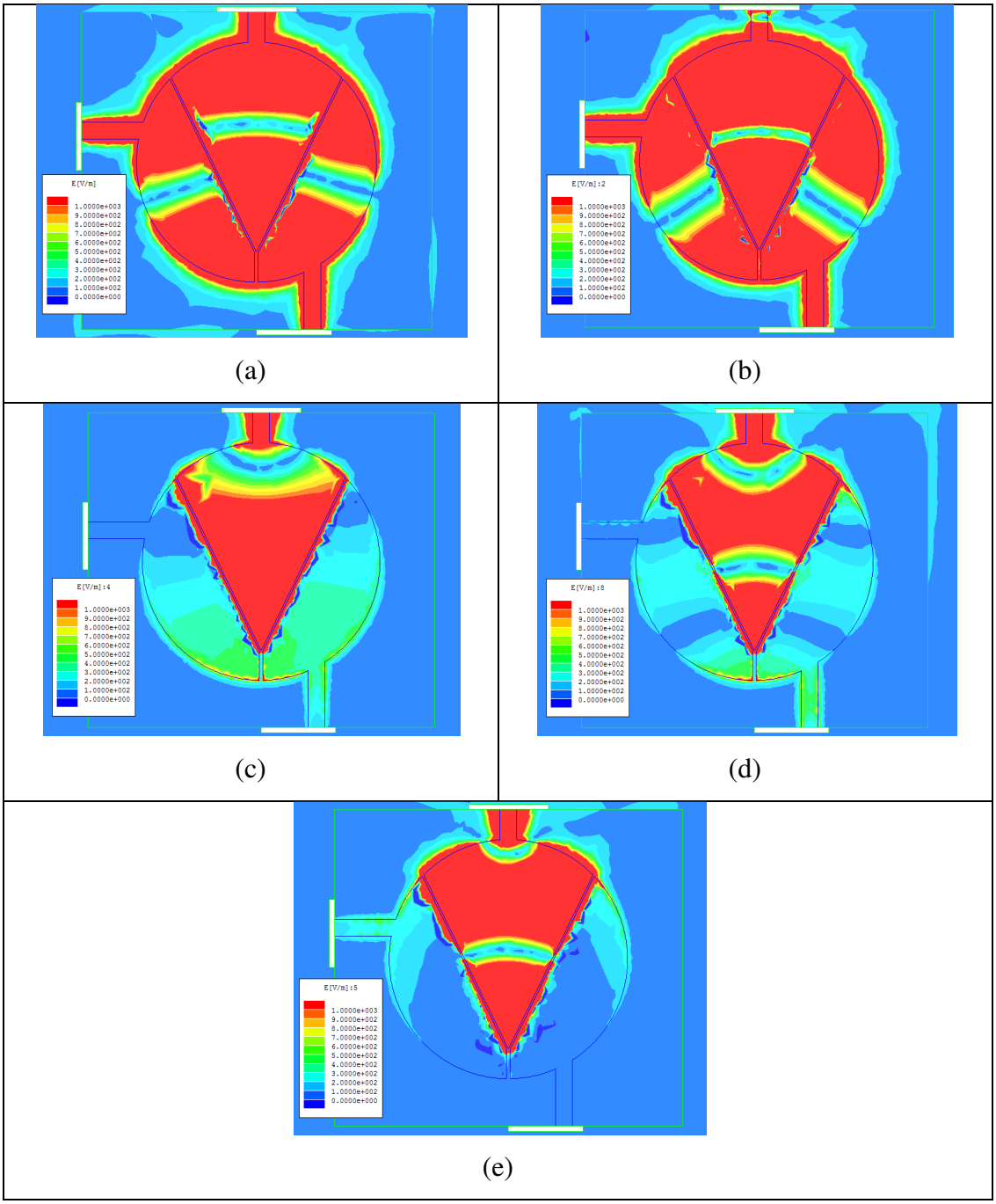

Figure 4.13: The electric field distributions of the proposed out-of-phase power divider at (a) 2.2 GHz near to P_1, and (b) 2.6 GHz near to P_2, and (c) Z_1 for S_{21} at 1.41GHz, and (d) Z_2 for S_{21} at 3.4 GHz, and (e) zero for S_{31} at 3.0 GHz.

4.3.3.1 Offset Distance *d* of Port 2

As this power divider comes with a new feeding position (*Figure 4.14*) at *Port 3*, which is slightly different from that in previous, the effect of the offset *d* on the frequency response is now studied. Similar to the in-phase case, the resonance frequency of the lower-bound zero of S_{21} decreases with a larger offset, although such phenomenon is not seen in S_{31}. With reference to the same figure, the upper-bound zeros are not so much affected, except when *d* goes below 8 mm.

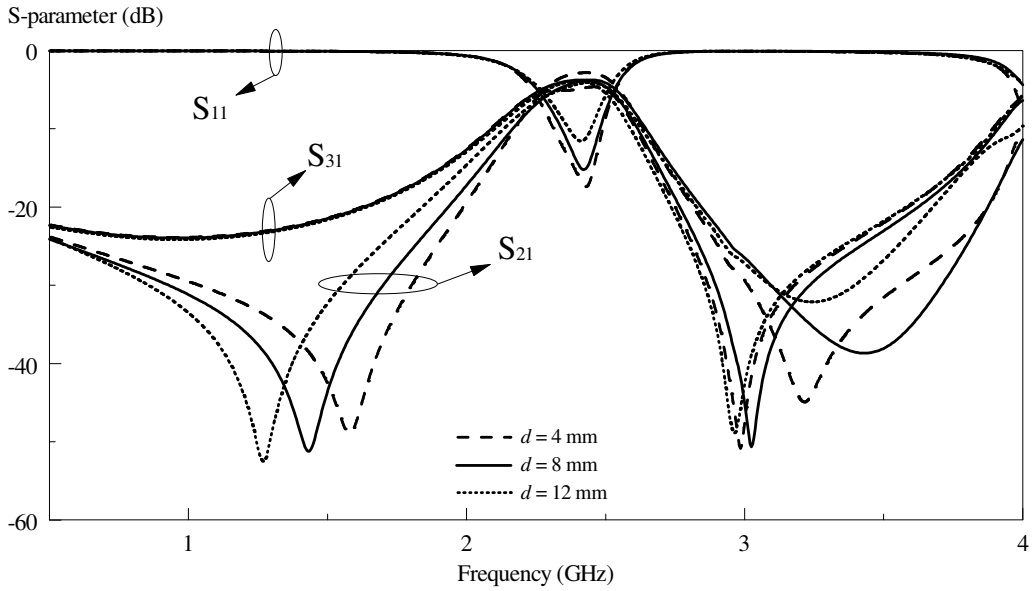

Figure 4.14: Effect of the offset d on the S parameters

4.3.3.2 Offset Distance *g* of Port 3

The effect the offset distance *g* (shown in *Figure 4.9*), being increased from 5.5 to 12.5mm, from *Port 3* is now studied as a function of frequency. The simulated S parameters, amplitude imbalance, and phase difference are illustrated in *Figure 4.15*, *4.16* and *4.17*, respectively. It can be seen from *Figure 4.15* that this parameter does not affect the frequency response much. Another fact is that g = 9.5 mm is the optimum gap distance that gives the best amplitude and phase bandwidths, as noted in the following subsequent two figures.

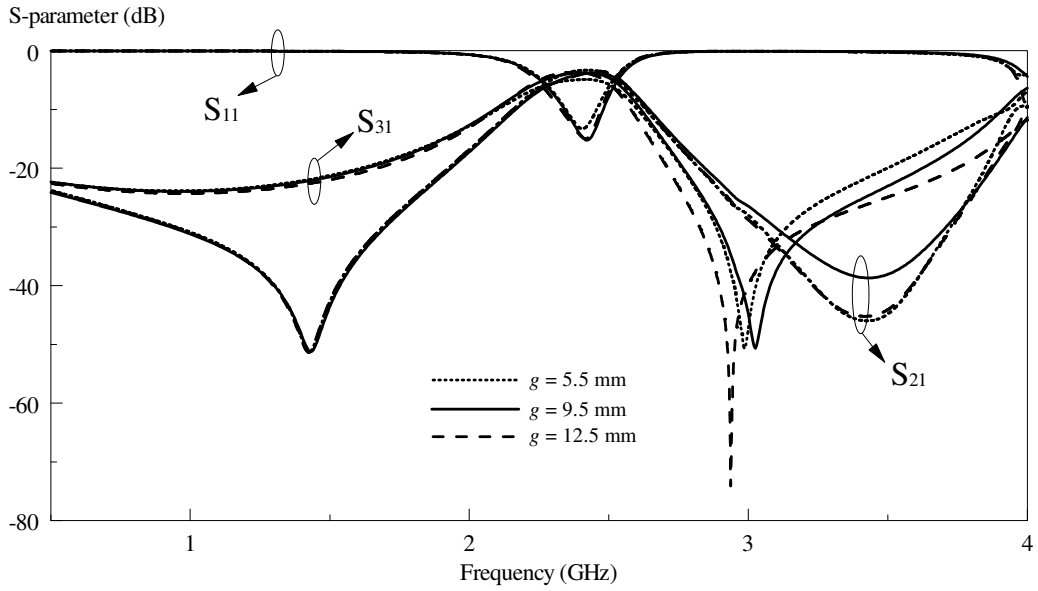

Figure 4.15: Effect of the gap distance *g* on the amplitude response.

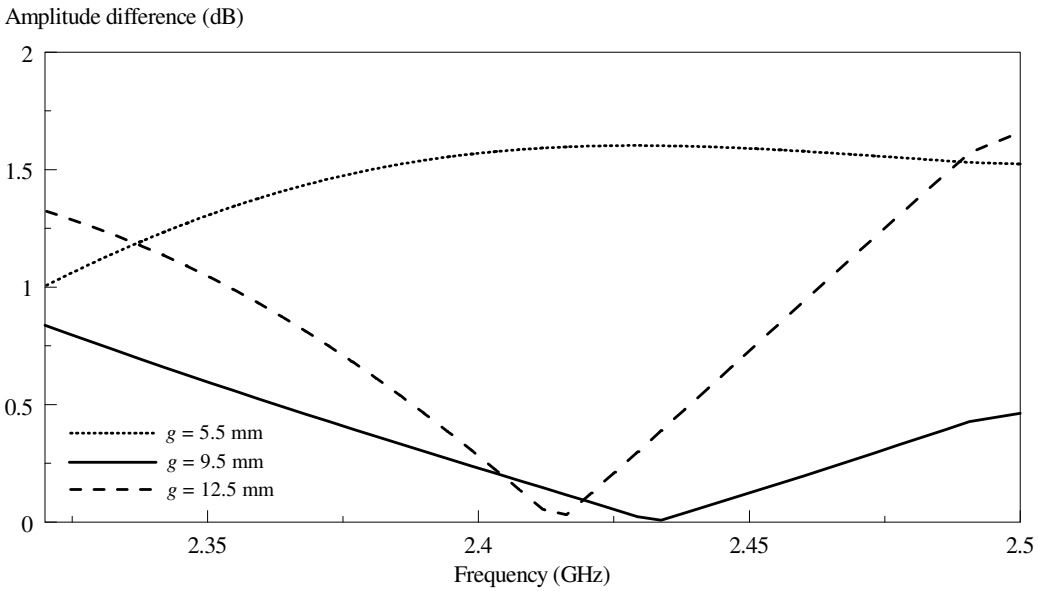

Figure 4.16: Effect of the gap distance *g* on the output amplitude imbalance.

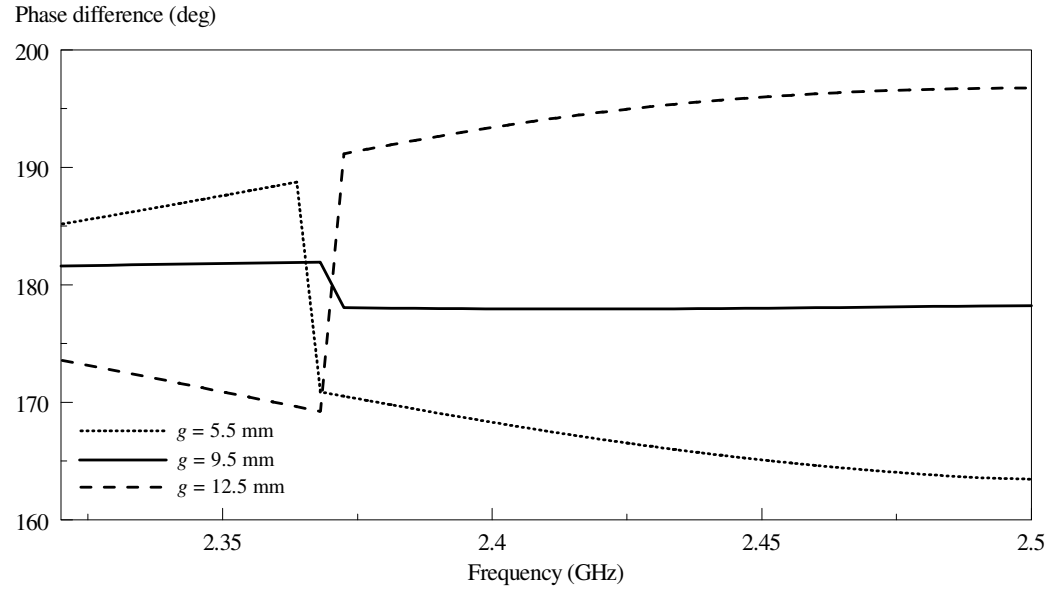

Figure 4.17: Effect of gap distance *g* on the output phase difference.

4.4 Reconfigurable Bandpassing Power Divider (BPD-3)

4.4.1 Configuration

In this section, the in-phase (BPD-1) and out-of-phase (BPD-2) power dividers are now combined to form a new device, called (BPD-3) with the schematic shown in *Figure 4.18*, that provides the two features in one piece. For this new design, the feedlines are incorporated with the BAR50-02V RF PIN diodes, manufactured by Infineon Technologies, for achieving reconfiguration. A good PIN diode can provide good isolation when it is reverse-biased but low insertion loss in forward bias. There are many RF PIN diodes available in the market. They are at variance with different operating frequencies, biasing points, isolation, insertion loss, and etc. However, only a few are capable in providing good performance at high frequency such as 2.4 GHz.

To facilitate simulation, the feedline is slightly tilted (θ_{port_3} = 65˚ from y-axis) at *Port 3* such that a DC block, as well as the diode model, can be included. The design parameters are given by: a = 6, b = 0.8 mm, c = 0.4 mm, d = 8 mm, e = 42 mm and θ = 52˚. The photograph of the prototype is illustrated in *Figure 4.19*.

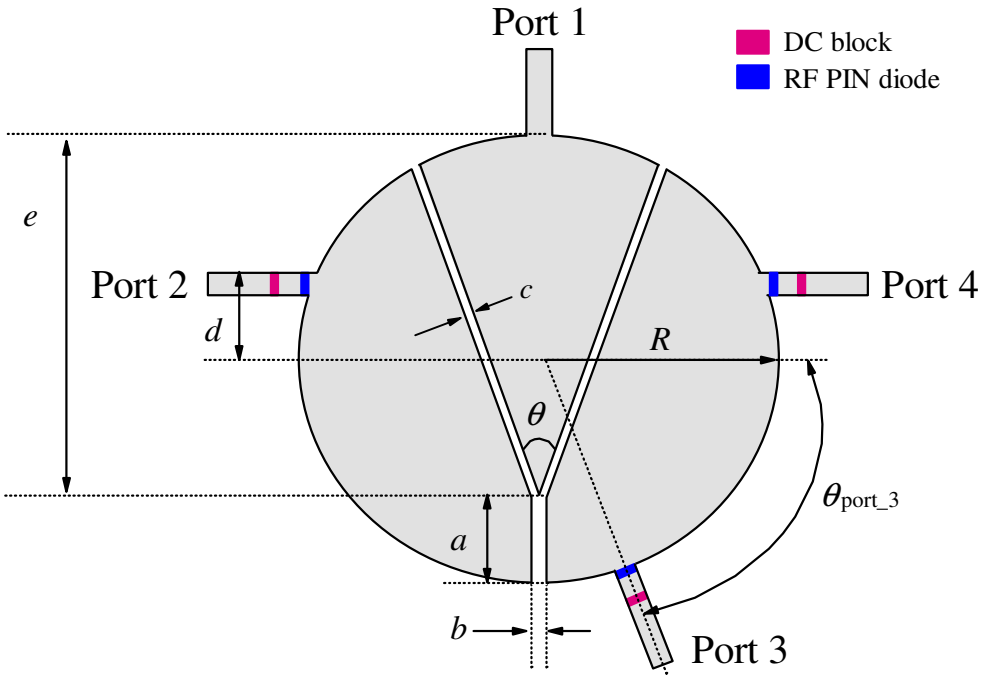

Figure 4.18: Schematic of the proposed BPD-3.

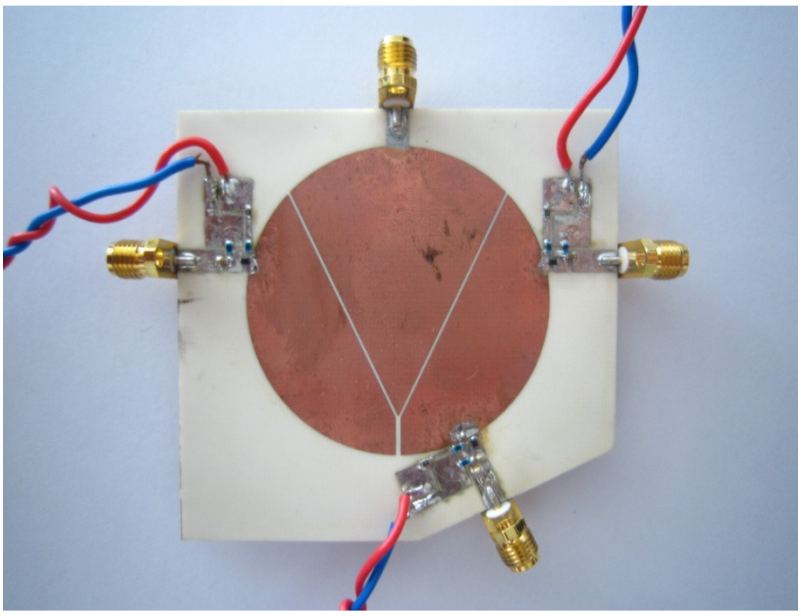

Figure 4.19: Photograph of the prototype of the proposed BPF-3.

4.4.2 Biasing Circuitry for RF PIN Diode

The biasing circuitry of the RF PIN diode is depicted in *Figure 4.20*. The RF and DC paths are highlighted. An RF choke is deployed to prevent the microwave leakage to the DC path. In this case, the diode is biased at a forward current of 100mA with voltage drop of 1 V. When turned ON, this diode is replaced by a resistance of 1.5Ω in simulation. It is simply left open in the OFF state.

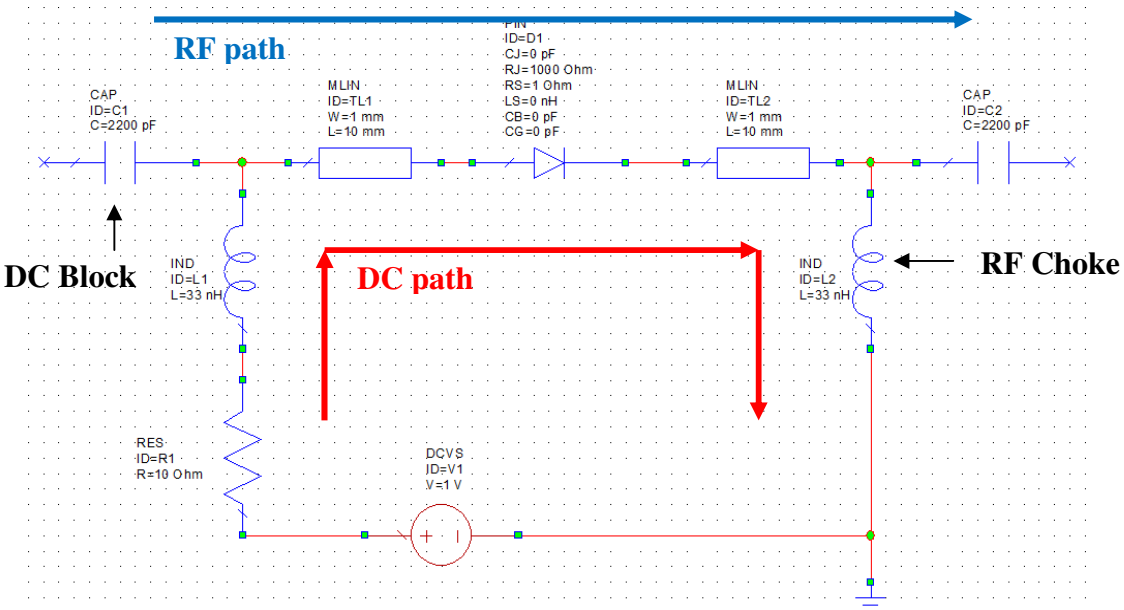

Figure 4.20: Biasing Circuitry for the RF PIN Diode.

As provided by the datasheet, with a 10mA forward current, the maximum forward resistance is 4.5Ω, meanwhile, the insertion loss is approximately 0.27 dB at 2.4 GHz. Low in both forward resistance and insertion loss is crucial, as power loss in travelling path is extremely undesirable in power divider. In order to further

minimize the power loss, several RF chokes are added to reduce microwave leakage to the DC path. Therefore, a high-impedance inductor is required for the design of the RF choke, which can be usually obtained by *eqn. 4.1*.

$$L = \frac{Z_L}{j\omega} \approx 33nH \tag{4.1}$$

According to the specification, in reverse bias, the diode is able to provide an isolation level of up to 18 dB at 2.4 GHz. With such high isolation, it is sufficient to isolate microwave signal from reaching the unused ports, as a result, it can be considered to be OFF state.

4.4.3 Simulation and Experimental Results

Ansoft HFSS is used for all simulations, with experiments conducted to verify. The unused ports were terminated by the 50 Ω loads. To begin, the BPD-3 is first configured in-phase by turning *Port 3* into OFF state. The simulated and measured S parameters are shown in *Figure 4.21*. Like its passive counterpart (*Figure 4.1*), two transmission zeros and a dual-mode performance have been observed. With reference to the figure, the measured and simulated center frequencies are 2.357 and 2.403 GHz, respectively, with an error of 1.91%. Besides, the maximum insertion loss of

the isolated port (S_{31}) is measured around -18 dB. It has been successfully showcased that the BAR50-02V diode can provide a good isolation. *Figure 4.22* shows the measured amplitude imbalance and phase difference. The measured and simulated bandwidths are 6.125 and 7.282%, respectively, with an error of 1.16%.

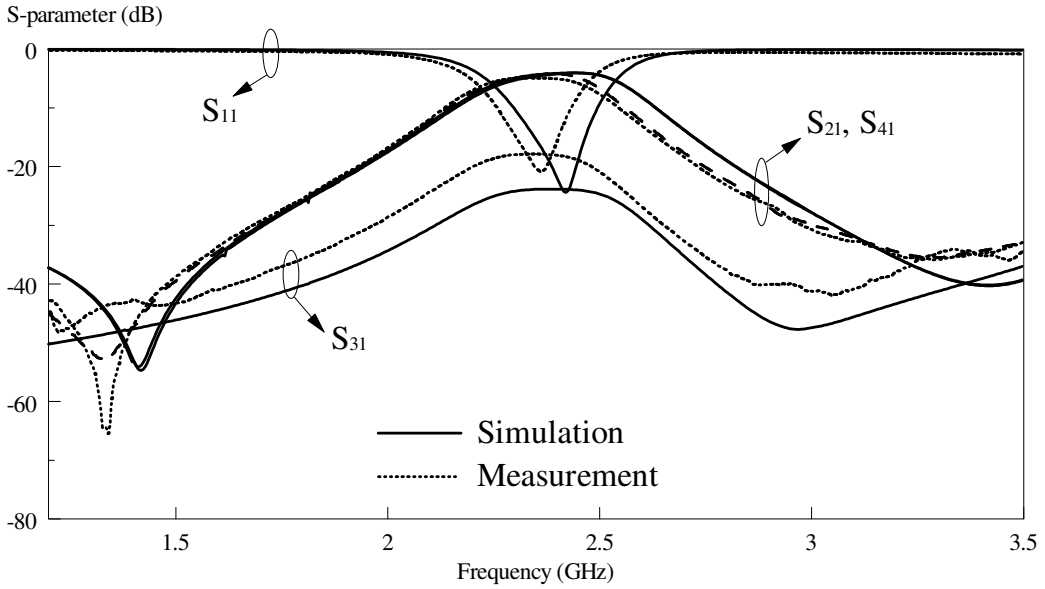

Figure 4.21: Simulated and measured S parameters of the reconfigurable and in-phase BPD-3 (with Port 3 switched OFF but others ON).

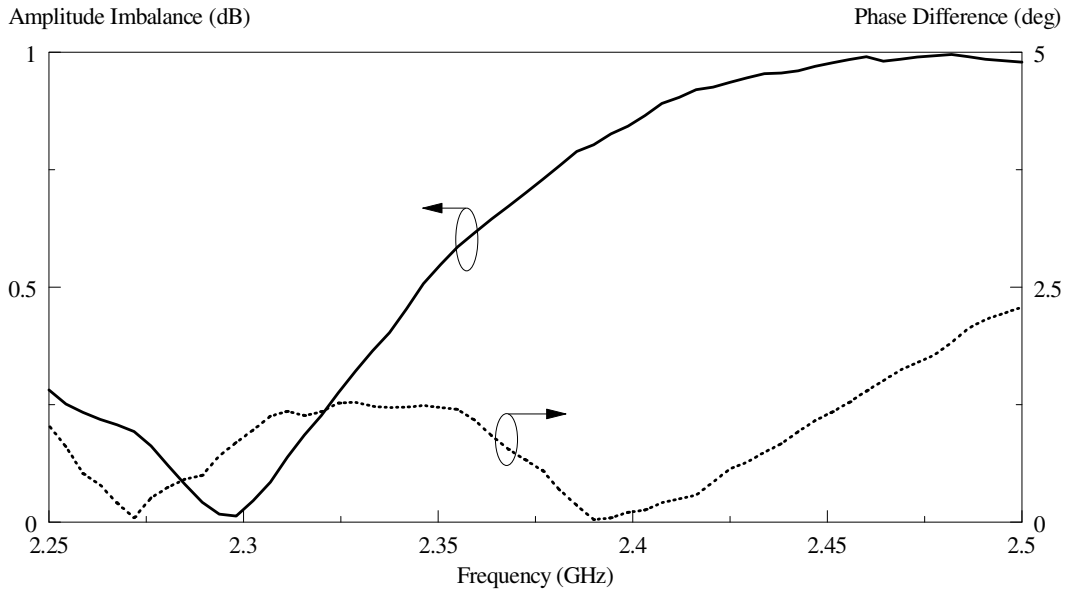

Figure 4.22: Measured amplitude imbalance and phase difference of the reconfigurable and in-phase BPD-3 (with Port 3 switched OFF but others ON).

Next, the power divider is made into out-of-phase configuration by turning off *Port 4*. The simulated and measured S parameters are shown in *Figure 4.23*, yielding the measured and simulated center frequencies of 2.34 and 2.41 GHz, respectively, with an error of 2.9%. Referring to the same figure, S_{41} can reach a maximum value of -20 dB. This again shows good isolation performance of the BAR50-02V RF PIN diode. The measured and simulated bandwidths (180±5°) are 2.25 and 4%, respectively, with an error of 1.75%.

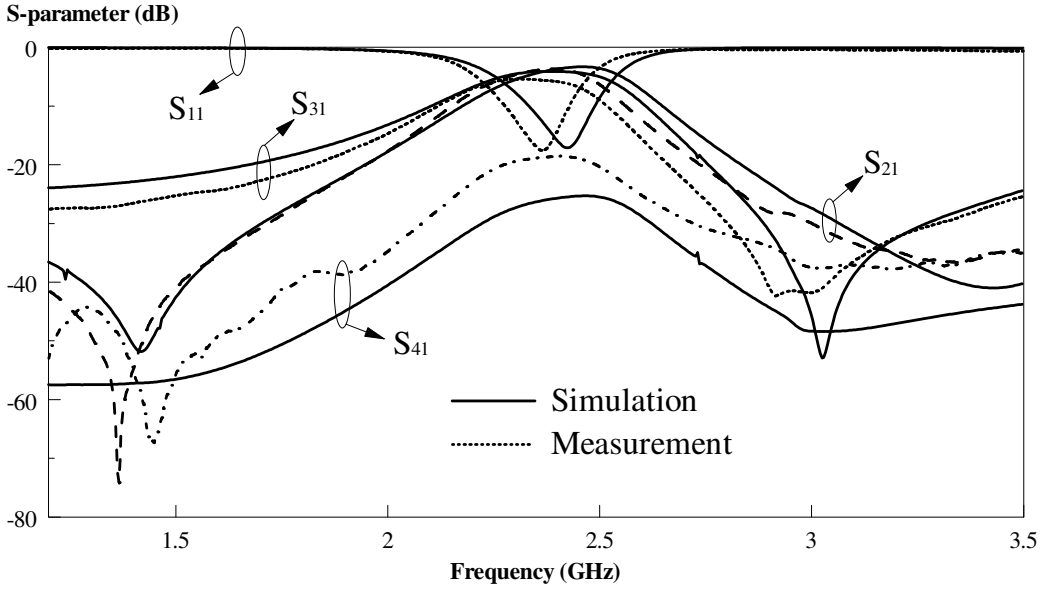

Figure 4.23: Simulated and measured S parameters of the reconfigurable and out-of-phase BPD-3 (with Port 4 switched OFF but others ON).

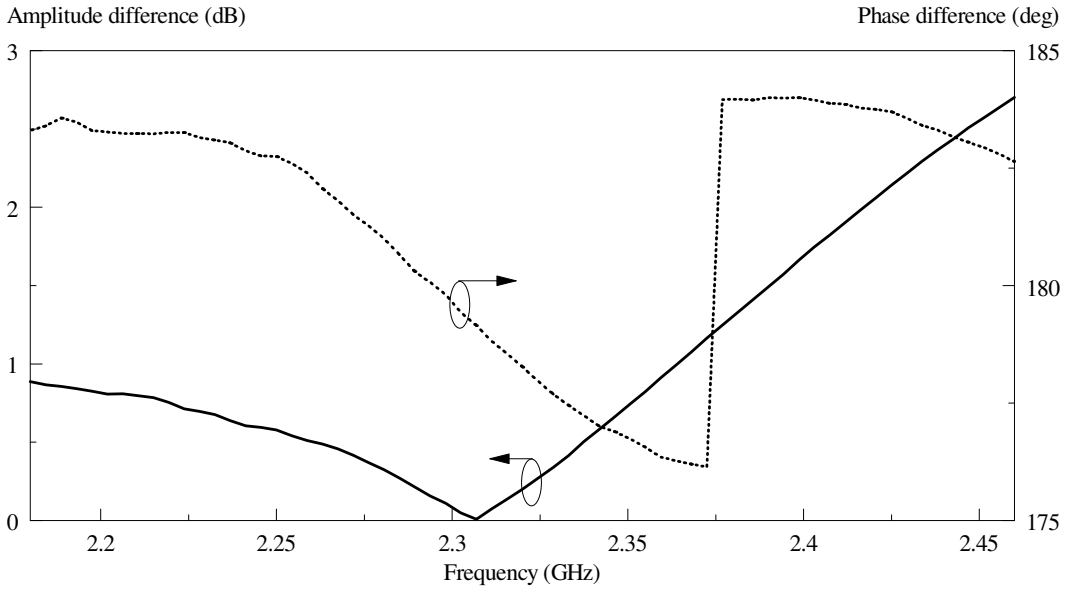

Figure 4.24: Measured amplitude and phase characteristics of the reconfigurable and out-of-phase BPD-3 (with Port 4 switched OFF but others ON).

4.5 Conclusion

In this chapter, an in-phase, an out-of-phase, and a reconfigurable band-passing power divider have been proposed and the design methodology has been described in each section. At the first stage, both the proposed in-phase (**Section 4.2**) and out-of-phase (**Section 4.3**) band-passing power divider were successfully optimized. It was found that the etched-away Y-slot is critical in creating tight coupling and providing filtering effect on a single-layered circular patch resonator. Also, it has been demonstrated that the out-of-phase band-passing power divider can be made available by **ONLY** shifting one of the output port (*Port 3*). Subsequently, in **Section 4.4**, they are combined together into one resonator to become the proposed reconfigurable band-passing power divider. Here, the BAR50-02V RF PIN diode has been integrated at each output ports, and effectively works as a switching element to enable in-phase or out-of-phase performance. The return loss, insertion loss, phase difference, amplitude difference and parameters for each of the band-passing power dividers have been analyzed. Reasonable agreement has been observed between the simulated and experimental data.

CHAPTER 5

Summary and Future Work

5.1 Summary

In this thesis, some of the fundamental concepts of the microstrip lines and patch resonators as well as those pertaining to filters are briefly visited in *Chapter 2*. Later, the multifunction concept has been deployed for designing several bandpassing power dividers. In the beginning, two novel double-layered 3dB and 4.8dB bandpassing power dividers were proposed and have been studied in Chapter 3. It was then followed by the exploration of the single-layered reconfigurable bandpassing power divider in Chapter 4. Commercial software Ansoft HFSS was used to simulate all the proposed configurations, with all verified by experiment. Reasonable agreement was observed between all the simulations and measurements. The research highlights are now re-captured in the following summary:

1) In the first part, two double-layered bandpassing power dividers were proposed and have been studied. With the use of a double-layered structure, the characteristics of the elliptical filters have been studied (as shown in *Figure 5.1*). It was found that the dual-mode performance can be achieved by cutting slit on the resonator. The design procedures for two novel

multiple-channel power dividers have been given at 6 GHz. Worth mentioning is that it does not involve any isolation resistors and quarter-wavelength impedance transformers. More importantly, it eliminates the usage of high-impedance lines, as required by the conventional Wilkinson power divider, when more output ports are involved. This is especially advantageous to the manufacturing process. High compactness in footprint can also be easily achieved in the new proposed designs. Also seen in *Figure 5.1* is that the selectivity of the proposed bandpassing power dividers is much better than that for the conventional one.

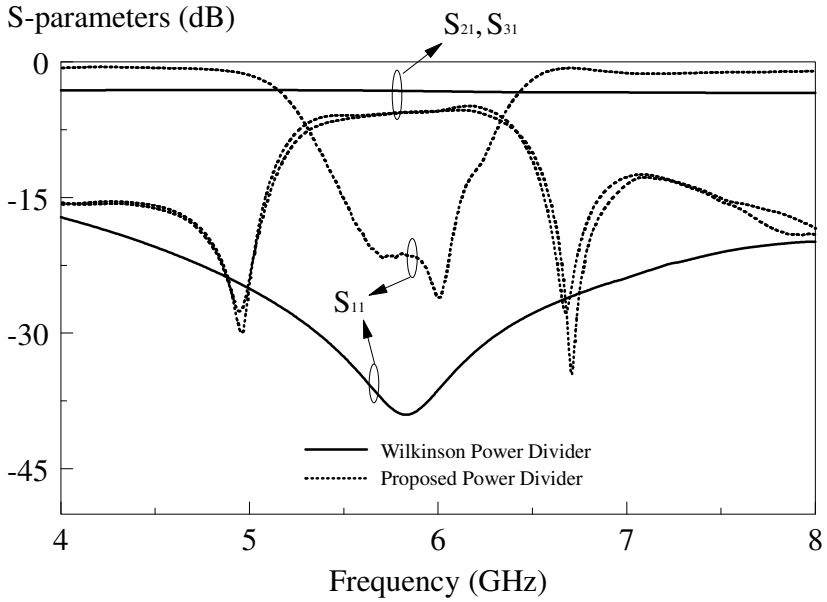

Figure 5.1: Comparison of frequency responses of the conventional Wilkinson power divider and the proposed double-layered bandpassing power divider.

2) Next, two single-layered in-phase and out-of-phase microstrip patch bandpassing power dividers, along with a reconfigurable one that is made out of them were proposed and have been studied. All the three designs are successfully simulated and measured in Chapter 4 of this thesis. By cutting a Y-slit on the patch, good selectivity has been achieved compared to the

conventional Wilkinson Power Divider, and the frequency responses are depicted in *Figure 5.2*. Again, the proposed power divider has a better selectivity.

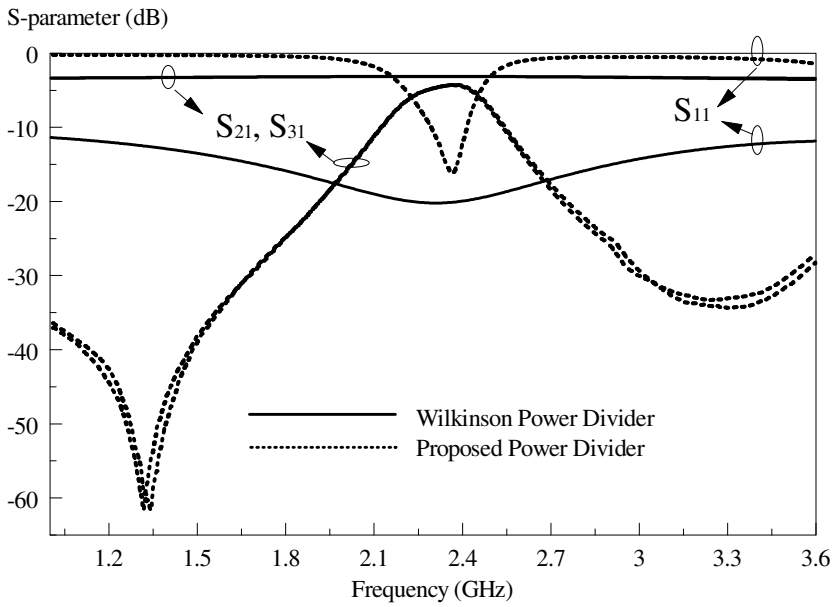

Figure 5.2: Comparison of frequency responses of the conventional Wilkinson power divider and the proposed reconfigurable bandpassing power divider.

.

In addition, reconfiguration was achieved by incorporating RF PIN diodes and the design idea was demonstrated at 2.4GHz. It was found that the same piece of resonator can be configured either in-phase or out-of-phase by tapping out the output microwave signals at different places. Since the proposed reconfigurable bandpassing power divider provides different outputs on a single piece, it signifies that it can be used for two very different applications, leading to tremendous cost saving.

5.2 Future Works

This thesis has successfully proposed and demonstrated two new design ideas, for the bandpassing power dividers. With the use of new resonators, the bandwidth of both the proposed designs can be extended to ultra-wideband (UWB) for future improvement. A more powerful reconfigurable bandpassing power divider may be possible to provide simultaneous 0˚, 45˚, 90˚, and 180˚ outputs, considering some other new technologies. By doing so, the circuit footprint can be made even more compact.

5.3 Bibliography

1. Y. C. Khor, E. H. Lim, B. K Chung, and K. W. Leung, 'Broadside-coupled Filtering Circular Patch Power Dividers', *IEEE Trans. Microwave Theory and Techniques*. (Submitted)

2. Y. C. Khor, E. H. Lim, B. K Chung, and K. W. Leung, 'Reconfigurable Sector-Induced Circular Microstrip Power Dividers', *IEEE Trans. Microwave Theory and Techniques*. (Submitted)

References

Abbosh, M., 2008 Design of Ultra-Wideband Three-Way Arbitrary Power Dividers, *IEEE Trans. Microw. Theory Tech.*, 56 (1), pp. 194-201.

Abunjaileh, A. I., Hunter, I. C., and Kemp, A. H., 2007 Application of Dual-mode Filter Techniques to the Broadband Matching of Microstrip Patch Antenna, *IET Microw. Antennas Propag.*, 1 (2), pp. 273-276.

Ansoft Corporation, High Frequency Structure Simulator (HFSS) v. 11 [Online]. Available: http://www.ansoft.com/products/hf/hfss/. [11 July 2010]

Basraoui, M. and Prasad, S. N., 1998 Wideband, Planar, Log-Periodic Balun, *IEEE MTT-S Int. Microw. Symp. Dig.*, 2, pp. 785-788.

Bialkowski, M. E. and Abbosh, A. M., 2007 Design of a Compact UWB Out-of-phase Power Divider, *IEEE Microw. Wireless Compon. Lett.*, 17 (4), pp. 289-291.

Chang, K., Bahl, I. and Nair, V., 2002 RF and Microwave Circuit and Component Design for Wireless Systems, New York: Wiley.

Chen, J. Y., Tsai, H. J. and Chen, N. W., 2011 Bandwidth Reconfigurable Microwave Bandpass Filter, *IEEE MTT-S Microw. Symp. Dig.*, pp.1-4.

Cheong, P., Lai, K. and Tam, K., 2010 Compact Wilkinson Power Divider with Simultaneous Bandpass Response and Harmonic Suppression, *IEEE MTT-S Int. Microw. Symp. Dig.*

Chiou, Y. C. and Rebeiz, G. M., 2011 A Tunable Three-Pole 1.5–2.2-GHz Bandpass Filter with Bandwidth and Transmission Zero Control, *IEEE Trans. Microw. Theory Tech.*, 59 (11), pp. 2872-2878.

Chiu, J. C., Lin, J. M. and Wang, Y. H., 2006 A Novel Planar Three-Way Power Divider, *IEEE Microw. Wireless Compon.*, 16 (8), pp. 449-451.

Cho, C. and Gupta, K. C., 1998 A New Design Procedure for Single-Layer and Two-Layer Three-Line Baluns, *IEEE Trans. Microw. Theory Tech.*, 46 (12), pp. 2514-2519.

Cohn, S. B., 1986 A Class of Broadband Three-Port TEM-Mode Hybrid, *IEEE Trans. Microw. Theory Tech.*, 16 (2), pp. 110-116.

David, M. Francois, B. and Ke, W., 1996 Microstrip three-way power combiners using a standard MIC technology, *Europ. Microw. Conf.*, 2, pp. 839-843.

Deng, P. H. and Jheng, J. H., 2011 A Switched Reconfigurable High-Isolation Dual-Band Bandpass Filter, *IEEE Microw. Wireless Compon. Lett.*, 21 (2), pp. 71-73.

Dey, S., Aanandan, C. K., Mohanan, P. and Nair, K. G., 1993 Modified circular patch antenna, *Electron. Lett.*, 29 (12), pp. 1126-1127.

Eccleston, K. W., 2005 Compact Planar 3-Way Power Divider Using Left-Handed Transmission Lines, *APMC*, 2.

Eriksson, A., Deleniv, A. and Gevorgian, S., 2002 Band-pass Filters Utilizing Dual-mode Circular Patch Resonators, *European Microw. Conf., Milan*.

Goldfarb, M. E., 1991 A Recombinant, In-Phase Power Divider, *IEEE Trans. Microw. Theory Tech.*, 39 (8), pp 1438-1440.

Hong, J. S. and Lancaster, M. J, 2001 Mirostrip Filters for RF/Microwave Applications, New York: Wiley.

Hsieh, L. H. and Chang, K., 2003 Tunable Microstrip Bandpass Filters with Two Transmission Zeros, *IEEE Trans. Microw. Theory Tech.*, 51 (2), pp. 520-525.

Huang, G. S. and Chen, C. H., 2011 Dual-Band Balun Bandpass Filter with Hybrid Structure, *IEEE Mocrow. Wireless Compon. Lett.*, 21 (7), pp. 356-358.

Huang, G. S., Wang, C. H. and Chen, C. H., 2007 Novel Balanced Coupled-Line Bandpass Filters with Common-Mode Noise Suppression, *IEEE Trans. Microw. Theory Tech.*, 55(2), pp. 287-295.

Huang, G. S., Wu, C. H. and Chen, C. H., 2011 LTCC Balun Bandpass Filters Using Dual-Response Resonators, *IEEE Microw. Wireless Compon. Lett.*, 21(9), pp. 483-485.

Hung, Y. Y., Chang, F. C. and Audeh, N. F., 1970 N-way TEM-mode Broadband Power Dividers, *IEEE Trans. Microw. Theory Tech.*, 18(10), pp. 682-688.

Jia, Z., Zhu, Q. and Ao, F., 2006 A 2-Way Broad-Band Microstrip Matched Power Divider, *Int. Conf. Comm. Circ. Sys. Proc.*, 4, pp. 2592-2596.

Jung, E. Y. and Hwang, H. Y., 2007 A Balun-BPF Using Dual Mode Ring Resonator, *IEEE Microw. Wireless Compon. Lett.*, 17 (9), pp. 652-654.

Kang, S. J. and Hwang, H. Y., 2010 Ring-Balun-Bandpass Filter with Harmonic Suppression, *IET Microw. Antennas Propag.*, 4 (11), pp. 1847-1854.

Kim, S. and Leong, J., 2009 Reconfigurable 1:3 Power Divider using Coupled Lines, *Electron. Lett.*, 45(22), pp. 1141-1143.

Kishihara, M., Yamane, K. and Kawai, T., 2004 A design of multi-stage, multi-way microstrip power dividers with broadband properties, *IEEE MTT-S Microw. symp. Dig.*, 1, pp. 69-72.

Lehmann, T., Hettstedt, F. and Knoechel, R., 2009 Reconfigurable Wilkinson Power Dividers with Minimum Number of Switches, *Electron. Lett.*, 45 (2), pp. 111-112.

Levy, R., 1976 Filter with Single Transmission Zeros at Real or Imaginary Frequencies, *IEEE Trans. Microw. Theory Tech.*, 24 (4), pp. 172-181.

Lew, D.-W., Park, J.-S., Ahn, D., Kang, N.-K., Yoo, C.S. and Lim, J.-B., 2001 A Design of the Ceramic Chip Balun Using the Multilayer Configuration, *IEEE Trans. Microw. Theory Tech.*, 49 (1), pp. 220-224.

Li, J. L., Wang, J. P., Yang, X. S., and Wang, B. Z., 2010 A Study of Dual-mode Patch Resonator-based Microwave Filters, *Microwave and Milimeter Wave Technology (ICMMT)*, pp. 48-51.

Li, Y. C. and Xue, Q., 2011 Tunable Balanced Bandpass Filter With Constant Bandwidth and High Common-mode Suppression, *IEEE Trans. Microw. Theory Tech.*, 59 (10), pp. 2452-2460.

Lin, Z. and Chu, Q. X., 2008 A Compact Spatial UWB Power Divider with 1 to 4 Ways, *APMC*, pp. 1-4.

Marim, M. F., Liu, A. Q., Alphones, A., Yu, A. B., 2006 A novel reconfigurable filter using periodic structures, *IEEE MTT-S Mocrow. Symp. Dig.*, pp. 943-946.

Mgombelo, H. R. and Gardiner, J. G., 1990 Three-way Power Dividers and Combiners Constructed on the Basis of a Three-way Luzzato Divider, *IEE Colloguium on RF Combining*.

Mung, W. Y. and Chan, W. S., 2011 Compact Tunable Lumped-Element Wilkinson Power Divider with High Isolation, *Microw. Opt. Tech. Lett.*, 53(2).

Nakatsugawa, M. and Nishikawa, K., 2001 A Novel Configuration for 1 N Multiport Power Dividers Using Series Parallel Transmission-Line Division and a Polyimide

Alumina-Ceramic Structure for HPA Module Implementation, *IEEE Trans. Microw. Theory Tech.*, 49 (6), pp. 1187-1193.

Ng, C. Y., Chongcheawchamnan, M. and Robertson, I. D., 2002 Analysis and Design of a High-performance Planar Marchand Balun, *IEEE MTT-S Int. Microw. Symp. Dig.*, 1, pp. 113-116.

Park, J. H., Lee, S., Kim, J. M., Kim, H. T., Kwon, Y. and Kim, Y. K., 2005 Reconfigurable Millimeter-Wave Filters Using CPW-Based Periodic Structures with Novel Multiple-Contact MEMS Switches, *Journal of Microelectron. Sys.*, 14 (3), pp. 456-463.

Rosloniec, S., 1996 Three-Port Hybrid Power Dividers Terminated in Complex Frequency-Dependent Impedances, *IEEE Trans. Microw. Theory Tech.*, 44 (8), pp. 1490-1493.

Saleh, 1980 Planar Electrically Symmetric N-way Hybrid Power Dividers Combiners, *IEEE Trans. Microw. Theory Tech.*, 28, pp. 555-563.

Serrano, A. L. and Correra, F. S. (2009) 'A Triple-mode Bandpass Filter Using a Modified Circular Patch Resonator', Microw. Opt. Tech. Lett., vol. 51, no. 1, Jan.

Serrano, A. L., Tan, P., Correra, F. S. and Ferrari, P., 2010a A Tunable Bandpass Patch Filter with Varactors, *IEEE Int. Micro. Symp. Dig.*, pp. 1752 - 1755.

Serrano, A. L., Tan, P., Correra, F. S. and Ferrari, P., 2010b Analysis of a Reconfigurable Circular Patch Filter, *IEEE Trans. Microw. Theory Tech.*, 58 (12), Dec.

Shao, J. Y., Huang, S. C. and Pang, Y. H., 2011 Wilkinson power divider incorporating quasi-elliptic filters for improved out-of-band rejection, *Electron. Lett.*, 47 (23), pp. 1288-1289.

Shor, 1988 Broadbanding techniques for TEM N-way Power Dividers, *IEEE MTT-S Int. Microw. Symp. Dig.*, 2, pp. 657-659.

Singh, Y. K. and Chakrabarty, A., 2008 Miniaturized Dual-Mode Circular Patch Bandpass Filters With Wide Harmonic Separation, *IEEE Microw. and Wireless Compon. Lett.*, 18 (9), pp. 584-586.

Song, K. and Xue, Q., 2010 Novel Ultra-Wideband (UWB) Multilayer Slotline Power Divider With Bandpass Response, *IEEE Microw. Wiless Compon. Lett.*, 20 (1), pp.13-15.

Sun, S. and Menzel, W., 2011 Novel Dual-Mode Balun Bandpass Filters Using Single Cross-Slotted Patch Resonator, *IEEE Microw. Wireless Compon. Lett.*, 21 (8), pp. 415-417.

Tae, H. S., Oh, K. S., Lee, H. L., Son, W. I. and Yu, J. W., 2012 Reconfigurable 1x4 Power Divider with Switched Impedance Matching Circuits, *IEEE Mocrow. Wireless Compon. Lett.*, 22 (2), pp. 64-66.

Tahara, Y., Oh-hashi, H., Miyazaki, M. and Makino, S., 2005 A Broadband Three-Way Tapered-Line Power Divider with Several Strip Resistors, *Europ. Microw. Conf.,* 1.

Tan, B. T., Chew, S. T., Leong, M. S., and Ooi, B. L., 2002 A Modified Microstrip Circular Patch Resonator Filter, *IEEE Microw. Wireless Compon. Lett.*, 12 (7).

Tang, C. W. and Chang, C. Y., 2002 A Semi-lumped Balun Fabricated by Low Temperature Co-fired Ceramic, *IEEE MTT-S Int. Microw. Symp. Dig.*, 3, pp. 2201-2204.

Tang, X., and Mouthaan, K., 2009 Analysis and Design of Compact Two-way Wilkinson Power Dividers Using Coupled Lines, *APMC*, pp. 1319-1322.

Vargas, S. R., Yang, R. Y., Weng, M. H., Wu, H. W. and Liauh, C. T., 2007 A Novel Circular Patch Bandpass Filter with Wide Stopband Response by Multi-order Harmonic Suppressed I/O Lines, *Proceedings of Asia-Pacific Microwave Conference*, pp. 1-4.

Watkins, J., 1969 Circular Resonator Structure in Microstrip, *Electron. Lett.*, 5 (21), pp. 524-525.

Wilkinson, E. J., 1960 An N-way hybrid power divider, *IRE Trans. Microw. Theory Tech.*, 8 (1), pp. 116-118.

Wong, P. W. and Hunter, I. C., 2009 Electronically Reconfigurable Microwave Bandpass Filter, *IEEE Trans. Microw. Theory Tech.*, 57 (12), pp. 3070-3079.

Wong, S. W. and Zhu, L., 2008 Ultra-Wideband Power Divider With Good In-Band Splitting and Isolation Performances, *IEEE Microw. Wireless Compon. Lett.*, 18 (8), pp. 518-520.

Wong, S. W. and Zhu, L., 2009 Ultra Wideband Power Dividers With Good Isolation and Improved Shapr Roll Off Skirt, *IET Microw. Antennas Propag.*, 3 (8), pp. 1157-1163.

Wu C. H., Wang, C. H., Chen, S. Y. and Chen, C. H., 2008 Balanced-to-Unbalanced Bandpass Filters and the Antenna Application, *IEEE Trans. Microw. Theory Tech.*, 56 (11), pp. 2474-2482.

Yau, W., Schellenberg, J. M. and Shih, Y. C., 1986 A New N-Way Broadband Planar Power Combiner and Divider, *IEEE MTT-S Microw. symp. Dig.*, pp. 147-149.

Yeung, L. K. and Wu, K. L., 2005 An Integrated RF Balanced Filter with Enhanced Rejection Characteristic, *IEEE MTT-S Int. Microw. Symp. Dig.*, pp. 713-716.

Yeung, L. K. and Wu, K. L., 2006 An LTCC Balanced-to-Unbalanced Extracted-Pole Bandpass Filter with Complex Load, *IEEE Trans. Microw. Theory Tech.*, 54 (4), pp. 1512-1518.

Yeung, L. K. and Wu, K. L., 2007 A Dual-Band Coupled-Line Balun Filter, *IEEE Trans. Microw. Theory Tech.*, 55 (11), pp. 2406-2411.

Zhang, Z. Y., Guo, Y. X., Ong, L. C. and Chia, M. Y. W., 2005 A New Wide-band Planar on a Single-layer PCB, *IEEE Microw. Wireless Compon. Lett.*, 15 (6),pp. 416-418.

Zheng, S. Y., Chan, W. S. and Man, K. F., 2011 Frequency-Agile Patch Element Using Varactor Loaded Patterned Ground Plane, *IEEE Trans. Microw. Theory Tech.*, 59 (3), pp. 619-626.